Post-processing of additively manufactured metallic alloys – A review

International Journal of Machine Tools & Manufacture 179 (2022) 103908

Contents lists available at ScienceDirect

International Journal of Machine Tools and Manufacture

journal homepage: www.elsevier.com/locate/ijmactool

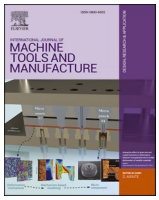

Post-processing of additively manufactured metallic alloys – A review

Amir Malakizadi [a,*], Dinesh Mallipeddi [a], Sasan Dadbakhsh [b], Rachid M'Saoubi [c], Peter Krajnik [a]

[a] Division of Materials and Manufacture, Department of Industrial and Materials Science, Chalmers University of Technology, Göteborg SE-412 96, Sweden
[b] Department of Production Engineering, KTH Royal Institute of Technology, Brinellvägen 68, 10044, Stockholm, Sweden
[c] R&D Material and Technology Development, Seco Tools AB, 737 82, Fagersta, Sweden

ARTICLE INFO

Keywords:
Additive manufacturing
Powder bed fusion
Direct energy deposition
Machining
Grinding
Mechanical properties
Machinability
Grindability
Laser polishing
Finishing
Electropolishing
Fatigue
Wear
Corrosion
316L
Ti6Al4V
Alloy 718

ABSTRACT

Additive manufacturing (AM) is characterised by several unique advantages, such as (freedom of) design, capability of fusing dissimilar materials, near-net-shape, and achieving a more sustainable production. While the increased precision of metal AM in recent years reduced the needed amount of post-processing to meet dimensional tolerance, the requirements for functional surfaces necessitate a well-understood post-processing, ranging from heat treatment to machining and finishing. The inherently rough initial (as-built) surface topography next to complex material microstructure affects the capability of post-processing/finishing operations to smooth the surface texture and obtain a favourable surface integrity. In this respect, a more fundamental understanding of the effects of material properties on post-processing/finishing is needed. Therefore, this review paper aims to establish the relationship between the characteristics of different AM technologies, microstructural properties of materials in as-built and heat-treated conditions, and the physical properties influencing the response of additively manufactured materials during post-processing/finishing operations. In particular, emphasis is placed on the physics-based understanding of how the microstructural characteristics of 316L, Ti6Al4V and Alloy 718 produced using the two principal technologies, Powder Bed Fusion (PBF) and Direct Energy Deposition (DED), influence their mechanical properties like tensile strengths, hardness and ductility. These properties are among the key factors influencing the response of material during post-processing/finishing operations involving material removal by shear deformation. This review paper also discusses the role of post-processing/finishing on fatigue performance, tribological behaviour and corrosion resistance of investigated AM materials. The paper summarises the state-of the art of post-processing/finishing operations and future research trends are highlighted.

1. Introduction

Additive manufacturing (AM) is currently perceived as a disruptive technology in production engineering. In a non-technical context, AM is referred to as 3D printing since the fabrication generally involves deposition of a material using a print head, nozzle, or other technologies and builds parts as specified by 3D model data [1]. The process of fabricating products by depositing material layer-by-layer instead of by conventional material-conversion processes (e.g., forming and casting) and/or material-removal (subtractive) processes offers numerous advantages in view of realizing new designs (e.g., lightweight engineered parts), and manufacturing with less tooling/assembly and with minimal material waste. Most of the established AM processes in use today were initially developed in the context of rapid prototyping (RP) over 30 years ago [2,3]. Since RP was historically the first commercialised application for AM it remains commonly used as a general term for this technology. The increased adoption of AM in recent years is to a large extent driven by fast-paced research and development in metal-additive manufacturing, featuring powder metals from steel aluminium and titanium alloys to Ni-based superalloys for high temperature applications. Metallic materials are hence in focus, whereas AM of polymer, ceramic and composite materials is deemed out of the scope of this work. AM is an industrialised and mature (high TRL) technology, implemented in real production lines, for example in manufacturing and remanufacturing of turbine parts (e.g., burners) in the energy and aerospace sectors. In other industries, such as the automotive industry, AM is primarily used for rapid tooling (i.e., using AM to produce tools and fixtures with short lead times), making spare parts and small-volume/near-net shape production [4]. This is a clear indicator that AM is currently more suited for high-value/small-volume

* Corresponding author.
E-mail address: amir.malakizadi@chalmers.se (A. Malakizadi).

https://doi.org/10.1016/j.ijmachtools.2022.103908
Received 15 February 2022; Received in revised form 27 May 2022; Accepted 9 June 2022
Available online 21 June 2022

manufacturing where higher production costs are compensated by added value, e.g., capability of forming complex 3D parts by addition of material. Despite these advantages, there are still major challenges and barriers to be overcome prior to even wider adoption. These technological challenges range from design (incl. materials design) to manufacturing. This review is clearly focused on the latter aspect, specifically on the role of post-processing, i.e., finishing processes taken after the completion of an AM build cycle in order to achieve the desired quality/properties in the final parts (e.g., surface roughness). Other manufacturing-related shortcomings, such as limited production capacity, high production costs, size limitations, and service/supply-chain issues are not specifically addressed in this review.

The motivation for writing this review paper is to make a critical analysis and to strengthen the role of finish post-processing in the AM value chain. This aspect is often overlooked and not sufficiently addressed in a scientifically inquisitive manner. For example, the understanding of the structure-property correlations in AM might be comprehensively addressed from the materials-science perspective [5]. Other perspectives in AM might focus on specific laser beam/sintering issues and carefully incorporate material aspects [6], but address post-processing to a limited extent. Then there are reviews available addressing post-processing effects on the surface integrity of materials produced by powder based fusion using a laser-based system (PBF-LB) [7]. However, these collective investigations do not provide a full understanding of how the history of a material which has undergone different stages along the AM value-chain can affect the surface integrity of the part after finishing and thus their functional performance during the application. In terms of post-processing/finishing, a recent review by Lee et al. [8] provides a valuable discussion on the availability and relevance of ISO/ASTM standards, but does not specifically address surface integrity aspects (beyond surface roughness and surface defects), nor the related effects of surface integrity on functional performance. The incentive for this review is hence that the ability to use AM metallic parts in precision engineering application depends on post-processing/finishing determining achievable surface integrity [9] and functional performance [10]. Specifically, the major concern is post-processing that result in an improved surface integrity in a variety of applications with constraints on fatigue performance, wear or corrosion properties. Finish post-processing includes subtractive processes such as machining to abrasive fine-finishing processes and non-contact finishing processes, such as laser polishing. Practical post-processing aspects such as removal of support structures and fixturing/clamping for machining are not considered, as they are more suited to other more specialised journals. Moreover, post-processes where the improvement of surface topography is not of major concern, such as in shot peening, are not discussed in great detail. The terminology used in this work is aligned as much as possible to ISO/ASTM 52900:2021 standard [1], to ensure the general principled definitions, terms and nomenclature are aligned to international norms.

The objective of this review article is to shed the light on the complex material-process- performance interconnected relation along the value-chain as shown in Fig. 1. The illustrated value-chain comprises a sequence of operations necessary for the part to achieve desired properties and functionality. The functionality of a part depends on a multitude of factors, ranging from geometry (e.g., dimensional tolerances), surfaces (e.g., functional surfaces, surface roughness) and material properties (e.g., mechanical properties set by AM, thermal post-treatment, final finishing post-processing). Depending on the functional requirements, AM processes almost always require one or more post-processing operations, such as thermal post-treatment (e.g., Hot Isostatic Pressing – HIP) and post-processing/finishing operations (machining, abrasive processes, etc.) to obtain all the designed properties in the final part.

The paper is structured as follows. Section 2 explains the background

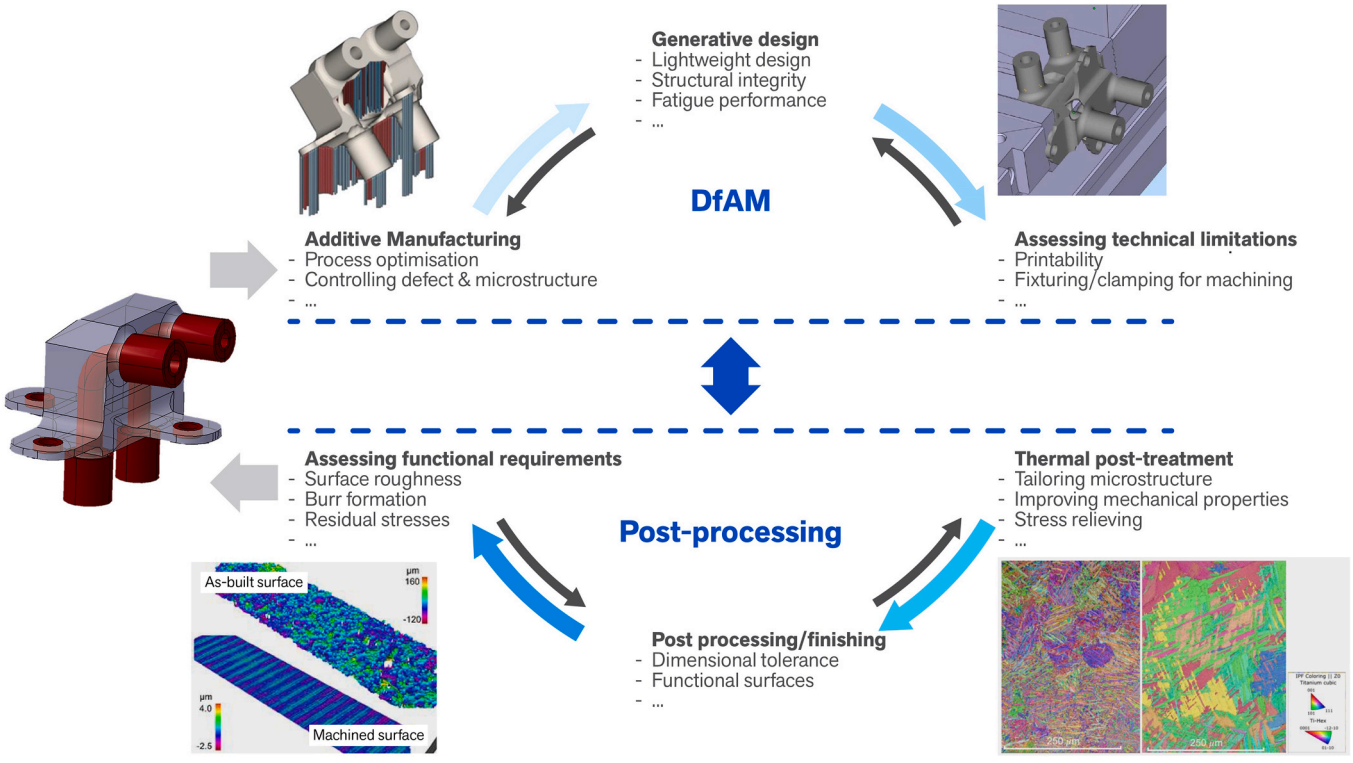

Fig. 1. Typical stages along the additive manufacturing value-chain. Iterative forward and backward strategies to optimise the final functional performance of a lightweight component. The original model often needs to be re-designed to unleash the full potential of additive manufacturing. The designers need to consider different aspects of the value-chain during the design process, e.g., the support structures, fixturing and clamping for post machining process [11,12] and distortion control and microstructure development during thermal post treatments [13] to ensure the functional requirements are met.

of the different indicators to assess machinability/grindability, as well as other finishing processes that are at the core of the undertaken approach, to a large extent determining the structure/outline of the paper. Here, we briefly cover AM-specific considerations that influence the microstructure development of additively manufactured materials and their physical properties, which in turn affect the response of material during and after post-processing. Section 3 covers the response of the additively manufactured 316L, Ti6Al4V and Alloy 718 during metal cutting processes including turning, milling and micro-milling. The reported observations are critically reviewed in this section with reference to the machinability assessment framework described in Section 2. Section 4 discusses the critical analysis of the state of the art with respect to grinding, abrasive fine finishing, electropolishing and laser polishing. Section 5 discusses the specific performance and functionality aspects of post-processed materials mentioned above. The paper concludes with Section 6 in which the state-of-the-art post-processing/finishing methods are summarised and future research trends are highlighted.

2. Background

This section provides a background to assessing the performance of the most common post-processing/finishing operations for AM parts, which are numerous – from conventional machining to laser polishing and electropolishing. Near-net shape additively manufactured parts generally require a marginal material removal from the as-built surfaces to set the dimensional tolerances and to achieve desired surface properties. Under conventional machining (metal cutting), the key processes are turning and milling. A careful selection of cutting conditions and tool geometries/material (e.g., wiper inserts or ball end mills with superior edge precision) can provide acceptable surface finish properties for most industrial applications. Higher quality in terms of form, accuracy and surface integrity can be achieved using other conventional and non-conventional finishing processes [14]. Compared to conventional metal cutting processes, finishing operations like grinding, abrasive fine-finishing and electropolishing typically remove a very small amount of material, on the scale of a few micrometres or less. Other methods like laser polishing do not remove but rather re-distribute the material on the as-built surfaces. In the context of this work, finishing processes are considered as post-processing following additive-manufacturing processes or heat treatment (including HIP).

Important considerations when selecting post-processing operations are the surface finish properties and complexity of as-built parts. These determine which post-processing technology is the most feasible and cost-effective to be implemented. Table 1 gives an overview of process parameters, capabilities and resulting surface finish and mechanical properties commonly reported for PBF and DED technologies. PBF-LB is capable of building the most complicated parts with the highest resolution, while PBF-EB and DED-LB generally lead to rougher surfaces with lower geometrical precision. These characteristics define whether a given technology is favourable and cost-effective for post-processing a part manufactured using different AM methods. The specific angle of this review paper is to emphasise the workpiece material effects on subtractive post-processing operations, which involve material removal by mechanical action (i.e., shearing). These effects are especially complex for additively manufactured parts due to inherent lack of robustness in 3D printing at scale. Here, the machinability/grindability assessment framework is discussed to serve as the baseline for a more systematic, and material-science focused approach to evaluate the ease of post-processing that involve material removal by shearing, though in different scales.

2.1. Machinability – definition and assessment methods

"Machinability of an alloy is similar to the palatability of wine – easily appreciated but not readily measured in quantitative terms" – this is how machinability was caricatured by Edward M. Trent [19] after his lifelong research in the field of metal cutting. Such an expression reflects the complexity in defining and evaluating machinability, because there are many factors partly associated with the cutting process itself which may influence the machinability of an alloy, such as the cutting tool material, tool geometry and machining method, and partly related to the inherent properties of the workpiece material e.g., its strength and thermal conductivity. In practice, however, machinability is perceived as the ease with which an alloy can be machined under given process conditions. Often, one or more of the following criteria are used to evaluate the machinability of an alloy: 1) tool life (or tool wear rate), 2) cutting forces, 3) surface finish, 4) material removal rate, 5) chip shape and 6) environmental impacts [20]. Nevertheless, where machining of AM materials is concerned, tool life, cutting forces and surface finish characteristics are often regarded as the machinability indicators and compared with those of wrought or cast materials as the reference point. The motive here is that if the machinability of an alloy is known, the machining processes can be executed more efficiently. For example, if the machinability of a given alloy is known, the right tool geometry and

Table 1
A general comparison between PBF-LB, PBF-EB, and DED. Adapted from different sources [15–18].

Parameter	PBF-LB	PBF-EB	DED-LB
Common markets	Direct metal parts, medical, aero, dental, tooling and high-tech applications	Direct metal parts, medical, aero, automotive, tooling and high-tech applications	Energy, aerospace, medical device, automotive, tooling and defence
Commercial materials	Stainless steel, Ti alloys, CoCr, tool steel, Ni-based alloys, Al alloys	Ti, Ti6Al4V, CoCr, Alloy 718	Tool steels, stainless steels, Ti alloys, Ni-based alloys
Typical powder size (μm)	15–45	45–120	Varied, spherical
Build envelop	Limited	Limited	Large and flexible
Build capability	Complex geometries, cellular structure, building hollow channels	Complex geometry, cellular structure, building hollow channels	Relatively simpler geometry with less resolution
Beam size (μm)	30–100	200–1100	300–3000
Layer thickness (μm)	20–100	50–150	40–1000
Min detail size (μm)	<200	250	500
Surface finish Ra (μm)	<10	10–50	20-50, depends on beam size
Residual stress	High	Minimal	High
Heat treatment	Stress relief is required, HIP is preferred	Stress relief is not required, HIP may or may not be performed	Depends on the case
Material properties	Typically, equal or better yield strength as compared to conventional materials, but lower ductility	Typically, within the same range as conventional	Typically, equal or better yield strength as compared to conventional materials, but lower ductility

tool material can be selected, the cutting data can be adjusted for improved productivity, and scrap rates can be reduced. These are considered critical factors when machining AM materials, as pointed in Section 3. Following the above role of machinability, grindability can be also considered as the ease with which a material can be ground (machined with abrasives) under given conditions while evaluating the process outcomes under criteria such as [21]:

- Mechanical – specific grinding energy (energy consumed per unit volume removed),
- Tribological – wheel wear, and
- Thermal – surface integrity (e.g., residual stresses, obtainable microstructure)

Over the last few decades, many attempts have been made to develop standard experimental procedures to rank the machinability of the materials in terms of a given indicator, like tool life. Astakhov [22] summarises the common experimental methods used for evaluating machinability of materials – with a major focus on tool life – along with the strength and weakness of each method. These methods normally aim to rank the machinability of a given alloy with respect to a reference material, and thus to develop a "machinability index" system. Given a number of examples, the author reasoned that developing a machinability index ranking system using the common experimental procedures and standards is not of practical value. The complex interactions between the tool and workpiece materials would differ as a new system (here, a system refers to a given tool and workpiece material combination) is investigated. Hence, the results of any machinability test will solely enable ranking the workpiece materials when machining using a specific tool material, tool geometry, cooling and lubrication condition and machining type and method. In addition, the variations in the microstructural properties of the workpiece materials would lead to large variations in their thermo-mechanical properties and thus in their machinability. These make it impractical to utilise the results of machinability indices developed solely based on machining experiments. In 1981, König and Messer [23] presented a similar attempt to account for all factors that influence a grinding process, and then addressed the grindability of a material. They highlighted the complexity of the system and that the grindability cannot be characterised by a single material characteristic alone. Instead, they mentioned the possibility of combining multiple process characteristics measured during grinding experiments, to form the so-called "grindability index". The machinability and grindability indices were quickly forgotten and are not widely used.

In parallel, many attempts have been made to relate the machinability of an alloy to its inherent thermo-mechanical and microstructural properties [20,24], for example, strain hardening, ductility, hardness, thermal conductivity and abrasiveness, and thus index its machinability with respect to a reference material using the concept of a polar diagram shown in Fig. 2. This approach is based on the notion that the thermo-mechanical loads on the tool surfaces and the tribological conditions controlling the tool wear in machining should in theory correlate closely with the physical properties of the workpiece material being machined. In polar diagrams, the mid-values for each axis (i.e., 0.5) are assigned to the properties of the reference material, which enables comparison of the machinability of different alloys with respect to the reference material in a qualitative manner. The potential of this approach for ranking the machinability of the materials in terms of tool life (tool wear) is demonstrated for machining of wrought Alloy 718 (batch-to-batch variation effects) [25,26], brass alloys [27], steels and other metallic alloys [24,28]. This framework would also be suitable to assess grindability, as the material properties such as ductility and strain hardening directly correlate to specific grinding energy, material hardness and abrasiveness affect tool (wheel) wear, whereas thermal conductivity influences grinding temperature (thermal aspects). Grindability, however, is not as meticulously defined as machinability and rarely follows a systematic investigation. In view of abrasive post-processing of AM materials this raises a particular concern as the material effects when processing at a small (chip thickness) scale become more dominant due to the size effect [29,30]. Nevertheless, the machinability- and grindability-related material aspects are comparable and interchangeable in the context of this review paper. Hence, the expressions for machinability/grindability can be exchanged with each other without addressing small process differences. Moreover, this concept further encompasses (non-grinding) abrasive fine-finishing processes, discussed in Section 4. Such an extension adds a certain complexity due to less defined geometry and kinematics of, e.g., pressure-copying processes utilising free abrasives, hence resulting in difficulty in attributing a certain material/post-processing effect with a specific measurable process (input) parameter. In turn, the material effects on abrasive fine-finishing processes are almost always ignored and/or insufficiently described.

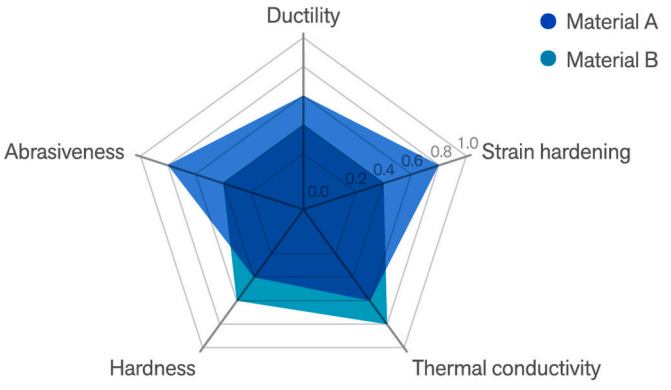

Fig. 2. Machinability assessment using the so-called "polar diagrams". In this approach, the machinability of Material A and B is compared with a reference material whose properties are given the mid-values (i.e., with 0.5 taking all axes of the polar diagram). Adapted from Ref. [20].

An example to illustrate the use of a polar diagram for ranking the machinability of materials in terms of tool life and tool wear is shown in Fig. 2. Here, material A, with larger strain hardening, ductility and abrasiveness, should result in lower machinability while material B, with lower strain hardening, ductility, abrasiveness and higher thermal conductivity, should lead to better machinability as compared with the reference material (with 0.5 taking all axes in the polar diagram).

Larger strain hardening and ductility of the materials would infer a larger amount of heat generation during the cutting process and thus higher temperature. This is based on the fact that somewhere between 75 and 90% of plastic work transforms to heat in shear zones in the vicinity of cutting edge. The plastic work in cutting can be estimated as [31]:

$$W = \int \sigma_e : d\varepsilon_p \tag{1}$$

where σ_e and ε_p are the equivalent stress and plastic strain tensors, respectively. The amount of plastic work at the shear planes increases with increasing the material strain hardening and ductility. Under the simplified unidirectional deformation, strain hardening may be approximated by the ratio between the tensile strength (σ_{UTS}) and yield stress (σ_y), and ductility may simply be expressed as the elongation at failure (ε_f) [25]. It should be noted here that if the flow stress properties of the workpiece material are known at the range of temperature and strain rate encountered in cutting, Eq. (1) would provide a more accurate estimation of generated heat. In addition, higher strength also means larger normal and shear stresses acting on the tool surfaces and thus larger wear rates are expected when machining high strength materials. Astakhov referred to this relation as the specific fracture energy (provided that Eq. (1) is integrated over the entire range of strain, up to

the material failure – ε_f) [22] and showed it can be used as a reliable indicator for indexing the machinability of alloys. Nevertheless, the amount of heat transfers to the tool depends on the thermal conductivity of the tool and workpiece materials. For a given tool material and under similar process conditions, the tool temperature depends on the amount of generated heat (plastic work and frictional stress combined) and also the thermal conductivity of the workpiece material. Hence, higher cutting temperatures and thus higher thermally activated tool wear are expected when machining materials with higher mechanical properties and lower thermal conductivity, like stainless steels, titanium, and Ni-based superalloys. These materials are often classified as difficult-to-cut materials. Excessive tool wear evolution worsens the surface integrity and dimensional tolerances and influences the process stability in metal cutting. In grinding and abrasive processes, excessive heat generation can lead to surface softening (tempering), changing the state of surface residual stresses from compressive to tensile, and in worst-case scenarios, it can induce microstructural changes (white-layer formation), referred to as re-hardening. Re-hardening and formation of the hard but brittle white-layer on the surface can drastically reduce the functionality of the ground surface (wear and rolling fatigue properties). The abrasiveness and (bulk) hardness determine the rate of mechanically induced wear mechanisms on tool surfaces during machining. The material abrasiveness depends on the type, amount and size of hard particles like carbides and nitrides or non-metallic inclusions like oxides. Materials with a large amount of large hard particles would show poor machinability and poor grindability. For example, high-speed steels containing large vanadium carbides can abrade (aluminium oxide) abrasives during grinding due to their high hardness [32]. Reducing the amount and size of hard inclusions can hence improve grindability, as the inclusions abrade the abrasive (tool) at a lower rate. This is analogous to the material effect observed in abrasive wear studies in metal cutting. Hence, the relative hardness and size of abrasive particles (i.e., micro-size carbides and nitrides in steels and superalloys) with respect to the tool material should be considered as a key machinability [33,34] and grindability indicator [32,35]. The behaviour of non-metallic oxide inclusions is rather complex. The presence of Al_2O_3 particles in steels is known to increase the tool wear by abrasion, whereas the modified Ca-rich aluminium oxide inclusions with lower hardness may smear out on the tool surfaces and form passive layers, protecting the tool from thermally-induced wear mechanisms like dissolution-diffusion and oxidation [36]. Chemical reactions between the coating and the oxide inclusions are also reported in some cases. These reactions are believed to increase the rate of tool wear [37,38]. These factors should be considered when comparing the influence of oxide inclusions on machinability of AM materials with their conventionally manufactured counterparts. This is of the utmost importance when comparing the machinability of AM 316L stainless steel with that of "inclusion engineered" wrought material, e.g., Ca-treated 316L stainless steel [39]. Nevertheless, application of this approach for evaluating machinability of materials faces a few shortcomings that must be taken into consideration:

- The ductility and strain hardening behaviours of the workpiece materials are not readily available at the high strain rates and temperatures encountered in machining processes. Moreover, it is well known that the ductility of the material (elongation at fracture) depends on stress triaxiality [40,41]. Thus, the response of a material that is examined using conventional mechanical testing methods like tensile or compression tests could differ greatly from the material behaviour during machining processes.
- The lack of a reliable gauge for the abrasiveness of materials. Although the hardness of abrasive particles like carbides and nitrides is widely available in the literature, a large range is observed for the reported values. The same applies for the hardness of coating materials applied on the tool surfaces. As a result, there is much uncertainty in estimated abrasiveness calculated based on the relative hardness of abrasive particles and tool materials. In addition, a number of investigations have shown that the size [42,43] and amount [44] of those hard particles play a significant role in rate of tool wear by abrasion. This suggests that abrasiveness of the workpiece materials should be evaluated using a more elaborate relation, taking into account the relative hardness as well as the size and amount distributions of present abrasive particles. Currently, such a complex model is not available.
- The relative impact and weight of each indicator on the machinability of an alloy is not clear in this approach. For instance, it is not possible to determine whether a 20% increase in strain hardening or hardness has the same effect as a 20% decrease in thermal conductivity. This limits the application of this method to, at best, solely in a qualitative manner.
- The properties of the tool material and chemical interactions between tool material and workpiece are not included in this approach (or at least only partly included if the relative hardness of workpiece and tool is considered for abrasiveness). It is well known that the chemical affinity of the workpiece and tool material play a decisive role in wear rate during machining. Hence, one-sided evaluation of the machinability of the materials without considering the properties of the tool would not provide the full picture.
- In grinding and abrasive processes, the material removal involves shear in an abrasive contact, whereas the magnitude of the shear fundamentally depends on process geometry and kinematics as well as specific energy. The latter is the main grindability characteristic, which captures the material effects, among others. However, there are no first-principle's laws available to correlate material properties to specific energy.

2.2. *Machinability of AM materials – specific considerations*

The approach described in Section 2.1, despite its limitations, can provide a useful framework for evaluating the machinability of AM materials under specific considerations. For example, if the conventionally manufactured alloy is taken as the reference material, the role of cutting tool properties would be neglected. This is based on the assumption that the chemical affinity of the AM materials with the tool would not greatly differ from those of wrought and cast materials (if the chemical composition and phase contents remain within a relatively narrow range). Yet the significantly different microstructural characteristics of AM materials as compared to those of wrought and cast materials [16,45–47] can influence their thermo-mechanical properties and thus their machinability/grindability:

- Very different grain size and shape distributions as well as strong preferred crystallographic orientation (texture) along the build direction would lead to anisotropic mechanical behaviour. This would, in turn, result in an anisotropic response during machining, depending on the material removal direction with respect to orientation of the densely distributed grains and the crystallographic texture on the cutting plane [46,48–51]. This phenomenon is well depicted in the comparative investigation on the influence of sample orientation with respect to the milling configuration (i.e., cutting plane direction with respect to the crystallographic texture) [48]. The authors reported directionality in measured cutting forces as shown in Fig. 3 (compare the colour codes in Fig. 3a and b). The lowest resultant force was observed when the cutting plane was perpendicular to the build direction. Highest cutting forces were achieved when the sample was oriented such that the {111} plane normal direction was parallel to the cutting plane. The influence of texture will be discussed further in Section 3.
- As-built AM materials normally possess a small amount of porosity defects. Pore formation is inevitable in AM due to the complex melt pool dynamics and can be of different types (e.g., gas porosity or lack-of-fusion porosity, depending on additive manufacturing

method and printing strategies), although the common goal is to fabricate parts with a density of above 99.5%. Pores tend to act as stress concentration regions with the material, reducing its tensile strength and ductility [52]. This phenomenon is depicted in Fig. 4 for PBF-EB/Alloy 718, where a large density of superficial defects, including surface voids and notches and subsurface defects, after a shallow machining led to premature failure during the tensile test. The tensile properties significantly improved after changing the printing strategy [53] and removing superficial defects using a larger depth of cut during machining [54]. The density of defects can also be reduced by application of HIP post-treatment, improving the ductility of AM materials [55–57]. In addition, the thermal conductivity is shown to be dependent on porosity [58]. Although the effect of porosity on thermal conductivity would be of minor importance for most practical applications (only about 2% and 4% reduction in thermal conductivity for 1% and 2% porosity, respectively), it can have larger impacts on cutting temperature when machining the as-built surface layers where the density of pores and defects is generally larger than pore content within the fabricated parts (i.e., in the bulk). In two-phase materials like Ti6Al4V or duplex-steels, the thermal conductivity can also be influenced by the amount of different phases formed during the AM process and after thermal post-treatments [59,60]. In fact, the thermal conductivity would be influenced by lattice defects, grain boundaries, dislocation, segregation of elements and other imperfections in the atomic structure [61]. Experimental observations suggest that thermal conductivity of materials decreases as the intensity of lattice defects and imperfections increases [61]. Unfortunately, to the best of our knowledge, there is no comprehensive quantitative assessment to date on the influence of these parameters on thermal conductivity of metallic alloys.

- The cellular structure and density of lattice defects such as dislocations have marked influences on the mechanical properties. Microscopic investigations showed clear differences in the dislocation density of materials fabricated using various manufacturing methods, e.g., PBF-LB, PBF-EB, DED-LB and wrought (recrystallised microstructure of hot rolled material) [46,62–64]. The larger density of dislocations leads to higher yield and tensile strengths, as larger forces are required to move the interacting tangled dislocations [65]. However, at the same time, larger dislocation density would lower the ductility of the materials, as the dislocation pile-up would potentially act as crack initiation sites during subsequent deformation [65]. The dislocation density can be reduced by the subsequent thermal post-processes. The role of dislocation density on tensile properties of materials is discussed in detail for AM 316L, Ti6Al4V and Alloy 718 in several studies [46,66,67].
- The amount, type and size of precipitates in as-built precipitation hardened alloys like Alloy 718 Ni-based superalloy would largely differ from those in conventionally manufactured parts of the same alloys due to very different thermal history and time scale [62,68]. This can lead to differences in precipitation hardening effects and thus the variations in tensile properties of as-built materials [46,69]. Similarly, the amount and morphology of phases in multi-phase alloys, for example the dimensions of α-laths and β-ribs (β-rods), the volume fraction of α/β phases, and the dimensions and volume fractions of α-colonies and basketweave structure in additively manufactured Ti6Al4V can all influence its flow stress properties [67,70,71]. These microstructural characteristics would be adjusted during subsequent thermal and HIP post-treatments [66,72,73] when the associated parameters (temperature, soaking time and pressure) are carefully selected.

The above distinctive characteristics are generally material-specific and depend on the fabrication technique, process parameters (e.g., scanning strategy, layer deposition thickness, energy density), metal powder properties (e.g., shape and distribution, atomisation method) and protecting gas flow and composition (or vacuum pressure in PBF-EB) and many other factors. Some of these key parameters are explored in Table 1 for PBF and DED methods, two of the most widely used AM metal technologies. A detailed summary of involved parameters can be found elsewhere [15,16,18,45]. Fig. 5 illustrates the relation between the major process parameters in laser-based additive manufacturing method (i.e., PBF-LB and DED-LB) and microstructural characteristics that can potentially influence the machinability of materials with reference to the polar diagram shown in Fig. 2.

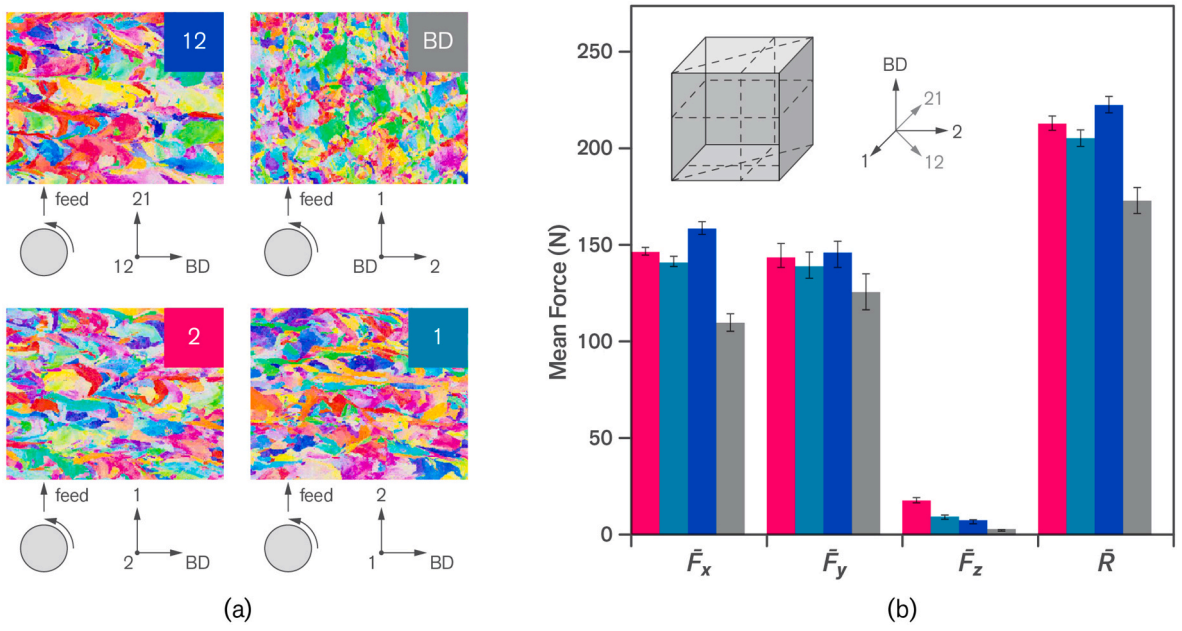

Fig. 3. Exemplary study illustrating the effects of AM material (CoCrMo) anisotropic behaviour on cutting forces during machining process. Sample orientations relative to the milling configuration where cutting action takes place normal to build direction (BD) and directions 1, 2 and 12 (a) and the measured cutting forces for each case (b). Adapted from Ref. [48].

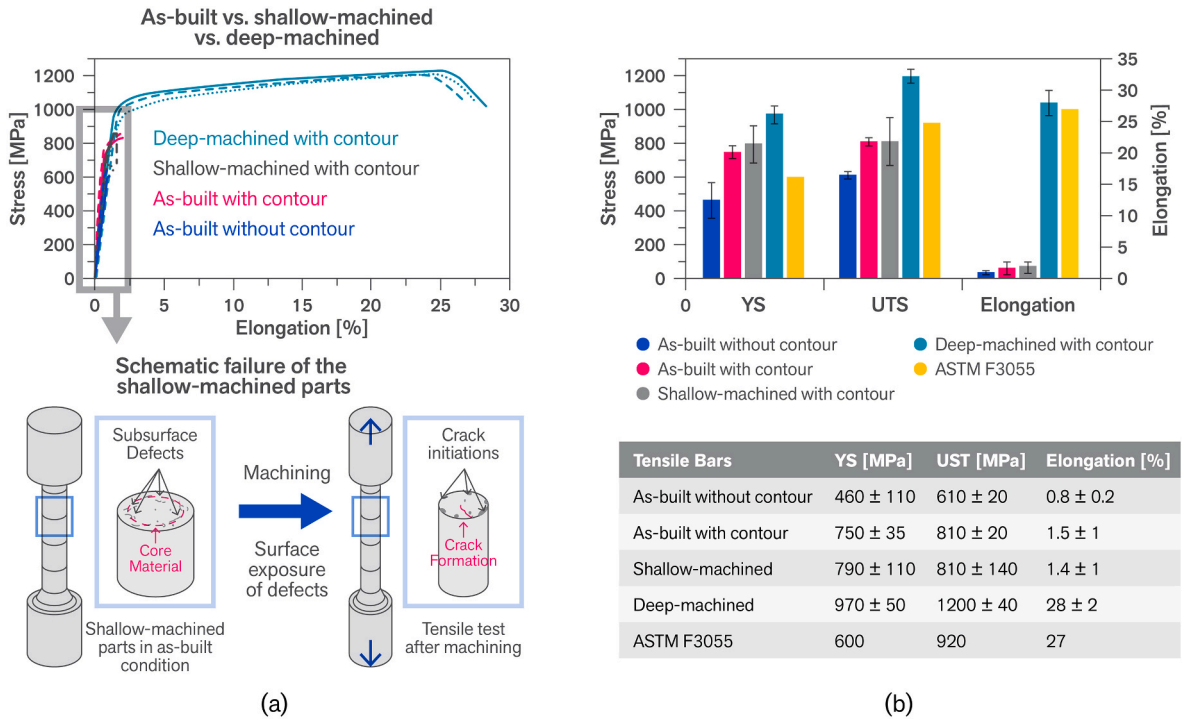

Tensile Bars	YS [MPa]	UST [MPa]	Elongation [%]
As-built without contour	460 ± 110	610 ± 20	0.8 ± 0.2
As-built with contour	750 ± 35	810 ± 20	1.5 ± 1
Shallow-machined	790 ± 110	810 ± 140	1.4 ± 1
Deep-machined	970 ± 50	1200 ± 40	28 ± 2
ASTM F3055	600	920	27

Fig. 4. Process induced superficial defects affecting the tensile properties of as-built and machined PBF-EB/Alloy 718 (a), and comparison of tensile properties of as-built, shallow-machined, and deep-machined parts with the reference values according to ASTM F3055 (b). Adapted from Ref. [54].

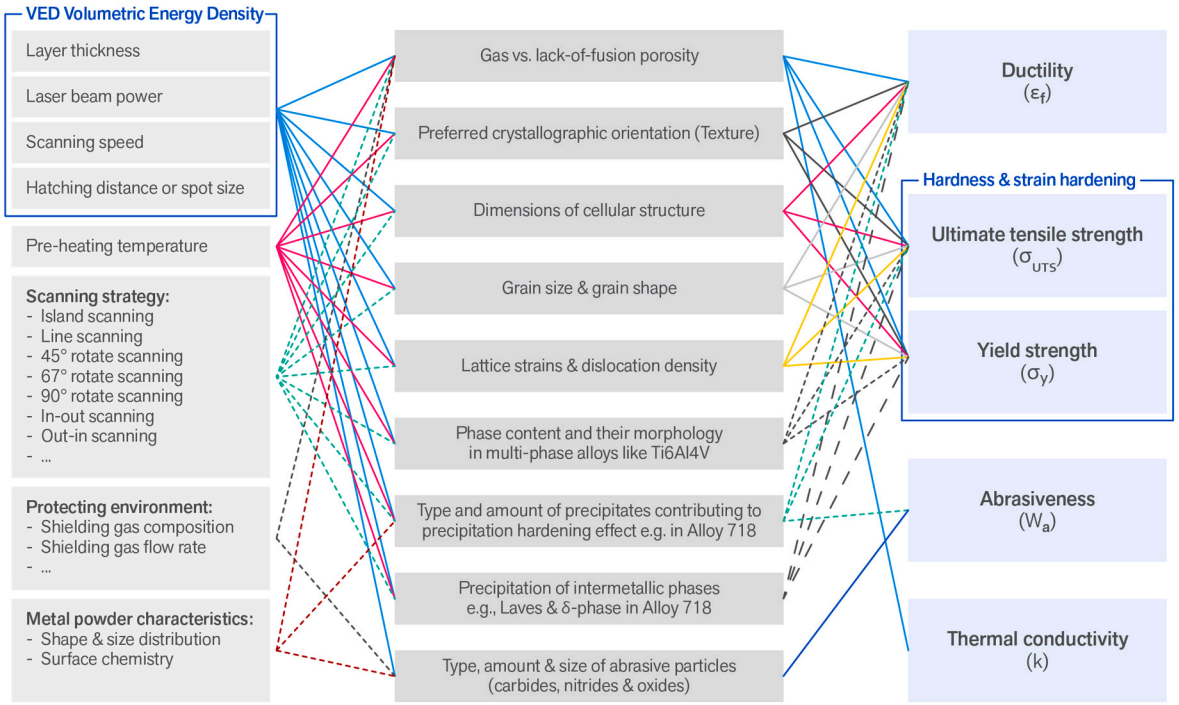

Fig. 5. Relation between some of the key parameters of PBF-LB and DED-LB technologies, the microstructural characteristics of AM materials and their potential influence on properties with large impacts on machinability.

3. Metal cutting processes

Metal cutting processes like turning, (micro-) milling, and drilling are generally needed to set the dimensional tolerances and to generate functional surface in the additively manufactured parts. The design requirements on functionality and performance, e.g., improved fatigue life, wear, and corrosion properties, are tightly connected to surface integrity (e.g., state of residual stresses, roughness, sub-surface deformation and microstructural changes). The impact of metal cutting processes on functional performance will be discussed further in Section 5.

Milling and micro-milling processes are often regarded as the most relevant conventional post-processing method due to their flexibility for

handling complex geometries of different size scales; however, the response of AM materials is also investigated in several studies during turning process. This section summarises the scientific reports on turning and (micro-) milling 316L, Ti6Al4V and Alloy 718 fabricated using different AM technologies, while in part we refer to other materials and processes as well. The emphasis is on the impacts of AM-specific microstructural characteristics on tool wear, cutting forces and surface integrity of machined workpieces. However, the machinability of conventionally manufactured materials (cast or wrought) is regarded as the reference point for comparison and will be discussed first in each case. This will provide a more fundamental understanding of the parameters that can potentially improve (or worsen) the machinability of investigated AM materials.

3.1. 316L stainless steel

Numerous studies have addressed the machinability of conventionally manufactured 316L stainless steels in terms of chip shape and its formation mechanisms [74,75], tool wear [39,74], surface integrity and cutting forces [76,77], using both experimental and computational approaches. Its low thermal conductivity, high ductility and substantial work-hardening during cutting often make machining of this material a challenge. In addition, the non-metallic inclusions (NMIs) are shown to have great impacts on chip formation and tool life when machining this material, as pointed out in Section 2. Bletton et al. [74] observed that tool life and chip formation when machining (turning, drilling and threading) wrought 316L largely depend on the type of NMIs. The attempts to produce NMIs with specific chemical compositions during steelmaking are often referred to as "inclusion engineering", as mentioned earlier in Section 2. For example, Ca-treatment is normally used to modify the properties of NMIs present in steels to improve their machinability. The efforts as such have (at least) a two-fold effect: 1) to reduce the hardness of Al_2O_3 inclusions present in the steels resulting in reduced abrasion wear, and 2) to improve their formability (malleability) to form a protective film on tool surface. The latter effect often improves the lubricity and thus reduces friction (and interface temperature as a result). The oxide inclusions with relatively lower melting points (e.g., anorthite: $CaAl_2Si_2O_8$ with about $T_m = 1400\,^{\circ}C$ compared to Al_2O_3 with about $T_m = 2000\,^{\circ}C$) are found to form a protective transfer layer on the tool surfaces and thus reduce the impact of thermally activated wear mechanisms like dissolution-diffusion. The effect of these NMIs would differ for different tool materials and under different cutting conditions. The temperature and shear stresses on the surface should be sufficiently high to smear out the NMIs and thus form a stable protective film on the surface of the tools, but not too high to break away the excessively softened oxide film from the tool surface [39,74]. In addition, the more ductile and low strength NMIs can deform more easily along the primary shear plane, facilitating the chip breakability. This is because the tips of the elongated NMIs can act as the crack initiation sites and reduce the strain threshold for chip breakability. In view of these observations, additively manufactured 316L stainless steels produced using different technologies would exhibit very different responses during machining. The microstructural characteristics of additively manufactured 316L such as crystallographic texture, grain size and shape, total dislocation density stored in the material, the volume fraction and dimensions of nano-sized oxide inclusions, and the dimensions of cell structure depend largely on the utilised technology, implemented process parameters, metal powder properties, and shielding gas type and flow (or vacuum pressure in PBF-EB) – as also illustrated in Fig. 5 [47,64,66,69,78,79]. The variations in these microstructural characteristics, along with the density of defects, influence the tensile properties like yield and tensile strength, ductility (elongation at fracture) and strain hardening [66] and thus a large scatter can be seen in the reported tensile properties. This scatter in collected data is observed not only when comparing the materials produced using different technologies but also within the domain of a specific AM technology. In addition, the tensile properties may largely differ after a thermal post-treatment depending on the temperature and soaking times (and the applied pressure in case of HIP), as can be seen in Fig. 6.

Besides the mechanical properties, the type, size and distribution of NMIs in additively manufactured 316L depend on process parameters such as VED, shielding gas composition and flow rate (or in case of PBF-EB, the vacuum pressure), and the composition of the metal powder [78,80,81]. The amount, size and distribution of NMIs can influence the machinability of additively manufactured material in different manners. While the uniform distribution of nano-sized oxide inclusions may provide some dispersion hardening effects [66,69,78], and thus increase the mechanical properties like ultimate tensile strength and hardness (see Fig. 7a), the micron-sized NMIs often act as crack initiation sites and lead to reduced fracture strain [82]. On the other hand, the micron-sized hard oxides like Al_2O_3 or SiO_2 can act as abrasive particles and thus influence tool wear, while the softer and more malleable oxides (if present within the material) may form protective transfer layers on the tool surface and thus reduce the rate of thermally activated wear mechanisms. The grain size and morphology, density of dislocations in cellular structure and the material texture are the other important parameters influencing the tensile properties and thus can potentially affect the machinability of AM materials. In particular, the material texture – the effect of which may be quantified using the Taylor or Schmid factor – and grain morphology (density of grain boundaries in specific directions) can result in an anisotropic behaviour in mechanical

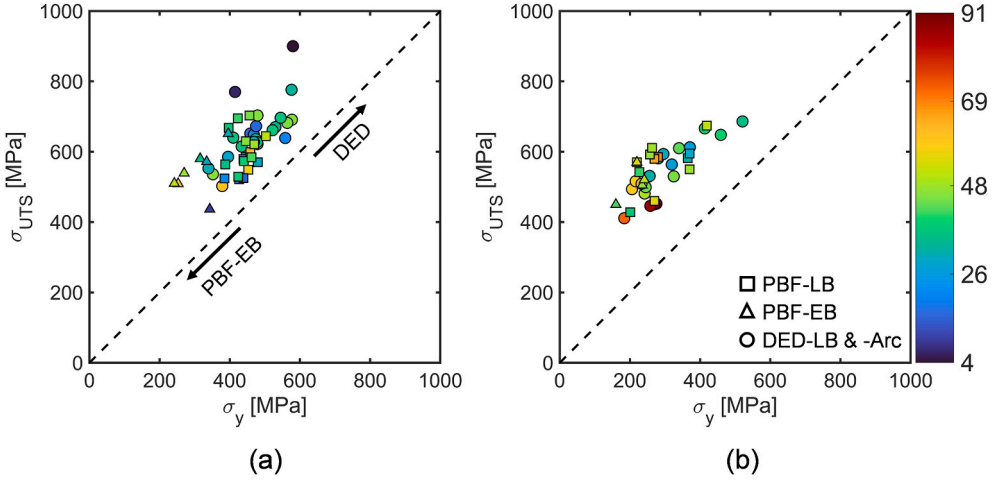

Fig. 6. Variations in the room temperature tensile properties of PBF-LB/, PBF-EB/and DED/316L reported in literature: as-built conditions (a) and post-treated materials (b). Plots include the supplementary data summarised in Tables A.1–A.5. The tensile properties reported for both vertical (longitudinal) and horizontal samples were included here. The colour code (colour bar) shows the reported fracture strains (elongation at fracture) in %. (For interpretation of the references to colour in this figure legend, the reader is referred to the Web version of this article.)

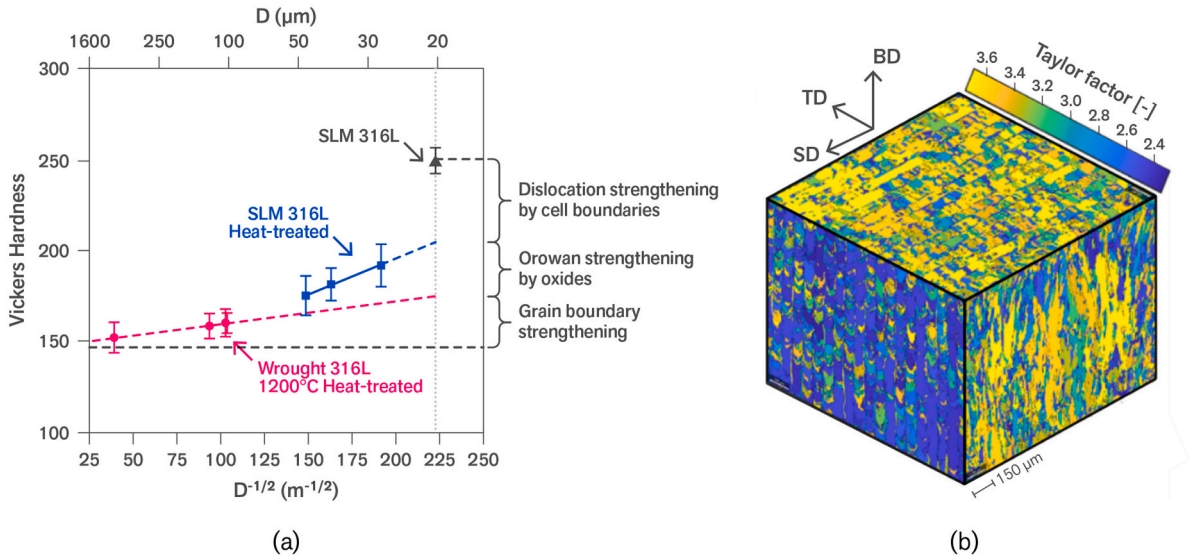

Fig. 7. The cumulative effects of various strengthening mechanisms contributing to the hardness (and thus to the overall tensile properties) of wrought and PBF-LB/316L (a) and calculated Taylor factor on SD-TD, TD-BD, and SD-BD planes under uniaxial loading normal to each plane (b). D is the average grain size, SD: scanning direction, TD: transverse direction, and BD: build direction. Adapted from Refs. [69,83].

properties. For example, Bahshwan et al. [83] attributed the differences in microhardness measurements on planes parallel and perpendicular to the build direction to their different Taylor factors and grain size distributions, as depicted in Fig. 7b. This can in turn lead to an orientation-dependent machinability of additively manufactured materials – as observed when machining other AM alloys [46,48,49]; see for example Fig. 3 in Section 2.

Machinability of additively manufactured 316L is addressed in a few studies. Kaynak and Kitay [84] investigated the surface finish properties of PBF-LB/316L using different methods: finish turning under dry and cold air conditions vs. mass finishing (vibratory finishing, and drag finishing using ceramic abrasives). The authors observed higher surface hardness and lower or comparable roughness (Ra) after finish turning at 40 m/min and 200 m/min compared to the utilised abrasive fine-finishing methods. However, the finish turning led to about 5 μm sub-layer deformation, supposedly with non-structured grains. This severely deformed layer with a nano-sized microstructure is often associated with tensile surface and sub-surface residual stresses and should be avoided because of its detrimental effects on functionality and performance (e.g., fatigue lifetime). Hence, the finish turning process is not recommended for load-carrying applications with high demands on fatigue and corrosion performance. In contrast, surface smoothing in mass finishing is achieved primarily via ploughing and sliding mechanisms, with a minimal fraction of cutting, resulting in high compressive residual stresses (e.g., −1000 MPa). Mass-finishing processes are discussed in more detail in Section 4.2. Alexeev et al. [85] studied the influence of build direction on cutting forces when milling PBF-LB/316L under different cutting conditions. The authors observed up to 11.3% higher cutting forces when machining the sample fabricated in the horizontal direction compared to those that were manufactured vertically. This observation was attributed to the different grain morphologies in vertically and horizontally manufactured samples, and thus different strain hardening behaviour of the material, depending on whether the plane of cut is parallel or perpendicular to build direction. As mentioned earlier, however, the material texture would play an additional role in the orientation-dependency of cutting forces observed in this investigation; see also Fig. 3 in Section 2. Gong and Li [86] studied the machinability of DED-LB/316L in terms of tool wear and surface finish. Relatively good surface finish was reported (Sa<1.6 μm); however, pits (or bumps) and burrs were observed on the machined surfaces and on the wall edges. The authors also reported better surface finish when using down-milling strategy and chipping and adhesion as the dominant wear mode and mechanism.

To date, no detailed comparative investigation on the potential differences in the machinability of additively and conventionally manufactured materials is available in literature. However, it is important to stress here again that the machinability of wrought 316L is also to a very large extent dependent on type, size and distribution of NMIs. Hence, the variability in the machinability of conventional materials can be as high as the variability in machinability of AM materials, although the underlying mechanisms would be different in practice.

3.2. Ti6Al4V titanium alloy

Machinability of cast and wrought Ti6Al4V is investigated in numerous studies. For example, chip formation mechanisms and chip shape [87–89], cutting forces and tool wear modes and mechanisms [90,91] and surface integrity [92] when machining wrought and cast materials using different tool materials under a wide range of cutting conditions are examined and reviewed [93] in previous studies. Within the practical range of cutting conditions, saw-tooth chip formation is often observed during machining Ti6Al4V, which is normally characterised by crack initiation and propagation from the outer surface of the chip. However, thermally activated microstructural softening within the thin shear bands also plays a role and facilitates the propagation of cracks. A number of studies showed that chip formation mechanisms and thus chip shape when machining Ti6Al4V largely depend on the material microstructure. For instance, a clear transition from continuous to saw-tooth chip formation was reported when machining the small colony-sized cast Ti6Al4V with increasing feed rates [87]. On the other hand, machining of large colony-sized cast material showed both chip formation behaviours simultaneously for all attempted feed rates. This observation was attributed to anisotropic behaviour of the material with the coarse microstructure [87]. The material texture and strain hardening are also shown to have large impacts on chip formation when machining Ti6Al4V. For example, Palaniappan et al. [94] have recently reported a gradual transition from saw-tooth to continuous chip formation when machining Ti6Al4V with increasing deformation hardening. This transitional behaviour was believed to be largely due to the weakening of transverse texture and fading basal texture when increasing the deformation hardening during cold rolling (where the thickness of test pieces was reduced up to 45%). However, such severe

deformations should, in principle, result in a large increase in density of dislocations within the cold-rolled test pieces. A large density of dislocations can also influence the onset of crack initiation and the rate with which the cracks propagate, as mentioned in Section 2. The potential effects of this phenomenon on chip formation were not investigated and not sufficiently discussed by the authors. Nevertheless, some degree of microstructural dependency has also been observed in cutting forces and tool wear when machining wrought and cast Ti6Al4V. Thermally activated mechanisms such as dissolution-diffusion as well as chemical reaction are believed to be dominant during machining this material [91, 95]. A wide range of microstructure can be obtained in this material during the forming and casting processes and subsequent thermal post-treatments. The microstructure variations lead to a rather broad range of thermo-mechanical properties, which in turn result in variations in the amount of generated heat and thus tool life during machining. Therefore, Ti6Al4V is often heat-treated to obtain a relatively soft and thus machinable microstructure. Table 2 summarises the recommended heat treatments for machinability improvement of wrought Ti6Al4V [96].

For the same reasons, the state of the material may greatly influence the machinability of additively manufactured Ti6Al4V. A wide range of microstructures can be obtained depending on utilised AM technology and the parameters used during fabrication and subsequent post-treatments [97–102]. This variation in microstructural features significantly influences the induced mechanical properties. Fig. 8 summarises the tensile properties of PBF-LB/, PBF-EB/and DED/Ti6Al4V reported in literature in as-built conditions and after post-treatments.

As evident, the PBF-EB/Ti6Al4V has generally lower yield and tensile strengths than those of PBF-LB/Ti6Al4V. DED generally shows intermediate tensile properties as compared with the other two manufacturing methods. On the other hand, the fracture strain (elongation at failure) is generally highest for PBF-EB/Ti6Al4V and lowest for PBF-LB/Ti6Al4V. The lower ductility/fracture strain of PBF-LB/Ti6Al4V is generally associated with its fine microstructure comprising of α′-martensite or mixed α/α′ with a large density of dislocations [103], provided that the density of defects is sufficiently small to play a major role in elongation at fracture. Following successive heat treatment, ductility generally improved at the expense of strength. This improvement seems to be more pronounced in HIPed samples as it results in 1) defect closure, and 2) microstructure modification: transformation of the non-equilibrium acicular α′-martensite into a near-equilibrium lamellar distribution of α/β phases. Nevertheless, these variations may give an indication of a significantly different machinability of additively manufactured Ti6Al4V, not only when different AM technologies are utilised for fabrication of the components, but also when a same AM technology is utilised but with different process parameters. It may be worth mentioning here that the collected tensile properties assessed in both transverse (horizontal) and longitudinal (vertical) directions indicate anisotropic behaviour [16]. However, no specific trend could be observed, for example, the tensile properties always being higher along the build direction than those of transverse direction, as also noted by Herzog et al. [16]. In either case, the anisotropic behaviour can manifest itself in intricate manners during machining and can thus influence tool wear, surface integrity, cutting forces and chip formation. These should be taken into account when comparing the results of different studies on machinability of Ti6Al4V in turning, (micro-) milling and drilling.

It is also important to emphasise here again that higher yield and ultimate tensile strengths (neither the higher hardness) are not necessarily an indication of poorer machinability of a given material variation. The work-hardening prior to fracture and the ductility of the materials (elongation at fracture) would in some cases give a better indication of the machinability of materials, as both are included in polar diagrams shown in Fig. 2. Yet the most reliable machinability indicator associated with the tensile properties of a given alloy is perhaps the amount of plastic work estimated using Eq. (1) (see Section 2), provided that the flow stress properties are available at ranges of temperature and strain rates encountered in cutting. In principle, a larger amount of plastic work is equivalent to higher cutting forces, higher heat generation and shorter tool life during the cutting process. In the absence of high temperature flow stress properties, one may use the room temperature data as a first approximation. The tensile properties presented in Fig. 8a would suggest higher cutting forces and shorter tool life when machining PBF-EB/Ti6–Al–4V (with lower tensile strengths but often with a significantly higher ductility) as compared with PBF-LB/and DED-LB/Ti6–Al–4V (with higher tensile strengths but often with a significantly lower ductility). Obviously, the microstructural characteristics and thus tensile properties change after thermal post-treatments (see Fig. 8b), and thus different behaviours would be observed during machining processes.

Table 2
Recommended heat treatments for machinability improvement of Ti6Al4V and typical tensile properties resulting after different thermal cycles [96].

Heat treatment	Thermal cycle and typical resulting tensile properties
Mill annealing	Holding the material around 730 °C in the lower range of the α/β region for 4 h followed by furnace cooling to room temperature. This recipe leads to the following typical tensile properties: σ_y = 945 MPa, σ_{UTS} = 1069 MPa, ε_f = 10%
Duplex annealing	Holding the material at 955 °C for 10 min, followed by air cooling to room temperature. The material is then hold at 675 °C for 4 h, and air cooled to room temperature. This recipe leads to the following typical tensile properties: σ_y = 917 MPa, σ_{UTS} = 965 MPa, ε_f = 18%
Solutionising & ageing	Holding the material at 955 °C for 10 min, followed by water quenching to room temperature, then aged for 4 h at a temperature between 540 °C and 675 °C. It is then air cooled to 25 °C. This recipe leads to the following typical tensile properties: σ_y = 1103 MPa, σ_{UTS} = 1151 MPa, ε_f = 13%

3.2.1. Turning

Machinability of additively manufactured Ti6Al4V in terms of surface integrity, cutting forces and tool wear is investigated in several studies. Shunmugavel et al. [104] conducted a comparative investigation on the machinability of wrought and PBF-LB/Ti6Al4V. The investigated AM material had higher yield and tensile strengths and hardness than those of wrought material; however, its ductility was almost one-third that of wrought material. Based on the provided micrographs, it seems the microstructure of additively manufactured material consisted of a mixture of acicular α/α', typically reported for PBF-LB/Ti6Al4V in as-built condition [100,103]. Higher cutting forces were reported when machining AM material, whereas the surface finish (Ra) was generally better than that of wrought material. The lower ductility of AM material was believed to be the reason for better surface finish properties. Sartori et al. [60] compared the machinability of wrought, PBF-LB/and PBF-EB/Ti6Al4V under dry and LN_2-cryogenic conditions. As mentioned earlier, the wear mechanisms in machining Ti6Al4V are dominantly thermally activated, and thus several studies demonstrated the potential of cryogenic cooling for prolonging the tool life by reducing the cutting temperature during cutting. Nevertheless, the highest crater wear depth was observed when machining the as-built PBF-LB/Ti6Al4V with the markedly higher yield and tensile strengths and hardness but with a lower ductility than those of wrought, heat-treated PBF-LB/and PBF-EB/Ti6Al4V. The authors also measured the thermal conductivity of the materials at various temperatures and reported the lowest and highest thermal conductivities for PBF-LB/and PBF-EB/Ti6Al4V, respectively. A combination of these thermo-mechanical properties led to a higher cutting temperature when machining PBF-LB and thus higher crater wear depths were observed under both dry and cryogenic conditions. The application of cryogenic cooling, however, reduced the depth of crater wear in all cases. Similar observations are reported in another investigation, comparing tool wear when machining PBF-EB/Ti6Al4Vand wrought alloys using LN_2-cryogenic cooling [105]. Besides tool life extension, cryogenic cooling was

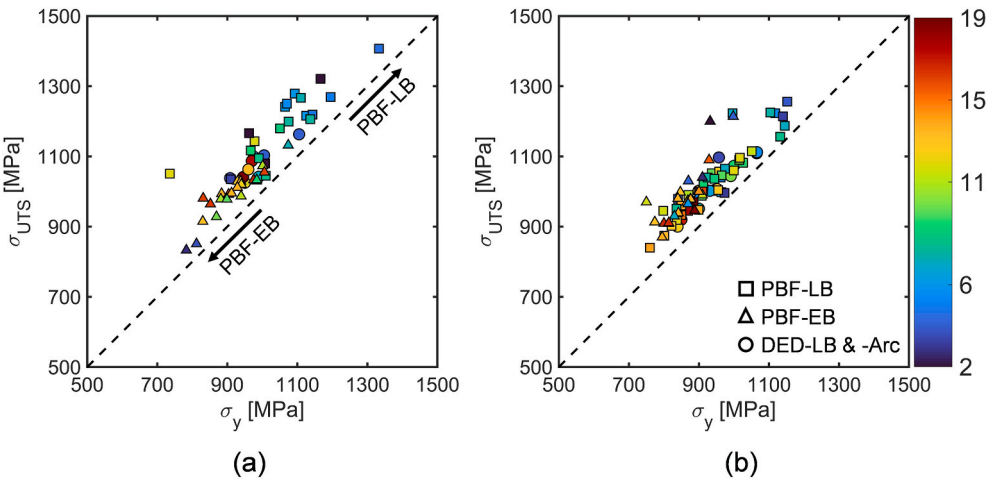

Fig. 8. Variations in the room temperature tensile properties of PBF-LB/, PBF-EB/and DED/Ti6Al4V reported in literature: as-built conditions (a) and post-treated materials (b). Plots include the supplementary data summarised in Tables A.6–A.10. The tensile properties reported for both vertical (longitudinal) and horizontal samples were included here. The colour code (colour bar) shows the reported fracture strains (elongation at fracture) in %. (For interpretation of the references to colour in this figure legend, the reader is referred to the Web version of this article.)

generally found to improve the surface integrity in terms of residual stresses and surface finish properties when machining additively manufactured materials [105,106]. For example, higher (and deeper) compressive residual stresses were achieved on (and beneath) the machined surfaces when machining as-built and heat-treated PBF-LB/Ti6Al4V using cryogenic cooling. The surface finish response was rather complex and was dependent on the feed rate and cutting speed. Distinct improvements in surface finish (Ra) were observed for cryogenically-machined PBF-EB/Ti6Al4V at high feed rates because of a better control on tool wear evolution; however, the machined surfaces in general exhibited more waviness and were often characterised by jagged feed marks, as shown in Fig. 9. Bordin et al. [107] reported higher evolution rates of flank and crater wear when machining PBF-EB/Ti6Al4V as compared with those of wrought material under wet conditions. This was in contradiction to the results reported by Sartori et al. [60], who observed the lower crater depth when machining PBF-EB/Ti6Al4V as compared to other materials under both dry and cryogenic conditions. In these studies, machining tests were conducted using TiAlN PVD coated tools with a similar geometry, but the lead angle was different as the tools were mounted on different tool holders. This contradiction perhaps indicates the importance of microstructure variation and the marked influence it may have on the tribological conditions influencing tool wear evolution when machining additively manufactured Ti6Al4V, as discussed earlier in this section.

Mallipeddi et al. [108] studied the influence of printing strategies and HIP post-treatment on the surface integrity of machined PBF-EB/Ti6Al4V. The aim was to determine the machining allowance, depending on the melting strategy (contour setting) and the subsequent HIP post-treatment. These two have a large impact on surface finish properties as well as the density of subsurface defects in as-built components, but they also largely influence the overall manufacturing time and cost. The material with no contouring resulted in the roughest

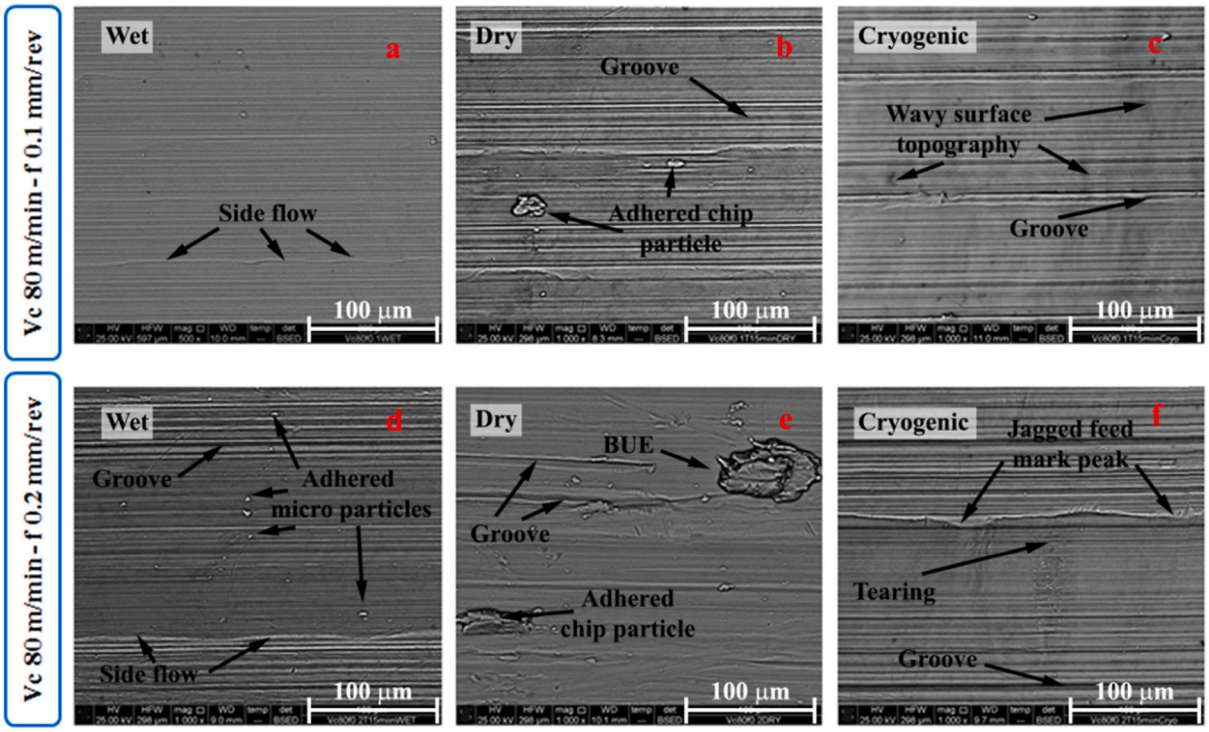

Fig. 9. Finish turning induced surface defects observed when machining PBF-EB/Ti6Al4V at two different feed rates using wet, dry, and cryogenic cooling strategies. This figure presents general observations on machined surfaces after 8 min of cut [105].

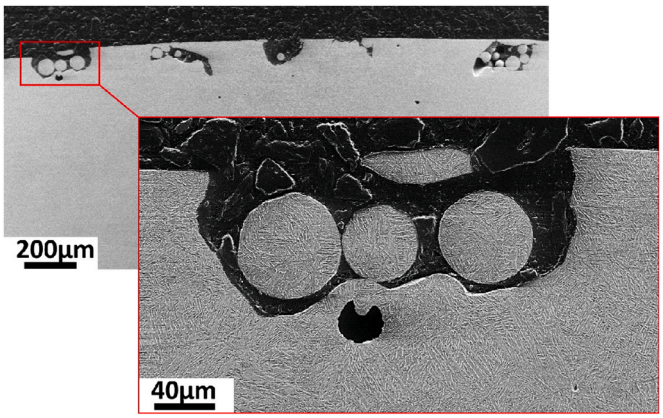

Fig. 10. Surface and subsurface defects were still observed after removing 0.5 mm from the surface of the PBF-EB/Ti6Al4V sample, where neither contouring nor HIP post-treatment was used [108].

surface as compared with three- and five-layer contouring strategies; however, printing without contouring gave up to 20% shorter build-cycle time. To obtain acceptable surface finish properties (Sa, Sv and S10z) at least 1 mm should be removed from the print surface for the sample with no contour setting, as shown in Fig. 10. As is evident, 0.5 mm allowance was not sufficient to obtain a defect-free surface after machining. However, the machining allowance for the no-contour sample could be reduced by half (0.5 mm) if the material was HIPed before machining. This is because HIP post-treatment with optimised settings can effectively reduce the density of surface and subsurface defects. The machining allowance was reduced to 0.25 mm when three- and five-layer contour strategies were used, regardless of whether HIP post-treatment was utilised or not. In other words, HIP was found to have no significant impact on pore closure of the sample. The authors reported compressive residual stresses on the machined surfaces in all samples, except when machining a three-layer contoured sample after the third cutting pass (i.e., 1 mm depth). The authors claimed that this is because 1 mm machining depth coincided with the depth of heat affect zone, and thus the tensile residual stresses were generated because of some sort of microstructural inhomogeneity present at this depth.

Machinability of DED-LB/Ti6Al4V has also been studied in as-built condition and after thermal post-treatment by Oyelola et al. [109]. This investigation showed a marked impact of microstructural characteristics resulted from two different annealing post-treatments on sub-layer deformation depth, cutting forces and surface finish properties. To remove the rough skin, at least 0.25 mm machining depth should be used for cleaning while an additional 0.2 mm of cutting depth may be needed to achieve a defect-free surface after machining. Thus, an overall machining depth of about 0.45 mm was recommended for machining the DED sample. This recommended machining allowance is almost half the machining allowance reported by Mallipeddi et al. [108] to achieve acceptable surface finish properties (at least 1 mm to be removed for untreated sample with no contour setting; see Fig. 10). This machining allowance seems to be rather small, since parts produced by DED-LB and PBF-EB processes often show comparable surface and sub-surface properties in as-built condition (e.g., compare the roughness (Ra) of as-built surfaces presented in Table 1). Nevertheless, the authors generally reported better surface finish properties (Ra) for the heat-treated DED samples after machining at all cutting conditions. Lower cutting forces were also observed when machining heat-treated DED. The thermal post-treatments below β-transus temperature led to slightly coarser microstructure (i.e., slightly larger width of α-lath) than that of as-built material, whereas heat treatment above β-transus temperature resulted in significantly larger width of α-lath and fewer colonies due to β-grain growth. These changes in the microstructure alter the mechanical properties and thus the shear resistance during the cutting process. The higher cutting forces induced larger sub-layer deformation in as-built material (up to 17 µm beneath the surface) compared to that of heat-treated samples (only within 5 µm below the surface) at low cutting speed (50 m/min). However, at higher cutting speeds (100–150 m/min), similar deformation depths were observed for both as-built and heat-treated AM materials.

3.2.2. *Milling and micro-milling*

Several studies were dedicated to assessing the machinability of additively manufactured materials during the milling process. The major emphasis was mainly on cutting forces and surface integrity; however, there were a few reports on tool wear behaviour.

Veiga et al. [110] studied the cutting forces, torque and surface finish when milling Ti6Al4V fabricated using a wire arc additive manufacturing method. The authors analysed the chemical composition, microstructure, hardness, and tensile properties of additively manufactured materials prior to the machining tests. The evaluated key elements, including Al, V, Fe, C and O, were within the range specified in AMS4928 standard for forged material certified for aeronautic applications. The typical columnar growth of β-grains along the build direction was reported; however, no additional information about other key microstructural features, e.g., volume fraction, distribution and morphology of α-phase and/or α′-martensite, were provided. Yet precipitation of α-phase at β-grain boundaries was evident in the micrographs, similar to those commonly reported in PBF-EB/Ti6Al4V microstructure [16,111]. The tensile properties, including yield strength, ultimate tensile strength and elongation at fracture, were all above the minimum requirements specified in AMS4928 standard, both in vertical and horizontal directions (i.e., parallel and perpendicular to build direction). Moreover, no significant gradient was observed in measured hardness values along the build direction. The measured torques along the build direction also showed no significant differences; however, the down-milling strategy led to slightly lower average torques than those measured for up-milling in almost all attempted table feeds, however, the difference was not statistically large due to large variations observed in measured values. A better surface quality (Ra) was reported during up-milling. The authors characterised this as the vibration-induced phenomenon caused by the slender dimensions of the manufactured workpiece. The Ra values reduced gradually from slightly above 1.5 µm–1 µm as the tool reached closer to the table. This was also attributed to the reduced vibrations with shorter distance from the clamp, although microstructure-induced variations in mechanical properties (e.g., ductility) along the build direction could also play a role. Woo et al. [112] studied the Laser Assisted Milling (LAM) of DED-LB/Ti6Al4V. Initially, the authors made some efforts to optimise AM parameters (laser power, scanning strategy, type of inert gas etc.) to obtain sound and representative workpieces. FE simulations were used to determine the maximum heat penetration depth during laser exposure. The results were then used to identify the depth beneath the surface that is subjected to sufficiently high temperatures to obtain desired thermal softening effects. The machining depth was selected accordingly to remove the heat affected zone ahead of the cutting edge. LAM resulted in 40% lower cutting forces and 30% better roughness values (Ra) than those measured when machining without laser preheating. The influence of microstructural characteristics on the machinability of Ti6Al4V manufactured using different AM technologies has been explored in several studies. Milton et al. [113] studied the machinability of PBF-LB/and PBF-EB/Ti6Al4V. The authors observed up to 50% higher resultant cutting forces when machining PBF-EB/Ti6Al4V than those of PBF-LB/Ti6Al4V, depending on the feed rate (f_z ranging between 0.05 and 0.2 mm/tooth, while cutting speed and axial and radial depth of cut kept constant). The difference was highest when machining at larger feed rates, regardless of whether the material was in as-built condition or HIP post-treated. However, about 10–12% lower resultant forces were measured respectively for the PBF-LB and PBF-EB materials after HIP, indicating that the microstructural properties and mechanical

properties are altered after thermal post-treatment. The grain boundary α-layer, Widmanstätten α-colonies, and intergranular α-lath structure were reported in PBF-EB fabricated material, whereas the microstructure of PBF-LB consisted of a uniform distribution of acicular α'/α with relatively fewer and thinner α-layers decorating the boundaries of prior β-grains elongated in the build direction. The authors reported no significant difference in measured cutting forces on surfaces perpendicular and parallel to the build directions when machining PBF-LB test pieces. However, the measured forces when machining PBF-EB test pieces depended on whether the plane of cut was parallel or perpendicular to the build direction. Up to 40% difference was reported between the measured resultant forces, indicating a rather significant influence of material microstructure on shear deformation during the cutting process. This was attributed to higher work-hardening in the investigated PBF-EB/Ti6Al4V material caused by thicker, more frequently observed α-grain boundary layers in this material as well as the presence of Widmanstätten α-colonies and intergranular α-lath structure. Milton et al. [114,115] also studied the machinability of PBF-EB/Ti6Al4V and PBF-LB/Ti6Al4V compared to that of wrought material (as the reference material) in two separate studies. Higher cutting forces and temperatures were reported when machining PBF-EB material compared to those measured when machining the wrought material, resulting in 50% shorter tool life when machining PBF-EB/Ti6Al4V under similar cutting conditions. Similarly, 22% higher axial forces were measured (on average) when machining PBF-LB/Ti6Al4V as compared with that of wrought material. In both studies, higher work-hardening behaviour of additively manufactured materials was believed to be the reason for the higher cutting forces as compared to the reference material. Although the authors did not present flow stress data to support their claims, they argued that the microstructure of the additively manufactured materials (e.g., finer distributions of Widmanstätten α-colonies, widths of intergranular α-lath, and widths of α′-laths) would lead to greater work-hardening behaviour during shear deformation in cutting. Higher wear rate and larger cutting forces were also reported by Al-Rubaie et al. [116] when machining PBF-LB/Ti6Al4V (402 ± 6.22 HV0.5), as compared to those of conventionally manufactured material (327 ± 8.67 HV0.5). The cutting forces were about 50% lower when machining the wrought material, while the surface finish properties (Ra and Rt) were generally better when machining PBF-LB/Ti6Al4V. Interestingly, only a slightly higher flank wear rate was observed when machining PBF-LB/Ti6Al4V, despite about 23% higher hardness. No significant difference was observed in terms of chip shapes. Overall, the authors concluded that a similar range of cutting conditions and tool materials can be used for machining wrought and PBF-LB additively manufactured Ti6Al4V.

Micro-machining of additively manufactured Ti6Al4V has been researched in several studies since this process is of great interest in medical applications. Lizzul et al. [50] studied the influence of anisotropic behaviour on tool wear during micro-milling PBF-LB/Ti6Al4V test pieces manufactured at four different orientations. Initially, all samples were heat-treated at 950 °C/30 min under controlled cooling and heating rates, resulting in a lamellar α/β microstructure. The machining tests were done under MQL condition using vegetable oils on the surfaces with 0°, 36°, 72° and 90° angles with respect to the build plate. Up to 40% difference in tool wear widths was noted when machining samples fabricated in different build orientations. The authors observed that columnar β-gains always grew parallel to the build-direction, independent of build orientation angles. However, the widths of columnar β-gains and α-lamellas after heat treatment depended on build orientations. A weak correlation was observed between the investigated microstructural characteristics and micro-hardness values; however, no clear correlation between tool wear rate and hardness was noted. Interestingly, the lowest and highest wear rates were reported for the samples with 0° and 90° orientations, with only a slight difference in measured micro-hardness values (372 ± 20 and 376 ± 22 HV0.1 for 0° and 90° samples, respectively). Other comparative investigation on machinability of wrought, DED-LB/, PBF-EB, and PBF-LB/Ti6Al4V showed that higher hardness of AM material does not necessarily lead to shorter tool life or higher cutting forces in micro-milling. For example, de Oliveira Campos et al. [117] observed about 9% lower cutting forces (on average) when machining PBF-LB/Ti6Al4V compared to that of wrought material, despite its ~16% higher hardness. Moreover, lower wear rates, lower burr formation sensitivity, and better surface finish (Ra) were reported in this investigation when machining PBF-LB material. The authors attributed the improved machinability of additively manufactured material to its relatively lower ductility and finer microstructure. Hojati et al. [118] reported a marked shift in the machinability of PBF-EB/Ti6Al4V at different ranges of uncut chip thickness (h_e). Whereas the cutting forces were about 10–15% lower when machining PBF-EB material at low uncut chip thicknesses ($h_e < 7.4$ μm), similar cutting forces were observed when machining this material compared to the wrought (extruded) material. The surface roughness was generally better when machining PBF-EB material, whereas burr formation showed a rather complex behaviour. A different burr formation response was observed depending on whether micro-milling is performed directly on the as-built surfaces or carried out after an initial clean cut, removing first the AM-induced surface defects. The burr formation was lower when machining as-built surfaces of PBF-EB material compared to that of wrought material. However, after removing the surface defects and irregularities, the burr formation when machining PBF-EB material became worse than that of wrought material. In general, the authors reported smoother edges (lower burr formation) with increasing uncut chip thickness for both materials. Conversely, Bonaiti et al. [119] observed higher burr formation than that of wrought material regardless of the uncut chip thickness (feed per tooth and axial depth of cut) when machining DED-LB/Ti6Al4V. In line with other studies, the surface finish (Ra) was better when machining additively manufactured material. However, in line with other investigations explored above, the cutting forces were lower when machining DED-LB materials despite the higher hardness compared to that of wrought material. These observations imply that material hardness is not the only parameter influencing tool wear, cutting forces and burr formation in micro-machining. In particular, microstructure induced "size-effect" and thus local micro-variations in material properties seem to be dominant in micro-machining. These micro-variations would not necessarily be reflected in simple micro-hardness tests. Khaliq et al. [120] investigated the micro-milling of PBF-LB/Ti6Al4V using a wide range of rotational speeds (ranging between 15000-35000 RPM) and table feeds (ranging between 30 and 90 mm/min) under both dry and MQL conditions. The authors claimed that the material grain size had a large impact on burr formation, surface finish and tool wear during micro-milling. Up to 28% improvement in tool flank wear was observed using MQL cooling, depending on the cutting speed and feed. Moreover, better responses were observed in terms of surface roughness when using MQL cooling; however, machining under dry condition led to reduced burr formation and higher compressive surface residual stresses.

3.3. Alloy 718

Machinability of conventionally manufactured Alloy 718 is researched in numerous studies. For example, chip formation mechanisms and chip shape [121,122], cutting forces and tool wear modes and mechanisms [34] and surface integrity [121,123] when machining wrought materials using different tool materials at a wide range of cutting conditions are well examined in previous studies. The chip formation mechanism and thus chip shape alter with cutting conditions (cutting speed and feed rate) and the material microstructure, e.g., grain size and amount of γ′ and γ'' precipitates (i.e., solutionised vs. solutionised + aged). Xu et al. [121] and Razanica et al. [124] observed a transition from continuous to serrated chip formation with increased cutting speed. This transition seems to occur at temperatures above 60 m/min when orthogonal cutting with 0.1 mm feed. The serrated chip

formation is generally associated with crack initiation and propagation facilitated by microstructural softening within the shear-localised zone at elevated temperatures [124,125]. However, serrated chip formation is also reported when machining Alloy 718 at cutting speeds below 60 m/min [126,127], indicating the important role of microstructural characteristics influencing the chip formation and chip shape when machining this material. The microstructural dependency has also been observed in cutting forces and tool wear when machining conventionally manufactured Alloy 718. For example, Hagberg and Malm [126] reported a marked difference in measured forces when machining the materials with small and large average grain sizes (~16 and ~127 μm, respectively). Olovsjö et al. [127] observed a significant increase in notch wear evolution on uncoated cemented carbide tools when machining the material with a larger average grain size. Interestingly, the variation in grain size (from ~16 to ~127 μm) had a significantly larger impact on notch wear evolution than that of heat treatment (solutionised vs. solutionised and aged). On the other hand, the average grain size had a minor influence on the rate of flank wear evolution. Nevertheless, both thermally- and mechanically-induced wear mechanisms such as dissolution-diffusion, oxidation, chemical reaction, adhesion and abrasion may play key roles [34,128,129]. Hence, those microstructural variations [25] that influence the tribological conditions on the tool surfaces (e.g., the distribution of temperature and stress) can, in principle, alter the rate of tool wear evolution when machining Alloy 718, depending on the tool material, range of cutting conditions and cooling-lubrication strategy. In addition, the variation in size and amount (volume fraction) of abrasive MC carbides and Ti-rich nitrides present in wrought and cast materials was shown to have large impacts on the tool wear rate, for example, when machining Alloy 718 using coated and uncoated cemented carbides [34,130].

For the same reasons, machinability of additively manufactured Alloy 718 would largely depend on the microstructure of the material in as-built condition and after subsequent thermal post-treatments. The microstructural characteristics like the size and amount (volume fraction) of γ′ and γ′′ precipitates, grain size and shape distributions, density of dislocations as well as the density of defects (e.g., porosity and lack-of-fusion) influence the mechanical properties [18,46,68,131]. The variations in these microstructural characteristics result in the large scatter in tensile properties as shown in Fig. 11. Hence, a large variation in machinability of the additively manufactured Alloy 718 would be observed. For example, higher cutting temperatures (and contact stresses) would be expected for an AM material with high tensile strength and ductility, as inferred from Eq. (1) (see Section 2), resulting in higher wear rates during machining.

However, no clear distinction between the machinability of Alloy 718 fabricated using different technologies can be deduced from the data presented in Fig. 11, as the tensile properties of PBF-LB/, PBF-EB/, DED-LB/and DED-Arc/Alloy 718 largely overlap. Besides, although the tensile strengths of as-built PBF-EB/Alloy 718 are in some cases larger than those of PBF-LB/Alloy 718, their ductility seems to be lower or within a similar range. This makes it difficult to make a general statement on the machinability of additively manufactured Alloy 718 based solely on its tensile properties. Besides, the AM Alloy 718 would generally contain Al-rich oxide inclusions, MC carbides and Ti-rich nitrides [46]. The variations in the amount and size of these hard particles can largely influence the rate of tool wear when machining AM Alloy 718. Hence, the relative impacts of the thermally- and mechanically-induced tool wear mechanisms differ depending on the tensile properties of additively manufactured material on the one hand, and the amount, size and type of abrasive particles present within the material on the other hand. In addition, the variations in the grain size and morphology as well as the crystallographic texture along the build and transverse directions would lead to directionality of machinability, as discussed in Section 2. Nevertheless, the machinability of additively manufactured Alloy 718 (in terms of tool life) should, in principle, worsen after solutionising and ageing treatment, as their tensile properties generally level up. This is evident from the data presented in Fig. 11, particularly for PBF-LB/Alloy 718.

3.3.1. *Turning*

Tool life, cutting forces and surface integrity of additively manufactured Alloy 718 during finish turning are investigated in several studies. Kaynak and Tascioglu [132] investigated the influence of feed rate and cooling condition (dry vs. cold air) on surface and sub-surface properties when turning PBF-LB/Alloy 718. The cutting speed and depth of cut were kept constant in this investigation. The authors reported surface roughness (Ra) ranging from 0.4 to 2 μm, depending on the feed rate and cooling condition. Up to 16% increase is observed in microhardness measured close to the machined surfaces as compared with that of the bulk material. Higher feed rates induced larger surface deformations and thus higher microhardness values were obtained with increasing feed rate. In a more recent investigation, Kaynak and Tascioglu [133] compared the influence of different post-processing/finishing operations including finish turning under dry and cold air conditions, drag finishing and vibratory finishing on surface and sub-surface properties of PBF-LB/Alloy 718. In order to obtain satisfactory surface finish properties, i.e., smooth and defect-free surfaces, the as-built surface layer with a large density of defects must be removed. The thickness of this layer varied between 80 and 130 μm. The lowest surface roughness was obtained using finish turning (Vc: 60 m/min, f: 0.12 mm/rev, and ap: 0.4 mm), followed by vibratory and drag finishing processes. The finish turning process led to the largest

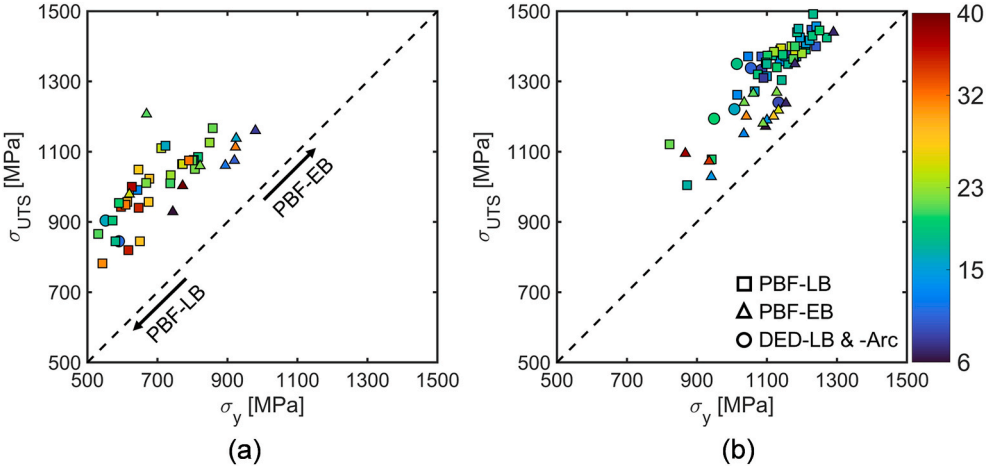

Fig. 11. Variations in the room temperature tensile properties of PBF-LB/, PBF-EB/and DED/Alloy 718 reported in literature: as-built conditions (a) and post-treated materials (b). Plots include the supplementary data summarised in Tables A.11–A.15. The tensile properties reported for both vertical (longitudinal) and horizontal samples were included here. The colour code (colour bar) shows the reported fracture strains (elongation at fracture) in %. (For interpretation of the references to colour in this figure legend, the reader is referred to the Web version of this article.)

surface and sub-surface deformations as compared with the other methods. Machinability of DED-LB/Alloy 718 is also investigated in a few studies. Chen et al. [134] investigated the tool wear evolution, cutting forces and chip formation when machining Alloy 718 deposited on 304 stainless steel bars (laser cladded), and the results were compared with the wrought material. The cladded and wrought materials both underwent a similar solutionising and ageing treatment according to AMS 5662 standard. Machining tests were performed using coated and uncoated cemented carbides. In the case of the cladded material, the authors studied the material response during machining surface and sub-surface layers. Whereas the tool wear evolution was almost similar when machining wrought, surface and sub-surface layers of laser cladded Alloy 718 using uncoated cemented carbide, the authors observed a significant difference in tool wear behaviours when machining using coated tools. The highest wear rate was observed when machining wrought material. The lowest wear rate was reported when machining the sub-surface layer of laser cladded Alloy 718 (within a range 0.4–1.0 mm beneath the as-built surface). Interestingly, the machining of the surface layer (up to 0.4 mm below the as-built surface) led to higher tool wear rates as compared to the sub-surface layer. In addition, lower cutting temperature, cutting forces and machining vibrations were reported when machining laser cladded Alloy 718 using coated tools as compared with those of wrought material.

Careri et al. [135] investigated the machinability of DED-LB/Alloy 718. The authors studied the influence of post-processing sequences (e.g., thermal post-treatment followed by machining vs. machining followed by thermal post-treatment) on surface roughness and surface and sub-surface hardness and residual stress. Three different scenarios were investigated: 1) machining the as-built specimens; 2) machining of heat-treated specimens undergoing the full homogenisation, solutionising and double ageing treatments according to AMS 5662 standard; and 3) as-built specimens that were machined first and then double-aged to level up their properties (without homogenisation or solutionising treatments). The authors observed 40–50% lower cutting forces when machining as-built material as compared to those of fully heat-treated material under similar cutting conditions. Hence, machinability of as-built material was better than that of the heat-treated sample. The sub-surface deformation and hardness increased with increasing feed rate and cutting speed. In addition, the best post-processing strategy was to machine the as-built material first, and then perform the double-ageing treatment to level up the tensile properties and to adjust the surface residual stresses induced by machining. This strategy led to compressive residual stresses and low surface roughness (Sa) on machined surfaces in most cases.

Malakizadi et al. [46] compared the machinability of PBF-LB/, PBF-EB/and wrought Alloy 718 in as-built (or as-received) conditions and after standard solutionising and ageing treatment (AMS 5662) when machining using uncoated cemented carbide. The authors made an attempt to explain reasons behind the very different machinability of PBF-LB/and PBF-EB/Alloy 718 based on the underlying deformation mechanisms and tribological conditions on the tool surface. A physics-based (dislocation-based) approach was used to evaluate the influence of different microstructural characteristics on tensile properties of PBF-LB/, PBF-EB/and wrought Alloy 718 in a qualitative manner. The authors reported markedly different microstructural characteristics in terms of 1) grain size distribution, 2) kernel average misorientation (KAM) as an indication of density of GNDs, and 3) preferred crystallographic orientation (texture) in the investigated materials as shown in Fig. 12 for the as-built (or as-received) materials. In addition, the authors argued that the PBF-LB/Alloy 718 should contain limited amount of γ′ and γ′′ precipitates as compared to PBF-EB/Alloy 718. This is because the material is subjected to relatively short thermal cycles during PBF-LB process. Hence, the authors claimed that the tensile properties of as-built PBF-LB/Alloy 718 would perhaps depend

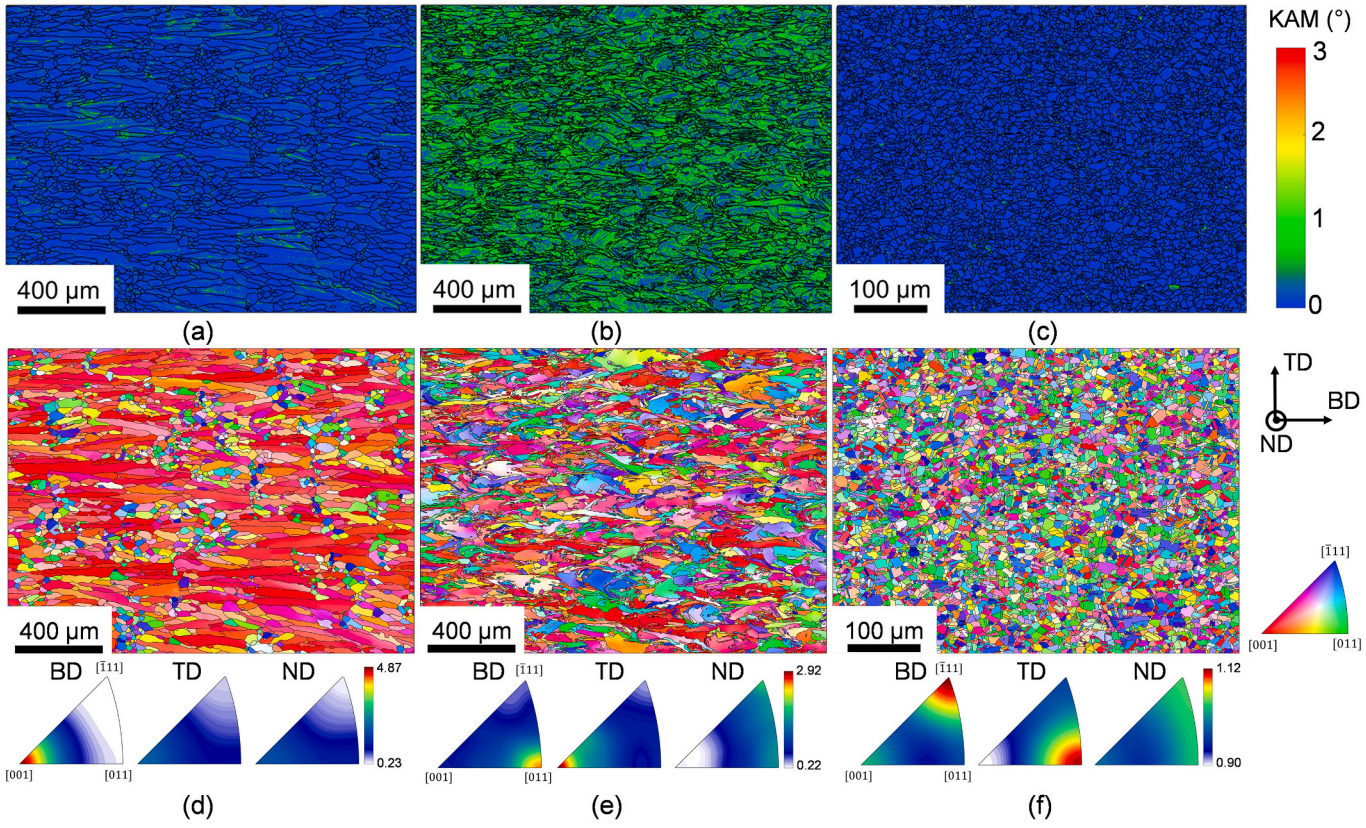

Fig. 12. Grain distribution, texture and kernel average misorientation (KAM) of PBF-EB/(a and d), PBF-LB/(b and e) and wrought/Alloy 718 (c and f) in as-built or as-received conditions. Adapted from Ref. [46].

exclusively on: 1) density of dislocations organised in cell structure [68], 2) amount and distribution of Laves-phase predominantly precipitated at grain boundaries, 3) the grain size distribution (and density of LAGBs and twin boundaries) and 4) texture [136]. PBF-EB/Alloy 718 would however contain some amount of γ' and γ'' precipitates in as-built condition since the material is subjected to high processing temperatures during AM process (975 ± 25 °C). The amount of γ' and γ'' precipitates was levelled up after the standard solutionising and double-ageing treatment (AMS 5662 standard), while the grain distribution, kernel average misorientation and texture remained mostly unchanged.

The authors reported the highest wear rates and cutting forces when machining PBF-EB/Alloy 718, regardless of whether the material was in as-built condition or heat-treated. Machining of PBF-LB/Alloy 718 in as-built condition showed the lowest wear rate, despite higher hardness than that of wrought material in as-received condition. Interestingly, the cutting forces were also almost similar when machining PBF-LB/and wrought Alloy 718 in as-built and as-received conditions. Heat treatment did not have a significant impact on the cutting forces when machining wrought and PBF-LB/Alloy 718, and the measured values were in the same range as those of as-built and as-received materials. The flank wear evolution increased when machining PBF-LB/Alloy 718 after heat treatment whereas a similar wear rate was noted when machining heat-treated wrought material. These suggest that the hardness is not the reliable indicator of machinability of the material in terms of cutting forces and tool life. In addition, no clear correlation between the tool wear rate and cutting forces was noted. For example, while the cutting forces were almost similar, significantly different flank wear evolution rates were observed when machining wrought and PBF-LB/Alloy 718; see Fig. 13.

The authors argued that the larger density of GNDs in as-built and heat-treated PBF-LB/Alloy 718 can lead to lower fracture strains as well as lower work-hardening during chip formation. This results in lower cutting temperatures when machining PBF-LB/Alloy 718. In addition, this material contained only a relatively small amount of oxide inclusions. Conversely, the wrought material contained a large number of NbC and Ti-rich nitrides, while PBF-EB/Alloy 718 was comprised of oxide inclusions as well as NbC and Ti-rich nitrides, but in lesser amounts as compared with the wrought material. These can explain the reasons behind lower wear evolutions when machining PBF-LB/Alloy 718. The strong 001 ‖ BD texture, larger work-hardening prior to chip separation and a relatively large amount of abrasive particles were believed to be the major reasons for higher wear rates observed when machining PBF-EB/Alloy 718.

3.3.2. *Milling and micro-milling*

Milling and micro-milling additively manufactured Alloy 718 is also investigated in several studies. Ostra et al. [137] compared the machinability of DED-LB/Alloy 718 with that of wrought (forged) material under similar cutting conditions. The authors observed shorter chips when machining DED-LB/Alloy 718 and attributed this to its almost 50% lower elongation at fracture compared to that of wrought material. The yield and tensile strengths of the DED-LB/Alloy 718 were comparable with those of wrought material. Calleja et al. [138] studied the machinability of laser cladded Alloy 718 and compared it with that of wrought material (i.e., base material used for cladding). The cutting forces were lower when machining laser cladded material in as-built condition as compared to the wrought base material. The solutionising and ageing treatment levelled up the tensile properties of cladded material and thus higher cutting forces were generally obtained when machining this layer after heat treatment. The surface roughness (Ra) was better when machining wrought material under similar cutting conditions. Periane et al. [139] investigated the influence of cooling media (dry, MQL and emulsion) on tool wear, surface roughness and specific cutting energy during milling PBF-LB/and wrought Alloy 718. Higher wear rates, specific cutting energies and surface roughness were observed when machining the wrought material under similar cutting conditions (i.e., cooling condition, feed rate and cutting speed). The energy consumption was the least when machining PBF-LB/Alloy 718 under wet (emulsion) condition. Ducroux et al. [140] compared the machinability of PBF-LB/Alloy 718 with that of wrought material in terms of tool life. Both materials were solutionised and aged (AMS 5662) prior to machining tests. The authors also developed a mechanistic approach for cutting force prediction in side-milling incorporating the effects of flank wear land widths. The authors reported lower forces (cutting, feed and passive forces) and almost two times longer tool life when machining PBF-LB/Alloy 718. Abrasion and attrition were identified as the dominant wear mechanisms controlling the rates of flank and notch wear evolution.

In a more recent investigation, Pérez-Ruiz et al. [49] developed a microstructure-sensitive mechanistic model for cutting force prediction in peripheral milling incorporating the effects of crystallographic

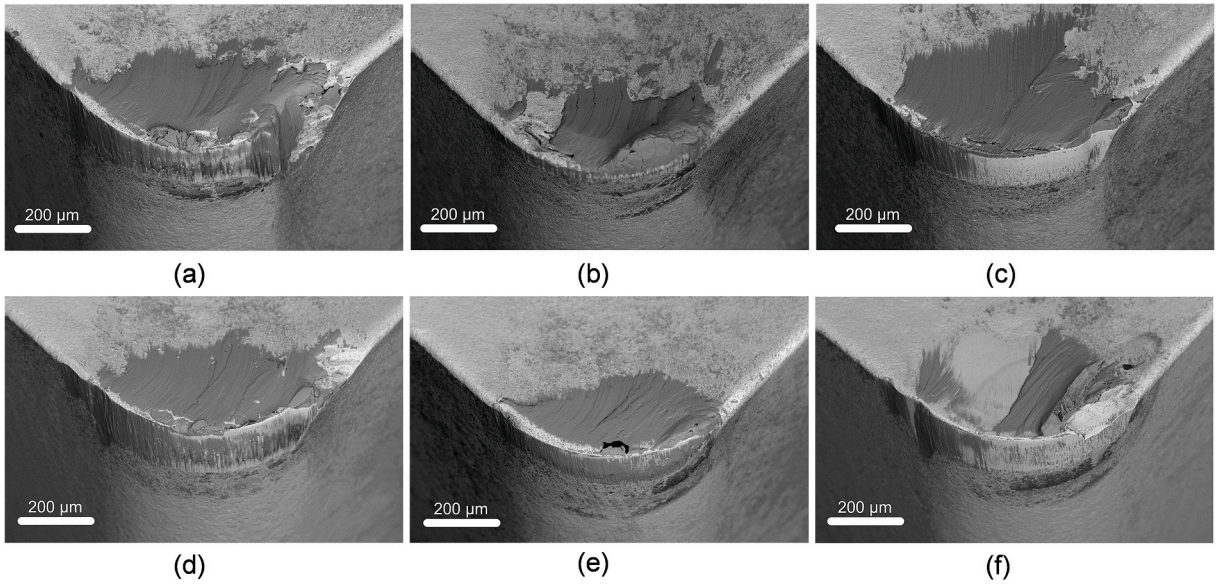

Fig. 13. Worn tools when machining PBF-EB/(a), PBF-LB/(b) and wrought/(c) Alloy 718 in as-built or as-received conditions, and when machining PBF-EB/(d), PBF-LB/(e) and wrought/(f) Alloy 718 after solutionising and double-ageing treatment (according to AMS 5662 standard). Adapted from Ref. [46].

texture and grain morphologies. This model attempts to present a generic framework for prediction of cutting forces, as the microstructural characteristics of the AM Alloy 718 vary with AM process parameters, e.g., scanning strategy and VED. It was claimed that the cutting force in peripheral milling is essentially related to the shear strength of the material. As mentioned in Section 2, the shear strength of the material depends on the microstructural features like grain size distribution and the crystallographic texture. These microstructural characteristics largely account for the anisotropic behaviour of Alloy 718 and thus the directional-dependency of cutting forces [46,48]; see also Fig. 3. Hence, the authors presented a mathematical relation to obtain the shear strength as the tool configuration varies with respect to the material crystallographic texture; see Fig. 14 for six different scenarios where the Taylor factor (M) maps were presented as a function of relative tool engagement angles (θ) and the shear angle (Φ_c). As soon as these maps are generated, it is possible to obtain the shear strength of the material and thus the cutting forces for different tool-workpiece engagements, for example, G(0 0 0), G(0 45 0) and G(0 90 0) configurations shown in Fig. 14. Furthermore, the authors evaluated the effects of grain morphology (i.e., size and shape distributions and orientations with respect to tool engagement angle) on cutting forces using an in-depth microstructural analysis. A clear correlation between cutting forces and grain morphology was observed, particularly for the cases where effects of crystallographic texture were rather weak (i.e., for parts manufactured using low VED).

Kim et al. [141,142] investigated the influence of build direction on tool wear during micro-milling PBF-LB/Alloy 718. The authors observed higher wear rates when machining wrought material despite its lower hardness compared to that of PBF-LB/Alloy 718. During machining PBF-LB/Alloy 718, the lowest wear rate was observed for the case where the plane of cut was perpendicular to the build direction, despite almost similar hardness on the surfaces parallel and perpendicular to the build direction. These observations show the important role of crystallographic texture and grain morphologies influencing the material deformation during the cutting process and thus the machinability of AM Alloy 718.

4. Finishing processes

This section is concerned with finishing processes that are primarily intended to modify surface texture, but also tailor surface integrity/material microstructure. The majority of concerned post-processes involve applications of finishing with abrasives, hence a mechanical post-processing. In addition, electro-chemical- and laser-polishing operations are analysed. The emphasis was placed on post-processing of additively manufactured 316L, Ti6Al4V and Alloy 718, while in part we refer to other materials like Alloy 625, 304 L and AlSi10Mg.

4.1. Grinding processes

Despite the importance of grinding as a finishing process, only a few research studies have been dedicated to grinding AM materials. Kirsch et al. [143] recently published a paper on surface grinding of PBF-LB/316L stainless steel using conventional aluminium oxide wheels. The objective of this work was to investigate the differences in grindability when grinding conventional steel (cast, rolled, solution annealed, and water quenched) vs. two AM materials having different defect sizes and densities resulting from low and high VEDs (33.3 J/mm^3

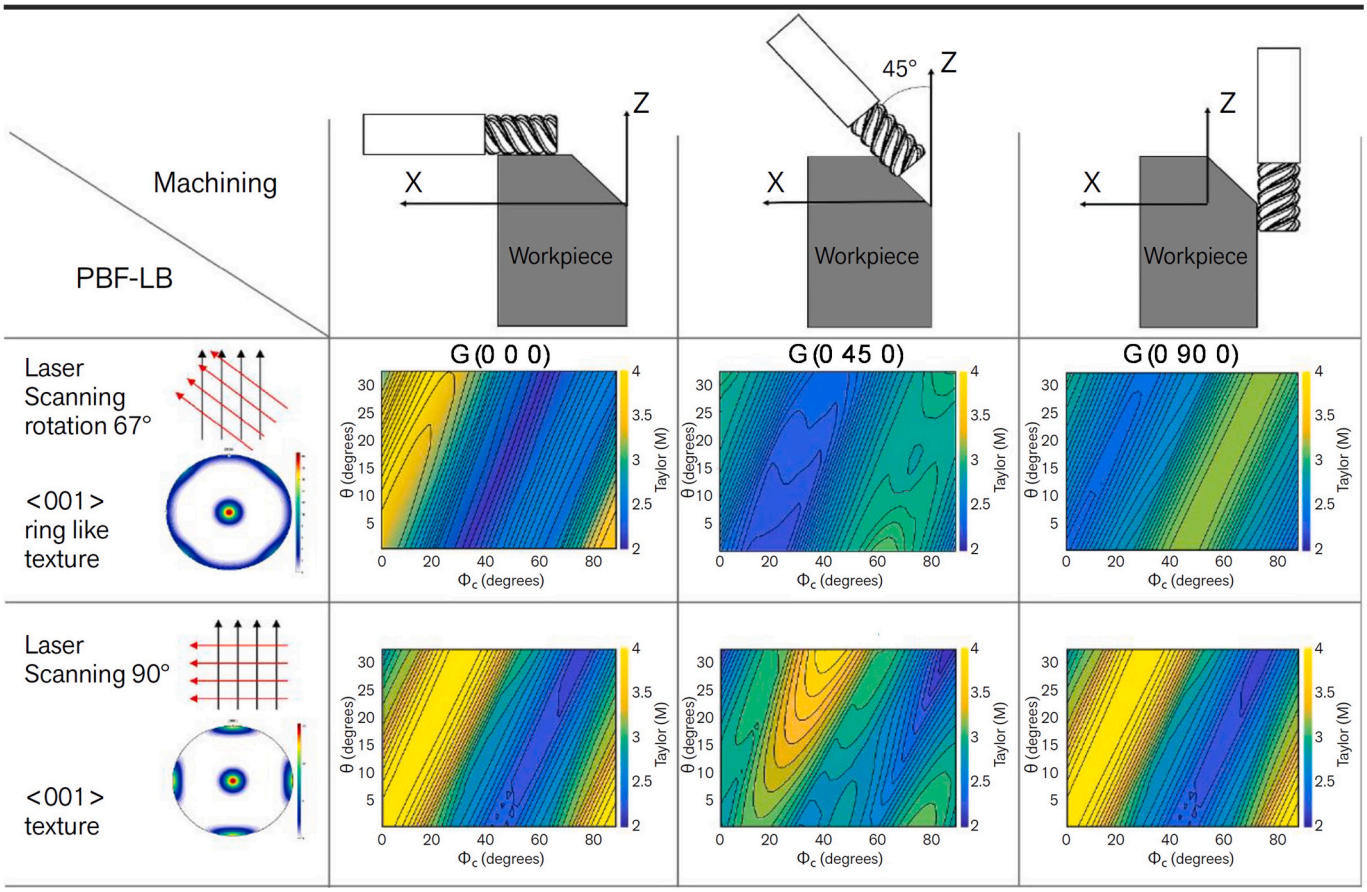

Fig. 14. The interaction between the tool and the microstructure (crystallographic orientation) of PBF-LB/Alloy 178. Taylor maps indicating the interaction between two laser scanning strategies (rotation by 67°and 90°) and three milling configurations (tool positions: G(0 0 0), G(0 45 0), G(0 90 0) for a helix angle of 30°, tool engagement angles between 0° and 32° and shear angles ranging between 0° and 90°). Adapted from Ref. [49].

vs. 119 J/mm^3). The grindability was assessed in terms of grinding forces and surface finish (roughness). For shallow-cut grinding with 5 μm depth of cut (Q_w = 1.25 mm^2/s), the specific tangential force was around 40% higher in the case of dense AM material compared to conventional. The authors attributed this to about 30% lower hardness of conventional material. Interestingly, in creep-feed grinding experiments with 0.25 mm depth of cut, the observed forces were very similar. Hence, hardness alone cannot explain the differences observed in grindability of materials. For shallow-cut grinding, the impacts of microstructural characteristics like pores and defects, grain size shape and size, micro-constituents, and material texture would be amplified, a phenomenon known as "size-effect" [144]. The obtainable surface roughness (Rz) is similar for all materials. Grinding reduced the as-built surface roughness by about 90%, from Rz = 42–44 μm to Rz = 3–6 μm, depending on the grinding mode. The cracks and voids/indentations were still present on the ground surfaces of the AM material with higher density of large lack-of-fusion defects. In this respect, the achievable surface finish is determined by the (residual) porosity, which depends on the material density and is grinding independent. Similar observations are reported by Kadivar et al. [145], who studied the role of specific energy in micro-grinding of conventional/extruded (340 ± 5 HV) and PBF-EB/Ti6Al4V (345 ± 10 HV) materials. In terms of finished surface properties, comparable surface topographies were observed using the same grinding parameters, regardless of the material manufacturing method. The surface parameter, Sa, and roughness parameters, Ra and Rz, were all nearly of the same order. In all cases, some material debris could be observed on the ground surface.

The specific energy is the energy expended to remove a unit volume of material, which is a fundamental grindability parameter that indicates the (cutting) efficiency of the process. The material microstructure resulting from different manufacturing processes (wrought vs. PBF-EB) was found to have a considerable influence on the obtainable specific energy, although the material hardness was the same. For example, 20–30% higher specific energy was observed when grinding in parallel to the material-build direction in comparison to grinding perpendicularly to the build direction. The specific energy when grinding perpendicularly was comparable to micro-grinding of conventional material. The observed differences in specific energy were attributed to the chipping ratio and strain-hardening effects. However, at higher aggressiveness (chip thickness) values, almost the same specific energy was obtained for all materials. This is in contrast to observations in micro-milling of the same materials, using a 3-fluted cutter measuring 1.8 mm in diameter [118]. Here, the size effect was distinct for chip thicknesses smaller than 7.4 μm, characterised by exponential growth in specific energy due to the dominant ploughing effect. In this range, the specific energies for conventional (extruded) material (350 HV) were about 5–15% higher compared to PBF-EB/Ti6Al4V (450 HV). This slight increase was attributed to higher ductility of conventional material. At higher values of chip thickness, cutting is predominant, resulting in similar values for specific energy, reaching a minimum at about 2.5 J/mm^3. These two studies also assert that measuring hardness alone is not sufficient to index grindability of additively manufactured materials with respect to their conventionally fabricated counterparts.

A special grinding process featuring a semi-elastic grinding tool with abrasive pellets refers to shape-adaptive grinding (SAG), developed by Beaucamp et al. [146]. This process enables a ductile-mode grinding and is capable of achieving surface finishes, typically required for optical applications. The SAG-based finishing of PBF-EB/and PBF-LB/Ti6Al4V alloy demonstrated the ability to remove the semi-sintered particles on the (as-built) surface texture, thus achieving a surface roughness around 10 nm Ra [147] andimproving the surface finish by about three orders of magnitude. The compliant nature of this process is especially suited for post-processing AM, due to its capability to machine free-form surfaces and to remove the workpiece irregularities resulting from the melting process more effectively. The precise control of the SAG process should now be available, thanks to the analytical models describing the process mechanics at multiple scales (macro- and micro-level) [148]. Moreover, the process can be further implemented on a dedicated (7-axis) polishing machine or a 5-axis machining centre [149]. The feasibility of using different machine types was demonstrated on SAG of PBF-LB/17-4 PH stainless steel. In addition to demonstrating the finishing capability, this work provides valuable insight into different modelling approaches to predict the process outcomes, ranging from empirical and semi-empirical to analytical methods. Finally, a novel analytical method is developed to model a compliant finishing process in a Folding Space, accounting for initial surface roughness, abrasive-grit distribution, compliant-tool deformation and process parameters.

4.2. Abrasive fine-finishing processes

Abrasive fine finishing is often applied as a final finishing process in the manufacture of precision components, and the selection of the right technology is crucial in obtaining the desired functional performance, such as fatigue life [150]. Most of the available studies are concerned with investigating the capability of abrasive fine-finishing to reduce the surface roughness of as-built AM components and are comparative in nature, i.e., when one or several finishing processes are compared with each other. Such observational studies have major shortcomings, as they fail to address the fundamental process aspects, such as discussion of material removal mechanisms and effects on surface integrity, and fundamental material effects on the process (e.g., effect of workpiece microstructure on specific energy). Very often, the experimental details are insufficient, for example, specifying the size of abrasives used [151]. Moreover, there are inconsistencies in terminology, e.g., magnetic-abrasive finishing (MAF) is used to refer to polishing [152] or linishing [153] is used in lieu of brushing [154].

The abrasive-fine finishing technologies that have been so far applied for finishing of AM-fabricated metallic components primarily include brushing, mass finishing (e.g., vibratory finishing, barrel tumbling and drag finishing), blasting, abrasive-flow machining (AFM) [155,156] and MAF.

4.2.1. Magnetic-abrasive finishing (MAF) processes

Guo et al. [152] investigated the feasibility of MAF of internal surfaces, where the workpiece, a hollow tube, was PBF-LB/Alloy 718. In MAF, the magnetic abrasives are forced against the workpiece surface by a magnetic force. Process kinematics consists of workpiece rotation and axial, reciprocal movement of the magnets, as shown in Fig. 15.

In the case of a hollow shaft, a cylindrical magnet is inserted into the workpiece bore, next to the two external magnets. The abrasive slurry consisted of stainless steel and SiC bound by a straight oil. Process modelling was founded on well-established Preston's law – commonly employed in modelling of material removal in a variety of abrasive fine-finishing processes, such as vibratory finishing [157], (bonnet) polishing [158,159], and compliant grinding [160,161]. According to Preston [162], the material removal rate is proportional to the relative velocity between the abrasive and the workpiece surface, the applied pressure and processing time. This empirical relationship accounts for the "system" properties, e.g., process geometry, abrasives/slurry used, workpiece material properties, etc., via a constant, specific to the finishing operation. Guo et al. [152] investigated the feasibility of MAF of a hollow tube – built of PBF-LB/Alloy 718. Here, the experimental results showed that the surface roughness of both the OD surface of the inner tube and the ID surface of the outer tube was reduced from 7 μm Ra for as-built samples to 0.5 μm Ra [152]. The reported process is slow; 3 h per experiment, where the bulk of the finishing allowance (100–120 μm) was removed in 1 h. The MAF mode, i.e., rotation vs. vibration or a combination of both, had little to no effect on achievable surface roughness, which was determined by the composition of the abrasive slurry. As expected, higher material removal was achieved when employing larger SiC grits. The analysis of the cross-section of the as-built tubes revealed dissimilar microstructures: larger near-surface

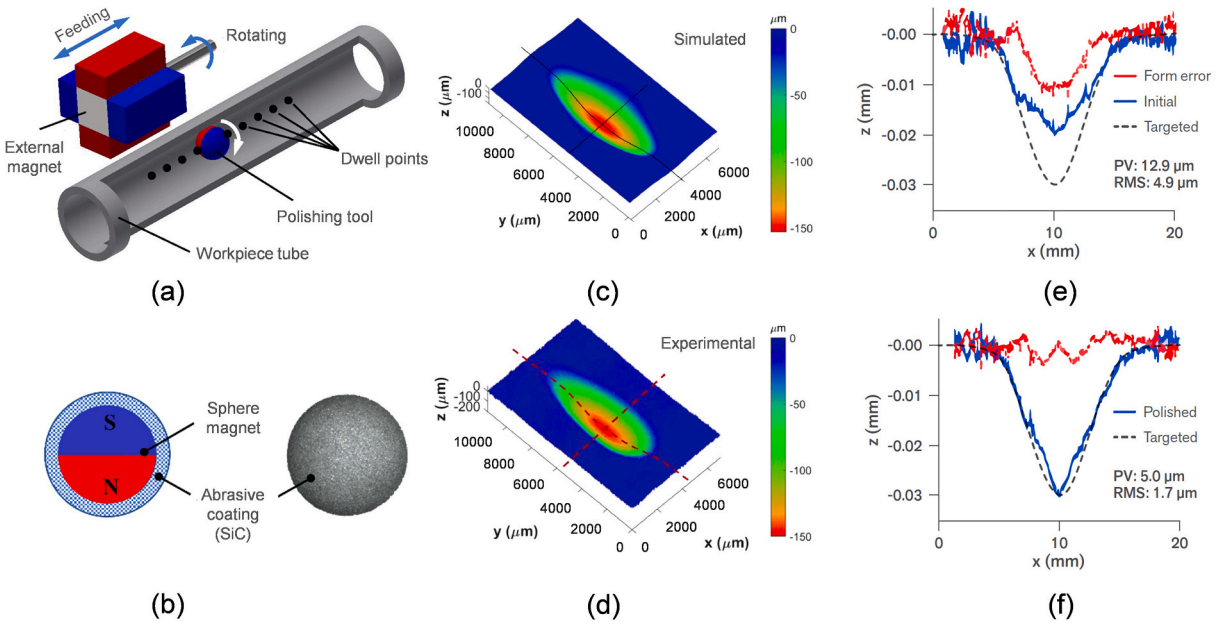

Fig. 15. Working principle of magnetically driven internal finishing and its application; 3D schematic of the working principle (a), design of the magnetic polishing tool and its digital twin (b), simulated and experimental footprint (c and d), after polishing, the form-error compensation of magnetically driven internal finishing by using the dwell-time algorithm (e and f) [163,164].

cellular structure in the outer layers (30 μm thick) as compared to cellular structure within the core. This microstructural difference was attributed to differences in the cooling rate closer to the surfaces. The cell dimensions of the material near the printed surface were about 5 μm in diameter and thus lower hardness than that of the core material (underneath layers) was expected. The outer layer (30 μm thick) was removed by MAF, revealing a damage-free surface. Near-surface residual stress measurements show release of compressive residual stress generated during the AM process in the normal direction (from about −230 MPa to −30 MPa), whereas the residual stresses in the shear direction remain similar (−20 to −30 MPa). Moreover, MAF caused a slight (5–10%) increase in nano-hardness (from 4.0 to 4.3 GPa).

MAF may be also employed for abrasive fine finishing of internal surfaces (channels and cavities) for fluid-flow applications, such as turbine buckets with cooling channels or fuel-mixing components for a combustion stage of a turbine [165]. Here, the internal-MAF process is controlled by size, hardness (e.g., 20–60 HRC), magnetic and chemical properties of particles, as well as the strength/direction of the magnetic field employed. The magnetic properties of the particles depend on their composition, e.g., the amount of nickel or cobalt in the Ni–Co–Fe alloy. The material removal is controlled by the magnetic field affecting the aggressiveness between the magnetic particles and the surfaces being machined. The size and shape of the particles affect the material removal as well, which is known in both fixed-abrasive and free/loose-abrasive machining. The capability of this technology to improve surface topography is not fully revealed in the patent. Increasing material removal in MAF of internal surfaces was recently achieved by coating conventional abrasives on the magnetic tool with a defined geometry (e.g., sphere) [164], as shown in Fig. 15. This tooling solution can increase the magnetic force to achieve localised finishing at a material removal rate of 15 μm/min – reducing Ra by 80% in only 2 min, which outperforms the MAF with loosely-bonded tools [166]. Moreover, this work postulates a modelling framework to investigate material removal mechanism and predict the finished surface based on contact mechanics and Archard wear theory. For this, a sphere-to-arbitrary geometry contact model was established to calculate the contact pressure distribution. This MAF technology is also used for a deterministic finishing process by implementing the concept of computer-controlled optical surfacing [163]. The key challenge is to model a tool influence function (TIF) which can account for the time-varying material removal rate. Hence, a time-variant TIF model – based on a partial differential equation – was developed and the corresponding dwell-time algorithm was proposed. These facilitate finishing of complex surfaces and compensate for a form-error, which is extremely challenging for conventional MAF methods.

The MAF is also capable of fine-finishing outer surfaces. Wu and Yamaguchi investigated the effects of magnetic particle size and abrasive type (magnetic/fixed vs. conventional/loose) on material-removal mechanisms in finishing PBF-LB/316L stainless steel [167]. Here, the magnetic abrasive refers to a composite abrasive (aluminium oxide fixed in the magnetic/iron matrix). In contrast, a simple mixture of aluminium oxide (Al_2O_3) abrasive and iron particles is also used. Since the Al_2O_3 abrasive is "loose," this mixture is termed conventional/loose type in this work. The authors observed that the as-built surfaces were too rough (Rz = 60–100 μm) for MAF using a magnetic abrasive featuring Al_2O_3 grits measuring below 10 μm in diameter. This necessitated modification of the tool, i.e., using a larger diameter of magnetic particles (steel grits) mixed with Al_2O_3 magnetic abrasive and diamond abrasive (120 μm diameter). The analysis showed that material was removed primarily by the diamond, not Al_2O_3 abrasives. The achievable surface texture was measured using areal height parameters, including Sa or Sz, Ssk (skewness) and Sku (kurtosis). The use of conventional abrasive created higher negative skewness compared to magnetic abrasive and larger kurtosis, indicating a "sharper" texture in terms of peaks and valleys. MAF is further capable of shifting tensile residual stresses induced by laser sintering to compressive residual stresses, if the mixture of magnetic particles and abrasive slurry is replaced by steel balls (with no diamond abrasive). This process modification refers to magnetic-assisted burnishing (MAB) [168], featuring a "stiffer" tool (still featuring abrasives) capable of modifying the surface topography (form and texture) by plastic deformation (without cutting/material removal). MAB is not to be confused with a conventional/non-abrasive (ball) burnishing process, which is also a viable post-processing technology of AM materials [169], as it improves the microstructure (grain refinement) and surface topography, as well as induces compressive residual stresses. The surface roughness, however, can be only slightly reduced by MAB. The real benefit of this process is in imparting compressive residual stresses through a mechanical action. For example,

the residual stresses in laser-scanning direction can be shifted from tensile (about +200 MPa) to compressive (approximately −80 MPa). The largest compressive residual stresses were observed parallel to the build direction (−150 MPa), as the initial tensile stresses were lower (20–80 MPa). The types of abrasives used also determine the process capability, especially with respect to the workpiece material being finished. For example, it was shown that the Ni-coated diamond abrasive is less efficient in removing material than an uncoated diamond in MAF of Ni-based superalloys [170]. The reason for an inferior material removal rate is that the Ni-coated abrasive is more attracted to the magnet than the workpiece, resulting in non-uniform finishing and fewer diamonds cutting in the formed magnetic-particle brush. MAF was also used to finish PBF-LB/316L stainless steel plates printed with various slope angles [171], as shown in Fig. 16. These stainless-steel plates show significantly different surface roughness and topography, resulting from the defects such as 'staircase effect', balling effect, rippling effect and semi-sintered particles. However, post-processing with MAF using 500 μm steel grits removed these defects gradually. The MAFed surface roughness was reduced by 75% while the deviation of the surface roughness from the slope remained unchanged.

4.2.2. *Mass finishing processes*

Mass finishing is an abrasive fine-finishing technology used for simultaneous processing of multiple components in a container, usually with abrasive media and a compound solution. Here, a cyclic movement of the container causes media to vibrate and rotate against workpiece surfaces, or workpieces to rub against each other. This type of finishing is often used as a final step after the AM build cycle to achieve low surface roughness and reflective surfaces (characterised by smaller standard deviation of heights, Sq). Mass finishing can be classified into 5 methods: vibratory finishing (using bowl or tub), rotary barrel finishing (tumbling), centrifugal barrel finishing, centrifugal disc finishing and drag (spindle) finishing [172]. The geometry and kinematics of the vibratory finishing are not well understood; however, Hashimoto et al. [173] modelled the material removal mechanism by deriving the relative velocity vector and the impact angle in the contact. In this respect the geometry and kinematics of the abrasive interaction could also be derived from the theory of aggressiveness [174]. Hashimoto et al. determined the characteristic specific energy curve against equivalent chip thickness h_{eq} [150,173], which is difficult as one also needs to estimate the depth of cut. As in other abrasive processes, the total specific energy is comprised of a chip-formation energy and the specific energy required for sliding and ploughing [173]. The dominant force in the contact occurs in a normal direction and depends on hydrostatic pressure (vibration); the cutting speed hence predominantly depends on the impact velocity of media. In a drag finishing process, a workpiece is clamped to a rotating carrier in a barrel and submerged into a mixture of abrasive media and liquid compound. Malkkora et al. [175] recently developed a model that enables a simulation of abrasive media flow, considered as a homogeneous and continuous media around a workpiece, as well as its interaction with a workpiece. The numerical modelling approach was based on the Arbitrary Lagrangian-Eulerian formulation, allowing calculation of process mechanics (e.g., sliding velocity, normal and shear stresses) and to correlate these fundamental parameters to surface roughness. Moreover, the authors also proposed a testing procedure, to identify the Drucker-Prager plasticity model, which has a demonstrated potential to investigate the effects of media (geometry, size, lubricant) on the rheological properties. The smoothing

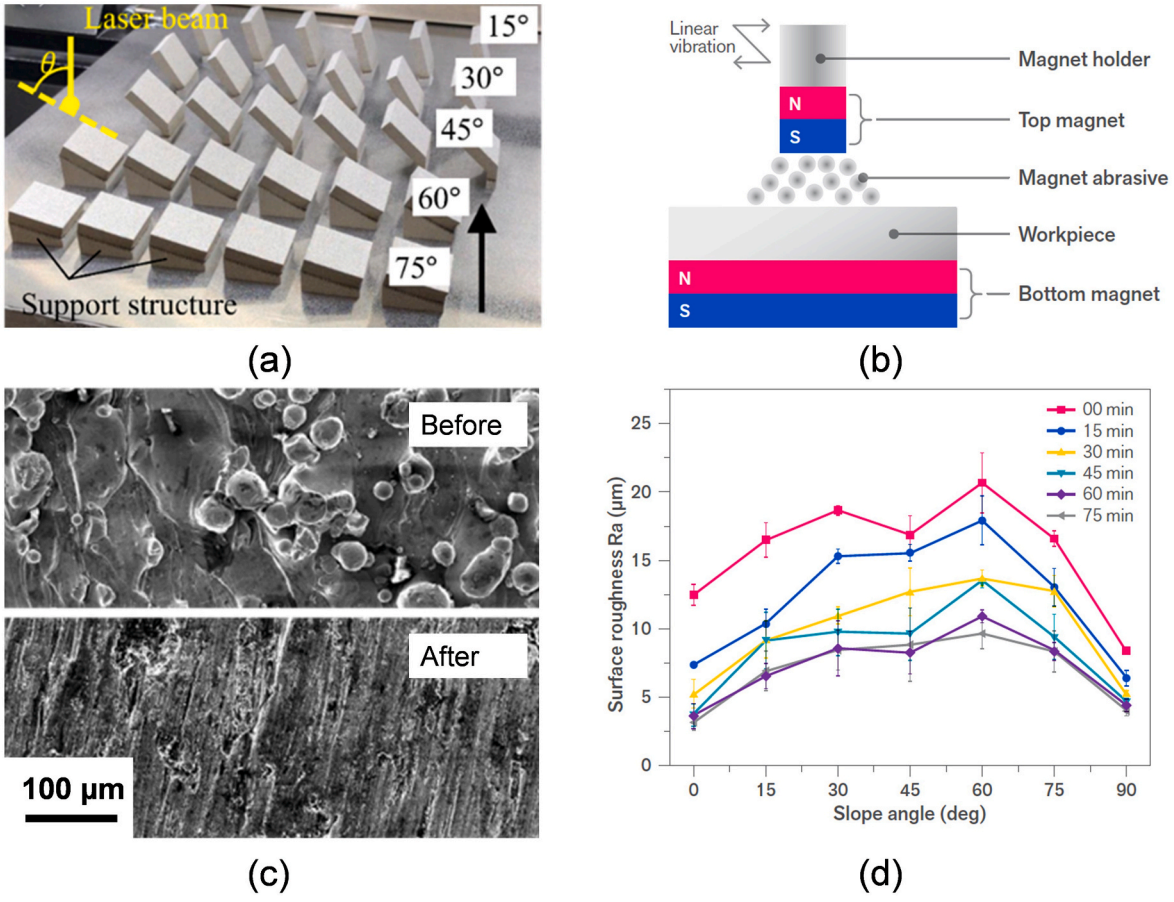

Fig. 16. Magnetic-abrasive finishing (MAF) of PBF-LB/316L stainless steel plates. As-built workpieces printed with various slope angles (a), schematic of the MAF setup (b), SEM images of workpiece surface before and after MAF (c), average surface roughness Ra vs. slope angle at different finishing time instants (d). Adapted from Ref. [171].

capability of drag finishing can be further increased by integrating electrochemical effects [176]. Note that the specific aspects of electro-polishing are discussed in greater detail under Section 4.3. In this innovative process, a part being finished is attached to a workpiece holder (vertical rotating shaft), which has a function of a positively-charged anode. The holder/workpieces are immersed in, and moved through electrically-conductive and negatively-charged abrasive media. The barrel containing and vibrating the abrasive media here serves as a cathode. In this process, the material removal is primarily mechanical, e.g., caused by three-dimensional abrasion. Addition of a water-based electrolyte to the process (e.g., containing 1–10% hydro-fluoric acid) enhances the surface-smoothing process by tapping the electrochemical etching effects (ion transport). This technology proved capable of reducing the roughness of PBF-LB/316L stainless steel by over 90% in 1.5 h, using only a small amount of sulfuric acid [177]. Spherical abrasive particles here were polymeric, with a diameter of 0.3–1.0 mm. The SEM analysis of the finished surface revealed a sequence of underlying material-removal mechanisms; 1) formation of an oxide layer; 2) cracking of an oxide layer; 3) fragmentation of an oxide layer; 4) shedding of oxide particles; and 5) formation of a new surface [177]. Electrical and chemical aspects of mass finishing are hence important to increase the capability of material removal.

Addition of only a chemical agent to the container where the parts are simultaneously finished can improve material removal due to a mechano-chemical effect, resulting in an isotropic (non-directional) surface texture and a high material-ratio curve. Mechano-chemical vibratory finishing was developed for isotropic finishing of roller bearings and was patented in 1996 by Hashimoto et al. [178]. Nowadays, this technology is widely used and is commercialised as isotropic superfinishing (ISF) technology, which is slightly misleading as it creates confusion with a genuine superfinishing process using a stone (or tape) oscillating at high frequency to produce a cross-hatched surface finish. Isotropic finishing (IF) is a more appropriate general term, as the process renders workpiece surfaces isotropic. The original IF is typically carried out in two steps. First an acidic liquid chemical (e.g., with pH = 1.5) is added to the process, where it reacts with the workpiece and produces a film loosely attached to the work material. This film can be easily detached by the abrasive media in the compound, enhancing material removal. The material removal is limited to the higher peaks of the surface, whereas the valleys remain intact. It is, however, insufficiently investigated how the agitation within the chemical regenerates until the patterns in a typical PBF-LB/EB layer caused by laser/beam tracks diminish and the surface becomes isotropic. Once the surfaces become isotropic, the delivery of acid is stopped and replaced by an alkaline (e.g., with pH = 8.5) burnishing liquid in the second step to neutralise the previous chemical reaction. Here, in the absence of the acid, the film is removed, revealing a mirror-like surface [178].

PBF-LB fabricated aluminium alloy (AlSi10Mg) was mechano-chemically finished, using an IF vibratory finishing process with unspecified abrasive media [179]. The finishing operation was done in two steps, utilising different media and the concentration of the dilution. This work is thorough in terms of surface finish characterisation, as it appropriately employs a wide variety of areal texture parameters from the ISO 25178 standard. The results show that the employed post-processing could reduce the mean dispersion of height values by a factor of ten, to Sa = 4 μm. Moreover, the finishing increases the negative skewness (from −0.21 to −3.66) and increases the Smr of the areal material ratio curve by nearly 50%. Therefore, valleys prevail over peaks in the surface texture, achieving a targeted isotropic surface. It should be noted, however, that the material removal is very slow, as the process takes 2–3 days to complete, indicating that the initial surface roughness was too high.

IF was also used for surface conditioning of PBF-LB/Ti6Al4V alloy intended for maxillofacial implants [180]. The as-built workpiece material was abrasive-blasted prior to finishing to remove the semi-sintered particles on the surface, reducing the initial surface roughness (Ra and Sa) by 25–30%. The vibratory-finishing parameters were not revealed, but the "tooling" was comprised of two types of abrasive media for roughing and finishing, i.e., pyramidal-shaped abrasive (density 2.5 g/cm^3, Mohs hardness of 8); and cylindrical-shaped abrasive (density 2.91 g/cm^3, Mohs hardness of 8.5), respectively. In addition, the chemical composition of the water-based fluid used was 2.5–5% sulfonic acids, C13-17-sec-alkane, sodium salts, 2.5–5% ethoxylated iso-tridecanol and 1–2.5% citric acid. The two finishing cycles took up to 20 h for roughing +2 h per finishing to accomplish. The obtained average surface roughness values were Ra = 0.22 μm (Sa = 0.15 μm), but the isotropic surface finish without distinct features such as deformation/-scratch marks was not observed nor assessed by additional areal surface parameters (beyond Sa). This may imply that the full potential of mechano-chemical processing was not tapped, due to either improper process parameter selection or inadequate processing time. The vibratory finishing was further benchmarked against electro- and plasma-electrolytic polishing [181], which were not able to achieve as a fine surface finish as vibratory finishing. In view of the medical application in focus here, vibratory finishing has further advantages with respect to edge rounding, which is needed to avoid tissue irritation. Moreover, cell attachment depends on surface topography, which is determined by the wettability angle, hydrophobicity [182] and adhesion properties. On the negative side, however, abrasive processing might lead to undesired surface chemistry of the finished surfaces (e.g., increased alumina content). This can be modified by careful selection of the abrasive/chemical media to minimise the cytotoxic, poisonous to living cells effects and to therefore improve initial adhesion of cells. Similar findings were reported for (ceramic) joint implants, where a polished nanoscale roughness (Ra = 1 nm) significantly reduced the bacterial adhesion (by 98% compared to ground Ra = 0.2 μm surface), and the risk of implant-related infection [183]. In this application the joint bearing surface requires surfaces with fewer peaks to avoid concentrated loading, and a damage-free surface with minimal micro-scale features, such as scratches, pits and grooves. Post-process finishing operations here included surface grinding (#800 diamond wheel) and subsequent "wheel" polishing [184] using a slurry of 0.75 μm diamond powder mixed in a 4 wt% concentration. The authors further showed that ground and (rough) polished surfaces generate hydrophobic surfaces (with larger wettability/contact angles) compared to fine polished, hydrophilic surfaces characterised by a smaller wettability/contact angle below 67°. In this way the surface wettability (hydrophilicity/hydrophobicity) is directly related to surface roughness and the employed abrasive fine-finishing process.

4.2.3. *Non-conventional abrasive fine finishing*

Ultrasonic cavitation abrasive finishing (UCAF) is a nonconventional

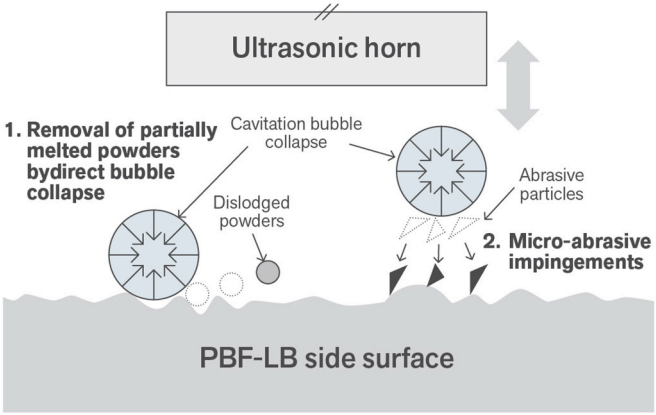

Fig. 17. Ultrasonic cavitation abrasive finishing (UCAF) process utilising cavitation effect and micro-abrasive mechanisms simultaneously for improving the surface roughness of PBF-LB/Alloy 625. Adapted from Ref. [187].

method specifically developed for abrasive fine finishing of 3D-printed materials and patented by Rolls-Royce [185]. The technology exploits the cavitation effect [186], caused by high-intensity sinusoidal ultrasonics, in the frequency range of 20–40 kHz. Here, the ultrasonic waves propagate through a liquid media – inducing cavitation. UCAF exploits the collapse of the cavitation bubbles close to the workpiece surface, producing high-velocity jets that can remove the PBF-LB/EB rough upper layer consisting of partially sintered powder by (heterogeneous) cavitation Fig. 17 [187]. Material removal and surface finish here can be enhanced by adding abrasive grits (e.g., 400–1200 mesh SiC) to the process. The kinematics of the grits – enabled by the bubble collapse – induce abrasive ploughing and cutting mechanisms in the contact between the grit and the workpiece.

The PBF-LB/Alloy 625 as-built surfaces were finished by two distinct UCAF process modes (material removal mechanisms), resulting in distinct topographies of a finished surface, shown in Fig. 18. The cavitation-induced erosion removed larger partially melted powder, leaving a crater on the surface. The smaller (fully-melted) structures were subsequently flattened/removed by an abrasive interaction. In contrast to MAF and mass finishing, UCAF is rather fast – capable of significantly reducing the surface roughness in 10 min' processing time. However, the reported Sa of 5.6 μm was obtained in 30 min; the final topography still features the initial surface form and texture (including discontinuities).

The capability of UCAF was also demonstrated for finishing of simple internal channels (3 mm diameter, 20 mm length) [188]. Here, the Ra values were improved by 20%. The authors reported on reduced efficiency of cavitation-based material removal due to attenuation effects, but this was improved by adding abrasives to the process, which aided cavitation (bubble) formation, depending on grit size and concentration.

Finishing of internal channels was further improved by controlling the upstream and downstream fluid pressure, resulting in an improved method, termed hydrodynamic cavitation abrasive finishing (HCAF) and patented by Rolls-Royce [189]. HCAF upgrades UCAF by closing the hydrodynamic loop, i.e., realizing a closed upstream and downstream hydrodynamic cavitation stream. Similar to UCAF, the material removal mechanism in HCAF consists of 1) erosion due to implosion of the cavitation bubbles (pure cavitation), 2) pure microparticle abrasion, and 3) cavitation-assisted microparticle abrasion [190], as shown in Fig. 19. The material-removal through cavitation seems to dominate over abrasive action; the latter, however, primarily erodes the larger semi-sintered particles on the surface [191]. In case of HCAF of PBF-LB/AlSi10Mg, the as-built surface of the internal channels (Sa = 34 μm) was smoothened to Sa = 10 μm, meaning a 70% improvement in surface finish [192].

Recently, the capabilities of HCAF were improved further by incorporating a multi-jet nozzle design [192]. The upgraded technology is termed Multi-jet Hydrodynamic Cavitation Abrasive Finishing (MJ-HCAF) and features high-pressure cavitation (up to 35 MPa) at the core, surrounded by low-pressure slurry (up to 5 MPa). The synergistic effect stemming from this cavitation bubble-particle interaction accelerates the abrasives to intricate zones in a complex channel and finishes the surface.

Improvements in the range of 60–90% (Sa <1 μm and Sz < 20 μm) were observed in MJ-HCAF of PBF-LB/Alloy 625 using an abrasive concentration of ≤1% weight with a processing time of up to 15 min,

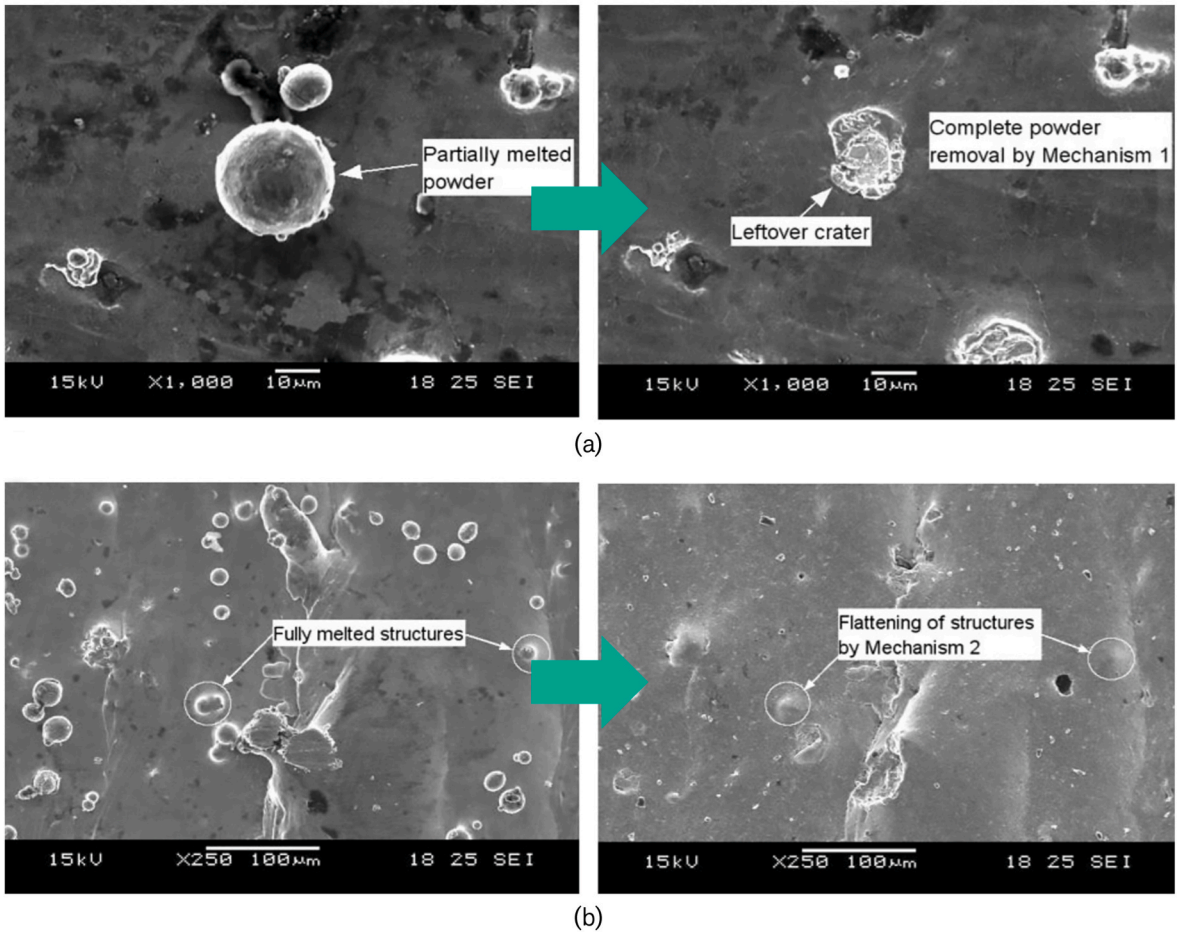

Fig. 18. The surface characteristics of PBF-LB/Alloy 625 after ultrasonic cavitation abrasive finishing (UCAF): removal of partially melted powders by cavitation-based erosion (mechanism I) (a), and surface peaks removal by abrasive impacts (mechanism II) (b). Adapted from Ref. [187].

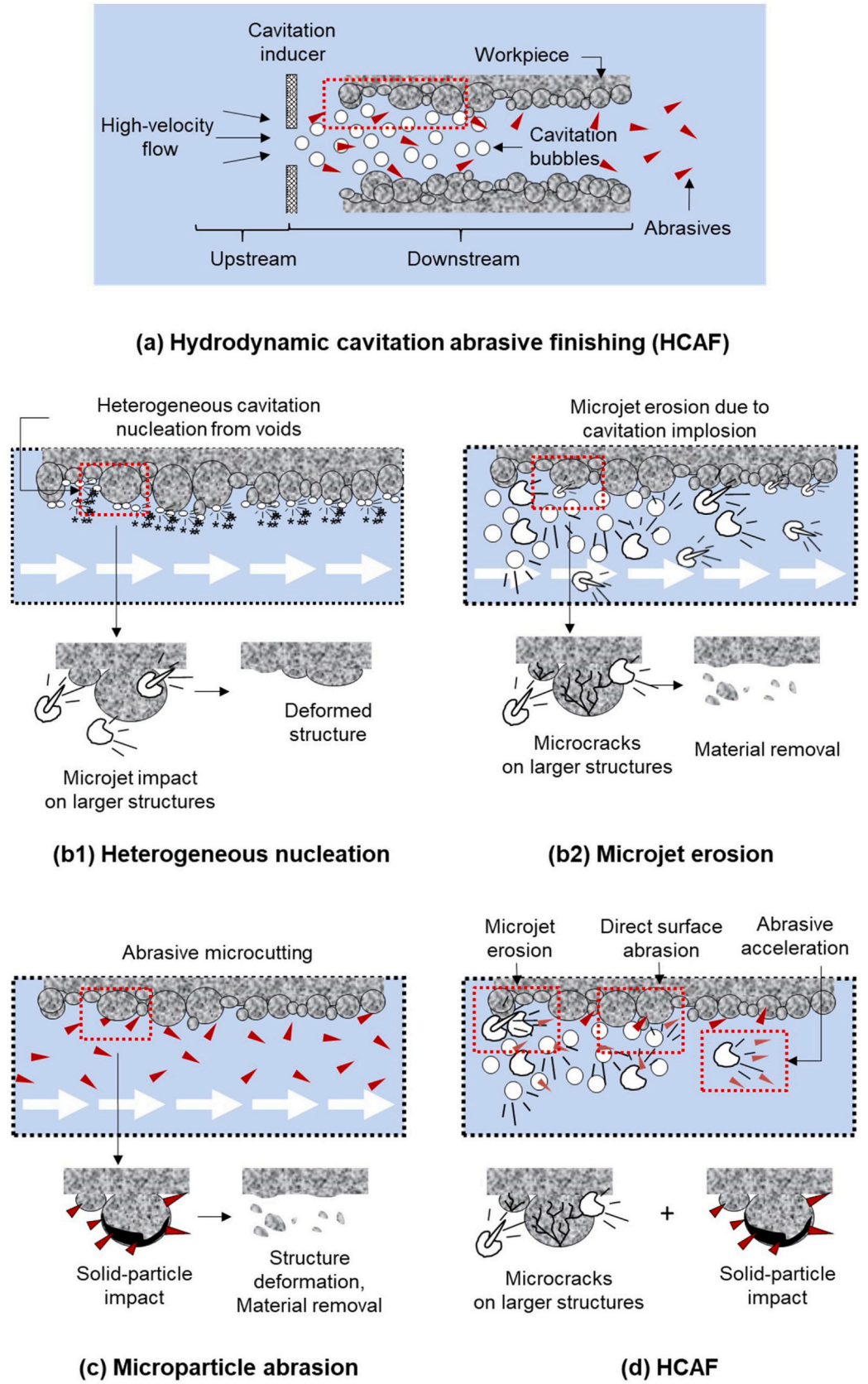

Fig. 19. Illustration of synergistic material removal mechanisms of hydrodynamic cavitation abrasive finishing (HCAF) of internal channels (PBF-LB/AlSi10Mg): overview of mechanisms in HCAF process (a); pure-cavitation finishing (b); pure-abrasive finishing (c); and synergistic effect of combined cavitation and abrasion processes (d) [190].

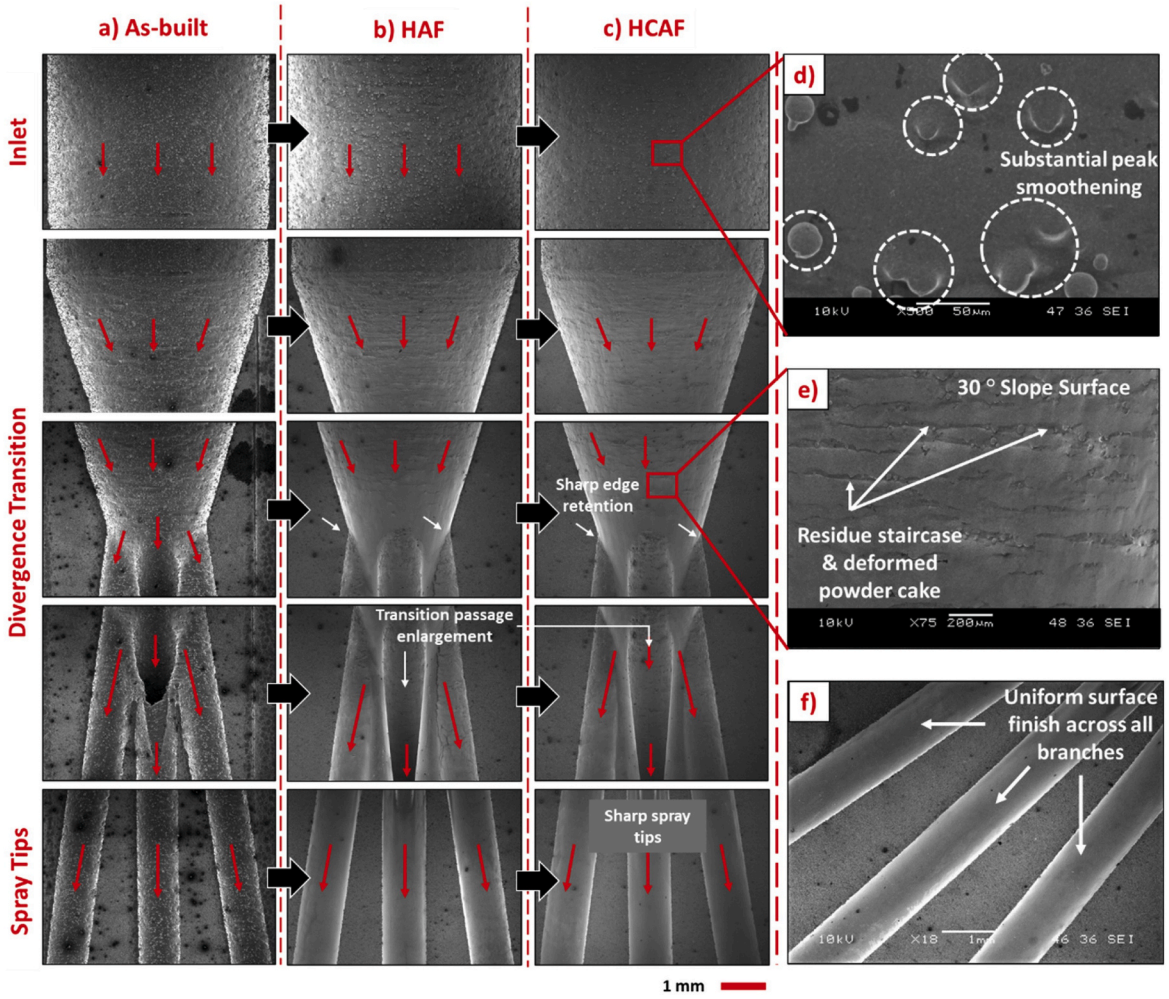

Fig. 20. Improvements in the topography of divergent fuel spray nozzle surfaces (PBF-LB/Alloy 625) at different locations after Multi-jet Hydrodynamic Cavitation Abrasive Finishing (MJ-HCAF): in as-built condition (a), after hydrodynamic abrasive finishing (HAF) (b), after hydrodynamic cavitation-assisted abrasive finishing (HCAF) (c) [193].

depending on the geometry of the channels [192]. The use of extremely low abrasive concentration provides the advantage of surface finishing while preserving the geometric accuracy of the channels (with diameter 1 mm, length 100 mm). The MJ-HCAF process has also been applied to finish complex channels in fuel injection/spray nozzles with multiple branches, as shown in Fig. 20 [193]. The authors reported substantial peak smoothing (75% improvement) with a staircase effect in the entrance zones, while observing a uniform finish across all branches of the nozzle with Ra < 2 μm and Rz < 20 μm (~80% reduction).

4.3. *Electropolishing processes*

Electropolishing (EP) removes a small but finite amount of metal from metallic surfaces that, in addition to smoothing and brightening, produces damage-free surface integrity (e.g., without crystallographic and grain-boundary alterations). EP is a batch-finishing process, where the parts are immersed in an electrolyte, and by applying electrical current, the material on the workpiece is removed. In comparison to previously discussed finishing processes, EP is capable of finishing complex, irregular or asymmetrical (including internal) surfaces. EP falls under the umbrella of electrochemical machining (ECM), which involves non-contact material removal by means of anodic electrochemical dissolution [194]. Here anodic refers to the anode-acting workpiece, which is electrochemically dissolved. The EP process was patented in 1930 by Jacquet [195], who also first reported on its capability to obtain a polished-like surface electrolytically by using a workpiece as the anode in an aqueous acidic solution while applying a certain current density. He proposed any metallic plate to serve as a cathode. Jacquet [196] later also introduced the current density-voltage curve to analyse the dissolution process. EP is typically carried out in the limiting-current plateau portion of the current density-voltage curve, where the voltages are higher than required by etching and passivating. Electrolytes used for EP are traditionally based on concentrated acids, such as phosphoric, sulfuric, etc. [197]. A typical electropolishing solution consists of an equal volume mixture of 96% mass fraction sulfuric acid and 85% orthophosphoric acid [198]. Electrolytes specially developed for EP of AM parts feature at least one phosphonic acid [199] and at least one polyalcohol to act as a complexing-/wetting-agent and viscosity modifier.

According to ISO 15730:2000 [198], EP is defined as the process of smoothing and brightening a metal surface by making it anodic in an appropriate solution. Here, smoothing refers to the elimination of surface roughness >1 μm, whereas brightening refers to the removal of surface roughness <1 μm. Such a distinction based on obtainable surface roughness is a simplification. From the fundamental material removal perspective, surface-roughness reduction on a macro scale is caused by the current concentration on most exposed peaks of a surface roughness profile, where a localised (ionic) dissolution rate is the highest. Brightening, however, is the outcome of eliminated surface defects. Consequently, a fundamental understanding of the process entails knowledge of atom removal from the crystal lattice, surface kinetics and passivation behaviour [197]. These theoretical aspects were recently reviewed by

Han and Fang [196]. The understanding of essential mechanisms of EP, however, is still not complete, despite years of research. This is evident by the prevailing experimental, trial-and-error approaches to design and optimise EP, according to the examined research papers and patents.

Metal parts are always passivated as a result of the electropolishing process. Passivation decrees the chemical reactivity of a metallic surface, by forming a thin (e.g., 2–4 nm) surface-oxide film [200]. In stainless steel, the passive films formed on surfaces exposed to acids consist of an inner oxide layer and an outer hydroxide layer (i.e., the passive film mainly consists of Fe and Cr oxides and hydroxides). While the thickness of such a passive film increases linearly with applied cathodic potential (mV), its stability depends on the compositions of the alloy, the temperature (of the electrolyte), and the processing time. In EP of PBF-LB/Ti6Al4V, the finished surface contained a passive film composed of TiO_x, Al_2O_3 and VO_x oxides [201]. In addition to improved passivation and consequent corrosion resistance of parts, EP is capable of providing surface-stress relief and removal of surface carbon and oxides. The indication of hydrogen embrittlement is not observed during EP. Since the metallic surface becomes passivated once submerged into an electrolyte with strong oxidizing properties, the passivation layer can be broken down in a controlled manner. Such a process, featuring material removal by passivated layer breakdown, is termed isotropic electrochemical etching (IEP) [202]. This process uses highly dissolved electrolytes at low temperatures. The shape of the etching holes is hemispherical, and they grow larger and overlap with the process duration. Such random formation, growth and merging of etching sites constitutes a main material-removal mechanism. The process was proven capable of finishing inner surfaces/bores and a maximum material removal rate of 15 μm/min.

The AM materials under EP consideration here include, but are not limited to, aluminium alloys, titanium alloys, and stainless steels. Rotty et al. [203] studied the effect of the material microstructure on EP. Here a conventional 316L stainless steel with a homogenous austenitic microstructure was compared to PBF-LB/316L, featuring melted clusters with cellular dendritic microstructure. These two crystallographic structures and surface morphologies are obviously different despite the same material compositions. It should be further noted that the hardness of PBF-LB/316L alloy was 25% lower compared to conventional material (i.e., 280 vs. 208 HV). To compare the material effects, the EP conditions were the same for both samples. These were immersed in a mix of sulfuric and phosphoric electrolytes. Different potentials and electrolyte temperatures were tested. It was observed that the EP outcomes in terms of obtainable surface topography were not the same, which means that the process is sensitive to the incoming microstructure. This poses a significant challenge as the surface smoothing/-brightening cannot be a priori predicted. The experiments revealed, however, that the optimal operating window (current density vs. voltage) is at the end of the limiting-current plateau.

EP can be further used to machine internal surfaces. A recent study by Zhao et al. [204] was concerned with ECM of internal holes of PBF-LB/304 L stainless steel, where the electrolyte was a 10 wt% $NaNO_3$ salt solution. The material-removal mechanisms responsible for removing semi-sintered particles/powder from the internal surface of the hole are shown in Fig. 21. The microscopy here reveals that the adhered powders and the band protrusions were dissolved simultaneously, where the most protruded surface irregularities – where the current density is localised and highest – were broken first to form half-spheres/craters and basin shapes, according to known smoothing mechanisms. In this case, the surface roughness was reduced by 55% from Sa = 14.151 μm to Sa = 6.287 μm. Further reduction of surface roughness, could be possibly achieved by optimising the EP system parameters, including the selection of the electrolyte.

ECM processes are widely established and have been used in the aerospace and medical sectors for more than 30 years [194]. An early example of ECM industrial application was Rolls-Royce's production of compressor blades for jet turbines, where ECM implementation was driven by the possibility of producing blades in smaller batch sizes and the process capability to machine complex geometry while achieving damage-free surface integrity, as the parts are not subjected to mechanical or thermal stresses. Similarly, ECM is also a long-established process in the production of artificial hip joints made of Ti and CoCr alloys. The ECM application areas are gaining a new momentum with the advent of AM, making EP a capable finishing technology for post-processing AM parts. For example, EP of PBF-LB/Ti6Al4V was able to uniformly smooth the highly scattered initial roughness values (Ra = 4–25 μm) due to different build-orientation angles down to Ra = 1–3 μm [205]. This result suggests that EP is capable of finishing parts with different (initial) levels of surface roughness, and that the amount of dissolved material is largest on the workpiece surface with the highest surface roughness (with the largest quantity of semi-sintered particles on the surface). The reported surface-thickness reduction time here was between 5 and 8 μm/min. Furthermore, 20 min of processing were required to achieve Ra<4 μm target, while removing 0.12 μm from the 0°-oriented surface and 0.28 μm from the 135°-oriented surface. This necessitates careful tolerancing of dimensional allowances for the as-built parts. Build angle also affected the achievable Rsk values. These were either positive or negative, indicating different levels of final surface isotropy (and level of the contact area).

The recent wider adoption of EP for post-processing AM metal parts is further driven by the availability of the commercially available turnkey post-processing solutions, such as the trademarked "Hirtisation" technology package developed by RENA Technologies Austria. "Hirtisation" is hence not a commercial name for electropolishing, but a three-step electrochemical post-processing spanning, (a) electrochemical jet machining (hydrodynamic electrochemistry) capable of removing support structures as well as powder cake, (b) EP smoothing (e.g., levelling the surface to Ra = 2 μm), and (c) EP brightening (e.g., achieving Ra = 0.5 μm). Other machine-integrated auxiliary operations include cleaning and a vacuum-drying process. Their patented EP [206] combines a 1) steadily-increased/ramped DC current with a 2) pulsed current – in a single-anodic pulse. The process, however, is controlled by the whole (input) pulse sequence, i.e., both anodic and cathodic pulse. In general, the anodic pulses have a wide current-density range, between 0.5 and 30 A/dm^2. In practice, the process is voltage controlled and the voltage increase of the ramp pulse depends on the initial surface roughness. The number, amplitude and frequency of the pulsed currents that follow the ramp pulse are material dependent. Examples of EP process design are illustrated in Table 3.

The illustrated case studies imply that control of the EP is complex and requires a careful selection of the current density (voltage signal) as well as pulse lengths, slopes and pauses – which are dependent on both workpiece material and initial surface roughness. The need to appropriately select a corresponding electrolyte (different acids, other solutions and mixtures) and its temperature further adds to this complexity. The exemplified "Hirtisation" of PBF-LB/316L above further implies that in certain cases – where the initial surface roughness is very high – a pre-treatment is needed to remove powder. In this industrial solution, such pre-treatment is done using electrochemical jet machining (EJM). This technique can achieve jetted material removal with an anodic workpiece [207]. EJM has been recently used to post-process EBF-LB/-Ti6Al4V parts, achieving an 87% surface roughness reduction from Sq = 18.6 μm (as-built) to Sq = 2.4 μm [208]. The underlying material-removal mechanism here was influenced by erosive loose-powder removal from the impinging jet flow and anodic dissolution (electrochemical removal). Smoothing was therefore achieved by 1) electrochemically and erosively removing semi-sintered particles from the surface, and 2) electrochemical surface etching and levelling. ECM can be also used for removing supporting structures of AM parts [209]. Here higher voltages are applied and the electrolyte preferably contains a stronger acid to achieve a targeted duration of the treatment between 30 and 60 min.

Despite all its advantages, EP also presents some challenges. First,

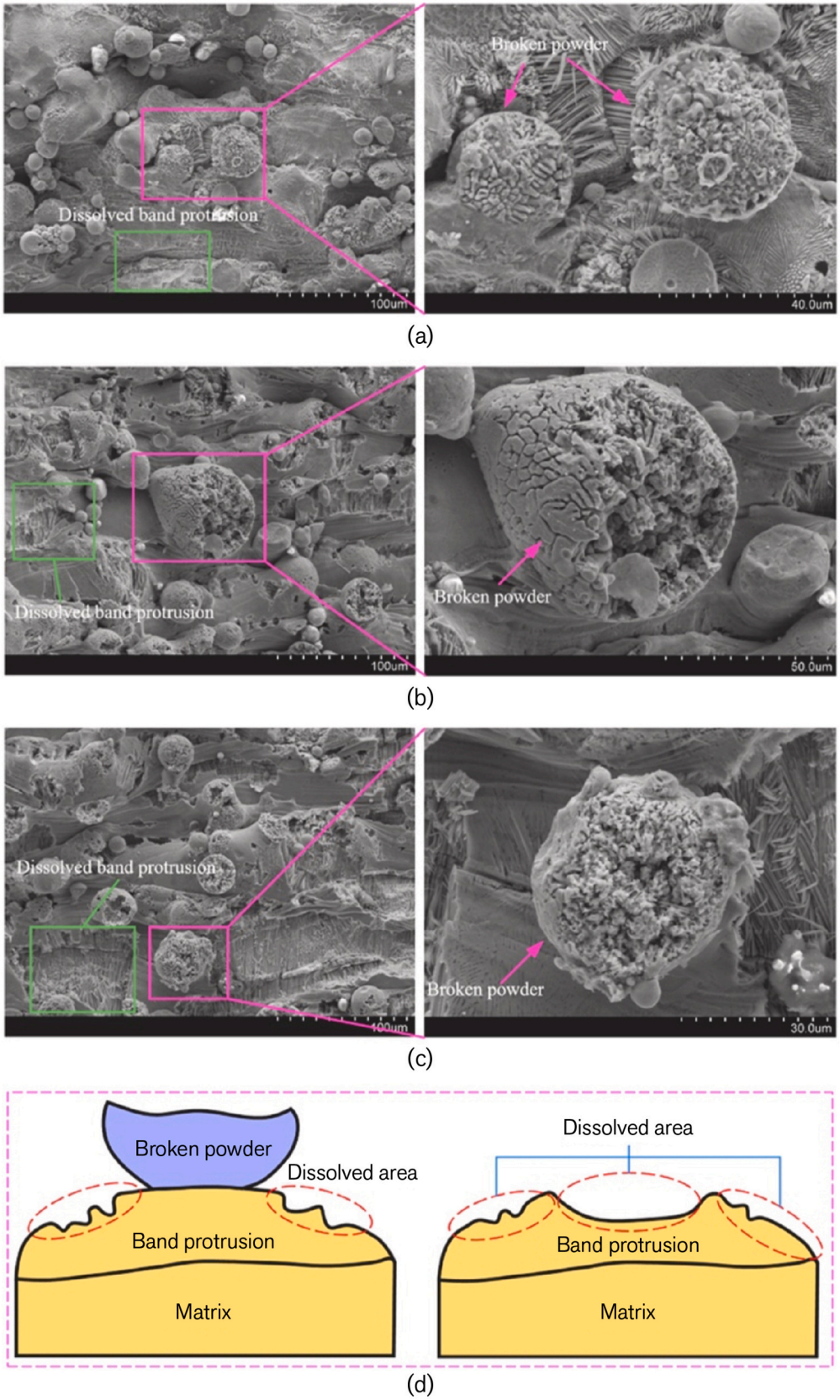

Fig. 21. Topography of electro chemical machined (ECM) internal surface with 5 A/cm^2 current density at different processing instants: 5s (a); 15s (b); 30s (c); schematic illustration of material removal mechanisms (d) [204].

Table 3
Examples of EP pulse-sequence design and finishing effects [206].

	PBF-LB/Ti6Al4V	PBF-LB/316L
Initial surface roughness	Ra = 14 μm	Ra = 50 μm
Pre-treatment/support removal	None	Electrochemical jet machining
Anodic pulse	• Ramp voltage: 0–3 V • Pulses: 3–12 V (5 Hz) • Pulse sequence: 10x • Cathodic pulse: 15 V	• Ramp voltage: 0–6 V • Pulses: 2.5–6 V (10 Hz) • Pulse sequence: 5x • Cathodic pulse: 0 V
Electrolyte solution (% by vol.)	• 25% sulfuric acid • 15% hydrofluoric acid • 60% glacial acetic acid	• 70% phosphoric acid • 20% sulfuric acid • 8% polyethylene glycol • 2% water
Operating temperature	N/A	45–55 °C
Final surface roughness	Ra = 0.5–0.8 μm (17x reduction)	Ra = 1 μm (50x reduction)

there is a need to investigate the complex relationship between the electrical process parameters and the chemical aspects of an electrolyte, as well as their individual and synergistic effects on the capability of EP to smooth and brighten AM surfaces. The majority of reported results are purely experimental, with some exceptions that attempted to model and simulate the current density distribution on the AM surface [204] or the evolution of material removal/surface smoothing [202]. Such efforts are needed to reduce the time-consuming experimental effort and/or dependency on commercial turnkey solutions. Moreover, there are certainly sustainability concerns associated with EP/ECM. Sustainable manufacturing should conserve energy and material with waste prevention and environment protection as integral parts of production [210]. As demonstrated here, there are attempts to use less aggressive and harmful acids, e.g., by using more environmentally-friendly salt solvents [204]. They might not be as effective in reducing surface roughness, but there is a space to develop more sustainable solutions that are safer to handle, and which could still be effective if combined with proper process parameters. Last but not least, non-conventional and hybrid EP processes, such as magneto-EP, EP with ionic fluids and plasma-electrolytic polishing are not discussed here, as they were recently included in the EP-focused review [196].

4.4. Laser polishing processes

As a non-contact method, laser polishing utilises highly intense laser beams as an energy source to smooth the surface of various materials [211–214]. It should be noted that surface finishing can be also achieved by non-laser energy sources, such as electron and plasma beam [215]. However, laser-beam irradiation is the focus of this review paper.

Laser polishing can also feature/combine several laser sources in a single finishing setup. For example, Liu et al. [216] combined pulsed laser and continuous wave laser (WL) to post-process DED-LB/Alloy 718. The finishing capability of such hybrid laser polishing (HLP) can be measured in terms of obtained surface roughness levels. Here, the initial surface roughness of the as-built workpiece (Ra = 15.75 μm) was first reduced to Ra = 6.14 μm by single-pulsed laser polishing (SPLP) and finally to Ra = 0.23 μm by the additional use of a continuous wave (CW) laser (Fig. 22). Here the CW laser has 8 times higher output energy compared with the pulsed laser in SPLP, which leads to enhanced re-melting of the surface, a surge in the depth and size of the molten pool and extended solidification time, which all lead to an improved surface finish.

The crystal growth in a smaller molten pool (i.e., in SPLP) is faster, which restricts the element diffusion and secondary phase precipitation.

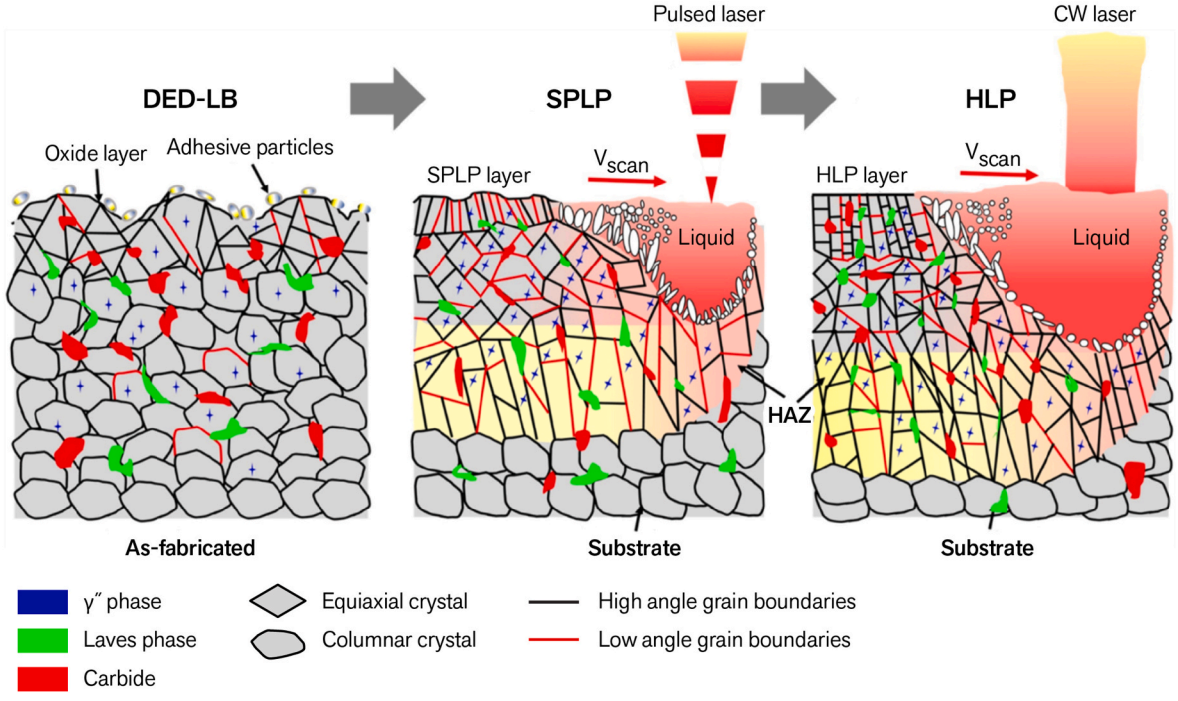

Fig. 22. Schematic illustration of the induced microstructure changes and crystal growth in DED-LB/Alloy 718 processed by hybrid laser polishing (HLP). HLP includes continuous wave (CW) laser polishing after single-pulsed laser polishing (SPLP) to further improve the surface properties [216].

During the cooling of the molten pool, the bulge is formed when the surface tension gradient in the molten pool is positive. Such wavy underlying shape of a part (i.e., protruded surface with characteristic height, depth, and width) formed in the centre of the polished track is not a phenomenon limited to AM-fabricated materials. For example, it was shown that bulges were introduced to the surface topography when laser polishing conventional 316L while the surface roughness (Ra) was reduced by 35%. This implies that it is possible to reduce surface roughness even if bulges are formed [217]. Therefore, the SPLP first yields a bulged/wavy surface form, whereas the final surface texture is determined by the CW laser processing. Moreover, the different lasers used in HLP have dissimilar effects on surface integrity. The SPLP largely refines the grains and secondary phases in the re-melted region, resulting in a cellular structure. The HLP also refines the grain and secondary phase, but the secondary phases still display array distribution. Moreover, the tangled dislocations organise along the interface of secondary phases. The SPLP reduces the microhardness, whereas the HLP increases the microhardness of the treated surfaces [216].

To overcome such conflicting effects on surface integrity, it seems necessary to gain a more fundamental understanding of the complex re-melting and its effects on mechanisms determining final surface integrity. The physics of the melt-flow/re-melting [218] in laser polishing are in principle similar to that of PBF-LB itself. This similarity should pave the way for more fundamental investigations to tackle materials/surface integrity challenges pertinent to laser polishing of AM materials.

Many studies are available covering a wide spectrum of different AM materials and different types of laser beams, from finishing planar to complex geometries [219–221]. One of the first papers on laser polishing of PBF-LB/stainless steel was published 15 years ago [222]. This particular application is still widely researched. The work of Chen et al. [223] was concerned with laser polishing PBF-LB/316L, where a fibre laser (1070 nm) could reduce surface roughness by over 92% (from 4.75 μm to 0.49 μm Sa) while also incorporating partially melted powders originally on the as-built surface layer. The XRD analysis revealed no substantial phase change after finishing and it was observed the process refined the columnar structure within the as-built sample into a fine cellular structure. Additionally, the sub-surface microhardness of the laser re-melted layer increased from 1.82 GPa to 2.89 GPa. Such an improvement of surface texture, combined with grain refinement, can improve corrosion resistance according to the authors. This was further elaborated in a dedicated material characterisation study, which revealed that laser polishing refined the grains of the re-melted region and that the areal fraction of grains with sizes smaller than 10 μm increased from 16.4% to 23.2% [224]. Compared with the as-built part, the proportion of cellular sub-structures increased after laser polishing. The dislocation wall and dislocation tangles occurred at the sub-structure boundaries and within some sub-structures and appeared to be more pronounced after finishing. The aspect ratio of the grains slightly increased from 2.36 to 2.49 after laser polishing. Obeidi et al. [225] also investigated the laser polishing of PBF-LB/316L using CW laser beam irradiation (CO_2 laser). The effects of various process parameters including the laser beam power, the rotational speed of the cylindrical samples, the number of laser scanning passes, the laser beam focal position, and the overlaps between successive laser scanning passes were studied. The authors reported a marked reduction in Ra surface roughness from 10.4 μm to 2.7 μm. However, the inconsistencies in the surface topography of AM sample posed a major challenge to unleash the full potential of laser polishing. This is because the surface inconsistencies of as-built materials, i.e., the local surface topography variations, make it difficult to determine the optimised laser polishing parameters for the entire surface.

Marimuthu et al. [226] laser polished PBF-EB/Ti6Al4V using a CW fibre laser at 1070–1090 nm wavelength, with a maximum power output of 200 W. The authors reported that excessive thermal energy input during the process can result in surface oxidation and carbonisation. Experimental results showed a reduction of Ra surface roughness from 10.2 μm to 2.4 μm when restricting the melt pool convection to a minimum. Similar application by Tian et al. [227] achieved comparable surface finish, but reported several surface integrity issues. For example, the re-melted layer underwent a change in texture and grain structure, and a martensitic transformation. In addition, a high level of near-surface tensile residual stresses was generated by laser polishing. Yung et al. [228] utilised laser polishing to improve the surface roughness of PBF-LB/CoCr alloys by using a strategy to adaptively adjust the laser defocusing distance according to the parts' geometry. Recent advances in controlling laser polishing refer to partitioning a 3D/freeform surface into triangular laser processing fields to maximize process efficiency [229]. During the demonstration of this method, the Sa/Sq surface roughness of PBF-LB/Ti6Al4V alloy was reduced by up to 96% using a nanosecond laser source. Laser polishing further proved feasible for finishing binder jetted stainless steel, BJT/316L [230]. Here, a nanosecond laser source with a maximum average power of 50 W and wavelength of 1064 nm was used to achieve over 94% reduction in surface roughness (from 3.8 to 0.2 μm Sa). All laser-polished surfaces were free of the build marks, pits, holes, lumps and irregularities that were observed on the as-received samples.

In addition to laser polishing, laser peening or laser shot peening (LSP) can be also used for post-process finishing of AM parts. In this process short, intensive laser pulses create a plasma in a confined geometry and thereby generate pressure pulses that create local plastic deformation normal to a workpiece surface [231], resulting in high compressive stresses in the surface and consequently an improved fatigue life. LSP generates a small amount of cold work (e.g., 3–5%), typically leaving the phase, hardness, and yield strength of the finished material unchanged. In this consideration, LSP is not intended to improve surface roughness, but to refine microstructure, impart deep compressive residual stress, and delay crack propagation in a narrow/limited area. As the scope of this review paper is limited to post-process finishing operations that primarily improve surface topography, a wide range of peening processes (LSP [232], shot-peening [233], waterjet-peening [234]) are not discussed in further detail despite their capability to improve material microstructure and improve functional performance of AM parts.

5. Functional performance

Functional performance of post-processed, AM-fabricated products, such as fatigue life, friction, wear, corrosion, etc., depend on product design, manufacturing methods, and material. Applications including high-fatigue load-bearing components in aerospace, internal passages for fluid-flow applications, and corrosion-susceptible medical implants require specific design considerations, determining manufacturing methods and material selection. In view of manufacturing methods, AM-processing (e.g., PBF-LB) to a large extent pre-determines the achievable surface integrity, whereas post-processing primarily determines dimensional and geometrical form (e.g., roundness, flatness) accuracy, as well surface topography (surface form and texture). For example, Blinn et al. showed that the AM process overrules the influence of post-processing (milling and grinding) on fatigue life due to pronounced effects of AM-induced defects [235]. Functional performance hence obviously depends on material as well, i.e., 1) its constitutive properties and 2) material-processing properties (AM-induced surface integrity, e.g., internal porosity, bond failures, residual stresses and cracks).

A post-processed, AM-fabricated product might need to satisfy multiple demands on functional performance at the same time, like high-cycle and low-cycle fatigue of turbine components. Sometimes a product might be required to meet only one, such as aesthetic appearance (e.g., mirror-like surface achieved by polishing) or fluid flow property (e.g., laminar liquid flow for cooling). The investigations of post-processing effects on functional performance of AM-fabricated products generally focus on three aspects, i.e.: 1) high cycle and low cycle fatigue life (HCF and LCF), 2) friction/wear, and 3) corrosion. These are briefly reviewed

in the following subsections for 316L, Ti6Al4V and Alloy 718.

5.1. Impact on fatigue performance

5.1.1. 316L

Shrestha et al. [236] reported on the effects of layer orientation and surface roughness on the mechanical properties and fatigue life of PBF-LB/316L round specimens. Quasi-static tensile and uniaxial fatigue tests were carried out on specimens fabricated in vertical and diagonal directions (as-built surface condition) and in horizontal, vertical, and diagonal directions after a subsequent machining process. It was observed that in the machined condition, horizontally built specimens displayed higher fatigue resistance, followed by vertically built specimens, and the lowest fatigue performance was observed for diagonal specimens. This was also observed in the as-built condition where vertical specimens demonstrated better fatigue performance when compared to diagonal specimens. Further, despite the important reduction of surface roughness in the machined LB-PBF specimens, the impact on fatigue performance was only marginal, suggesting that the presence of larger internal lack-of-fusion defects had a dominating effect on initiation of fatigue cracks in PBF-LB/316L. Elangeswaran et al. [237] compared the fatigue performance of the as-built and stress-relieved PBF-LB/316L prior to and after machining with that of wrought material as the reference point. The authors observed a significant improvement in fatigue performance (HCF) after machining, comparable with that of wrought material. This improvement was attributed to the much better surface finish properties of the machined samples: The initial surface roughness (Ra) was reduced from 7.2 ± 1.3 μm to 0.5 ± 0.06 μm. The results also showed stress relieving did not have a major impact on HCF of PBF-LB/316L, and the influence of surface roughness was more pronounced. Removal of the surface and sub-surface defects using an appropriate machining process (within finishing range) was necessary to obtain reasonable fatigue performance for high-end applications where the parts are subjected to high alternating loads. Blinn et al. [235] compared the HCF performance of PBF-LB/316L in as-built condition and after machining (milling and grinding) with that of continuously cast material subjected to similar finishing processes. In addition, two different printing strategies were examined to reveal the role of surface and sub-surface defects on the HCF before and after finishing processes. The authors reported a significant improvement in surface finish properties of AM material, which was even better than those of cast material in some cases. Interestingly, a better surface roughness (Sa and Sz) was obtained after milling as compared with pendulum grinding. Fatigue lifetime of PBF-LB/316L depended mainly on the density of defects inherited from the AM process itself, and improved surface finish had a minor impact on HCF performance of additively manufactured material. It was then concluded that an optimal selection of process parameters to reduce the density of defects (e.g., gas porosity and Lack-of-fusion) is of greater importance than the subsequent post-processing. In other words, it is not possible to improve the fatigue performance of the AM parts unless the density of defects is kept minimal. This can be achieved by optimising the AM process parameters and application of HIP post-treatments.

5.1.2. Ti6Al4V

Products manufactured by AM processes are characterised by significant surface roughness and surface-integrity related (internal) defects, which are detrimental for aerospace applications subject to highly stressed and cyclical loads. An early work from Airbus was concerned with investigating the effects of milling, (Al_2O_3) blasting, vibratory finishing, and mechano-chemical finishing of PBF-LB/Ti6Al4V [151]. Here the details of abrasive fine finishing are to a large extent missing, except that both processes took 48–50 h. The authors showed that milling achieved minimum surface roughness and the most improved fatigue performance due to ample material removal. This may imply a too-rough initial surface texture, which could not be improved using the selected finishing processes. In general, abrasive fine-finishing processes – characterised by very low specific energy (and low aggressiveness/chip thickness) – should yield reduced surface roughness compared to metal-cutting processes [150]. The authors further claim there is no direct correlation between (a specific) roughness value and fatigue life, which implies the necessity of investigating wider surface integrity effects, such as subsurface defects and microstructure. This was addressed by Witkin et al. [238], who observed that surface roughness improvement in abrasive fine finishing does not necessarily enhance fatigue performance if only geometrical irregularities are removed from the surface, while the roots of surface defects, where fatigue cracks initiate, are left intact. Kahlin et al. [153] published a similar investigation of post-processing effects on fatigue strength. The workpiece material here was both PBF-LB/and PBF-EB/Ti6Al4V, post-processed by shot peening, laser shock peening, centrifugal barrel finishing, laser polishing and brushing (linishing). In contrast to the results of Bagehorn et al. [151], centrifugal barrel (mass) finishing gave the best results in terms of fatigue strength, i.e., +125% for PBF-LB and +100% for PBF-EB material, respectively. This is due to a combination of low surface roughness, large compressive residual stresses (about −550 MPa), and absence of material defects. The performance of a finished AM product is hence comparable to wrought and machined Ti6Al4V. Centrifugal barrel (mass) finishing in this case was carried out in three stages: 1) 120 min of roughing with ceramic 10×10 mm triangular media and 50 ml acidic compound for descaling, 2) 90 min of smoothing with lower-concentration ceramic media (6×10 mm triangular shape) and 50 ml concentrated lubricant, and 3) dry finishing for 60 min with plastic media without a liquid compound. The main conclusion of this work confirms the necessity of addressing both surface topography and surface integrity in evaluating functional performance of post-processed AM products, as the fatigue strength depends on a combination of surface roughness, residual stresses, microstructure and sub-surface defects [153].

Another illustration of this can be found in the recent work of Childerhouse et al. [239], who investigated the implications of machining stock allowance on the surface integrity of PBF-EB/Ti6Al4V, subsequently followed by finish machining (face milling). Low cycle fatigue testing using a four-point bend test method was conducted on the machined PBF-EB specimens to assess the effect of the exposed surface defects on the fatigue performance of the material; see Fig. 23. Their results indicated that the PBF-EB specimens subsequently machined to a depth of 1.00 mm performed significantly better than those which were not subjected to machining or had been machined to a depth of only 0.50 mm, as evident from the data shown in Table 4.

In a subsequent and more comprehensive investigation following a similar testing protocol [240], the same authors reported on the influence of finish machining depth and hot isostatic pressing on defect distribution and fatigue performance of PBF-EB/Ti6Al4V specimens. Their results again confirmed that when employing a sufficient material removal depth during finish machining, a significant improvement in fatigue performance could be achieved, and this was attributed to the removal of a material zone rich in lack-of-fusion defects that were concentrated in the subsurface, as shown in Fig. 24. The application of HIP post-treatment was found to improve the fatigue performance to a smaller degree, as the treatment was only effective at reducing the volume of gas porosity but ineffective at healing the near-surface defects.

5.1.3. Alloy 718

The microstructure and basic mechanical properties (e.g., yield strength, ultimate tensile strength) of Alloy 718 produced by different AM methods have been extensively studied in recent years, as indicated by the recent review of Kok et al. [241] on this subject. Numerous studies showed that through an adequate post-processing heat treatment, the quasi-static properties of additively manufactured Alloy 718 could be comparable to or even outperform those of wrought material

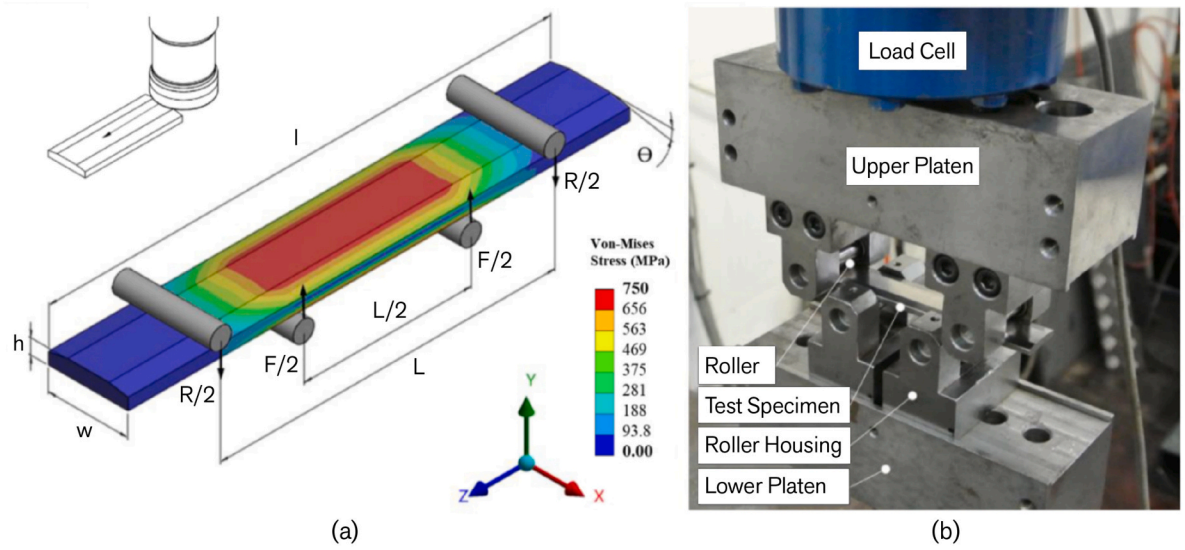

Fig. 23. Four-point bending test method used to obtain fatigue performance of the specimens. Schematic representation of the test method with superimposed predicted stress distribution (a) and the four-point bending test-rig (b). Adapted from Ref. [239].

Table 4
Summary of four-point bend fatigue test results at S_{Max} = 750 MPa [239].

Specimen condition	Mean Cycles to failure, Nf	Standard deviation (%)
As-built	1351	29.7
machined-0.5 mm	1705	17.7
machined-1.00 mm	3446	4.8

[242]. The fatigue properties are, however, found to be more affected by the surface condition (topography, roughness) of the AM Alloy 718 material [243] – as generally expected. Balachandramurthi et al. [244] investigated the influence of defects and as-built surface roughness on fatigue properties of PBF-LB/and PBF-EB/Alloy 718 using a four-point bending fatigue test setup. The AM materials were subjected to two different post-treatments, HIPing and machining. It was found that both HIPing and machining resulted in an improvement of the fatigue performance when compared to the as-built condition; see Fig. 25. According to the authors, the higher number of crack initiations from the as-built surface could be attributed to the valley-like features in the surface causing stress concentration and acting as micro-notches. The machined surface had a relatively lower number of crack initiating sites, thus explaining the better fatigue performance of the machined specimens. Witkin et al. [245] reported on the high-cycle fatigue performance of PBF-LB/Alloy 718 specimens tested using round uniform-gauge or hourglass specimens for various specimen orientations, stress ratios and surface conditions (as-built and machined). Only surface conditions, specifically near-surface process defects were shown to influence the fatigue properties where machined specimens consistently displayed a higher fatigue endurance limit than the as-built specimens.

Lee et al. [246] investigated the effect of various surface treatments, including sand-blasting, drag-finishing, turning, grinding, and grinding

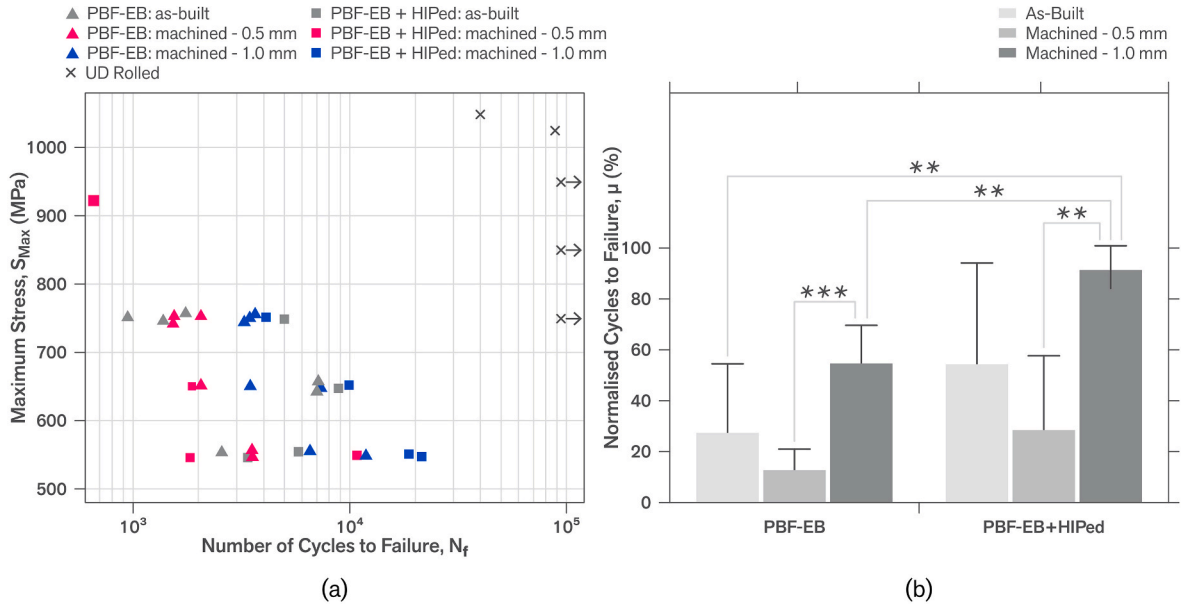

Fig. 24. S–N data for HIPed and non-HIPed PBF-EB specimens tested compared to those specimens machined from conventional wrought (UD rolled) material (a) and normalised cycles to failure data for HIPed and non-HIPed PBF-EB specimens machined at each stock allowance condition (b). *** indicates a significant difference $p < 0.001$, **$p < 0.01$. The error bars represent ±1 standard deviation. Adapted from Ref. [240].

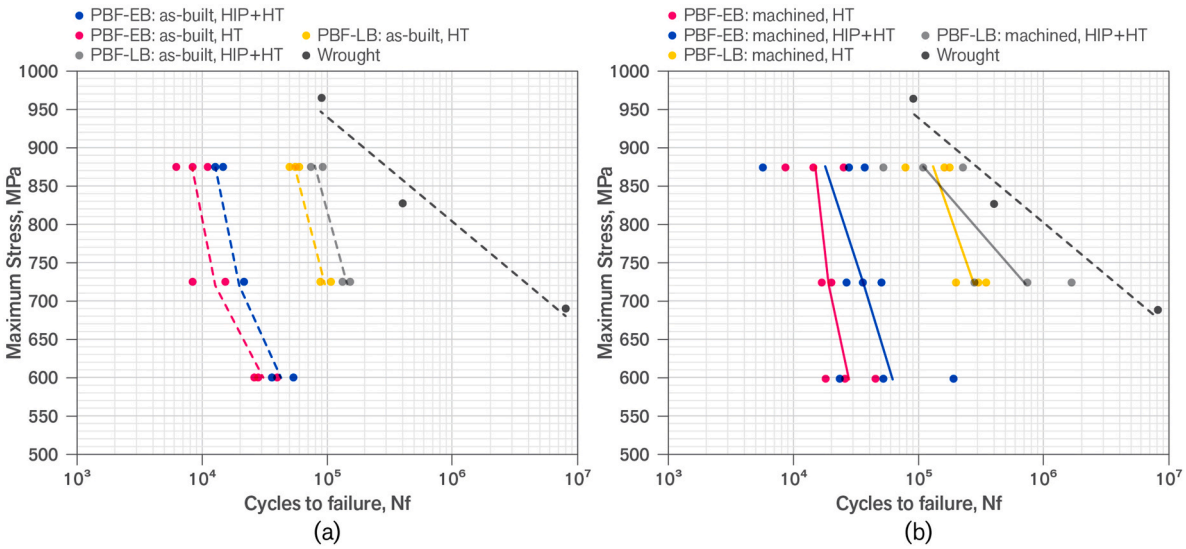

Fig. 25. S–N curves for PBF-EB and PBF-LB/Alloy 718 specimens in as-built and machined conditions. Adapted from Ref. [244].

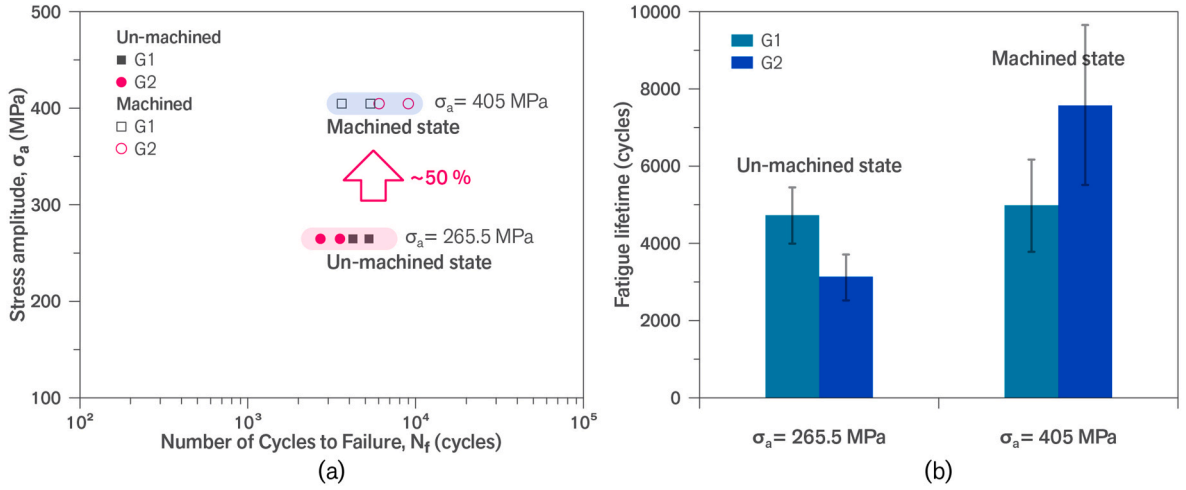

Fig. 26. Comparison of fatigue strength of G1 (thin, 1.3 mm) and G2 (thick, 3.3 mm) PBF-LB/Alloy 718 specimens before and after machining (a), and fatigue lifetime of the G1 and G2 specimens under the same surface state (un-machined state at σ_a = 265.5 MPa or machined state at σ_a = 405 MPa) [247].

+ drag-finishing, on surface roughness and fatigue properties of PBF-LB/Alloy 718. All the surface treatments resulted in improvement in surface roughness and fatigue performance with sandblasting and drag-finishing showing the least performance while grinding + drag--finishing displayed the highest. It was also found that only the cracks of grinding + drag-finished specimens initiated from crystallographic facets while those in other conditions were surface initiated.

Wan et al. [247] investigated the effects of surface roughness and build thickness on the high temperature (650 °C) fatigue properties of PBF-LB/Alloy 718. The authors reported that fatigue strength could be improved by ~50% after surface machining and polishing where the surface roughness Ra was reduced from ~14 μm to ~110 nm. The thinner un-machined specimens exhibited a longer fatigue lifetime than the thicker ones, while the opposite trend was observed in the machined specimens (see Fig. 26).

5.2. Impact on tribological performance

Many applications have distinct bearing-surface requirements, determining tribological behaviour in a sliding contact. These requirements are commonly set by specific surface-texture parameter targets, from the most used Ra (and areal Sa) to parameters related to material ratio curve. It was shown that even manually-removed material using coated abrasives (220–1200 mesh), combined with short-time polishing using a diamond slurry, can reduce as-built surface texture of PBF-LB/X40CrMoV5-1 tool steel to mirror-like finish at Sa = 0.15 μm [248]. The as-built layer (30 μm thick) here could not be removed by polishing alone, but the combined abrasive post-processing lowered the friction coefficient by about one order of magnitude (i.e., from 0.1 for as-built to 0.01 of finished sample). The abrasively finished surface furthermore showed a hydrodynamic lubrication for all tested sliding speeds, which was not the case for a laser-textured surface. Wear mechanisms in dry sliding of polished PBF-LB/316L stainless steel were studied by Bahshwan et al. [83]. Microstructural effects of AM-fabricated material (grain morphology and crystal texture) on wear are compared to annealed wire-drawn reference workpiece. Special attention is given to porosity-induced fracture, which not only affects fatigue life but also accelerates wear rate. The observed surface fractures are attributed to the pre-existing porosity, e.g., resulting from insufficient fusion of pores below the sliding surface (Lack-of-fusion defects), as shown in Fig. 27. The density and distribution of porosity depends on PBF-LB build orientation and scanning strategy and cannot be removed

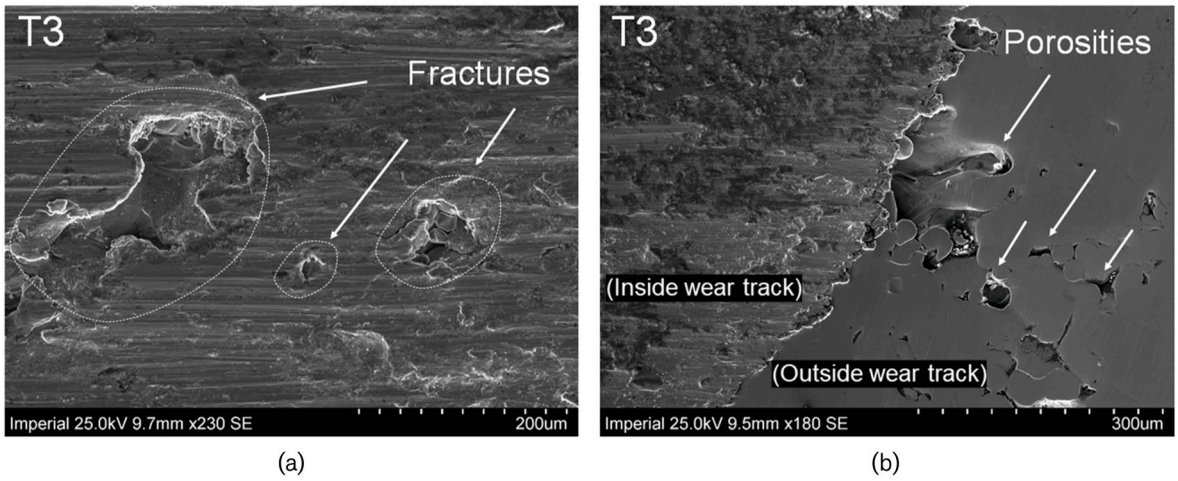

Fig. 27. Micrographs showing the fractures caused by presence of Lack-of-fusion pores inside the wear track of PBF-LB/316L (a) and evidence of Lack-of-fusion pores on unworn surface (b) [83]. T3 in the micrograph represents sliding surface parallel to reference TD-BD plane (the plane containing transverse and build direction vectors, see Fig. 7b).

by polishing, which is only able to remove material at nanometre-level depth of cut. Under load, stress concentrations induced by sharp corners of pores lead to large fracture chips. The authors argue that wear mechanisms can be controlled based on surface microstructure, and that wear resistance of a PBF-LB workpiece is not better or worse compared to conventional material. With this in mind, it is necessary to advance the understanding of abrasive fine-finishing processes on surface integrity and take work-hardening effects into consideration as well.

5.3. Impact on corrosion resistance

The influence of post-processing on corrosion properties of additively manufactured materials is also investigated in a few studies. For example, Melia et al. [249] studied the impact of build angle and post-processing on the susceptibility of PBF-LB/316L stainless steel to localised corrosion. The authors investigated five different surface finish treatments: 1) chemical passivation of as-built surface according to ASTM A967/A967M-1; 2) in-process surface re-melting by contouring implemented during the building process; 3) vibratory finishing (tumble polishing); 4) electropolishing and 5) grinding. The susceptibility of surface treated and as-built PBF-LB/316L was then compared with that of wrought material in ground condition. It was observed that a decrease in surface roughness (Sa) generally leads to an increase in breakdown potential (Eb), suggesting a reduced susceptibility to the initiation of localised corrosion for smoother surfaces. In this respect, material removal using coated abrasives (grinding) and electropolishing was viable option for smoothing the surface roughness and reducing the susceptibility to pit initiation (at increased Eb). Other finishing methods demonstrated mixed results. For example, vibratory finishing featuring a multitude of ceramic media could not completely remove distinct as-built surface features (e.g., highest asperities) after 3 h of processing. This might be improved by reducing the incoming roughness and/or optimising the abrasive media/compound used. The other important observation was that the roughness and topography of the as-built surfaces varied on top plane normal to BD and side walls, as shown in Fig. 28. This leads to directionality in corrosion properties of AM parts both in as-built condition and after post-treatment, since the process fingerprint may remain on the post-treated surfaces, as evident in this figure. Similar observations are generally made for other AM materials and processes. However, it is worth stressing here that the corrosion behaviour of the materials also largely depends on other factors such as the microstructural characteristics like cell and melt pool boundaries,

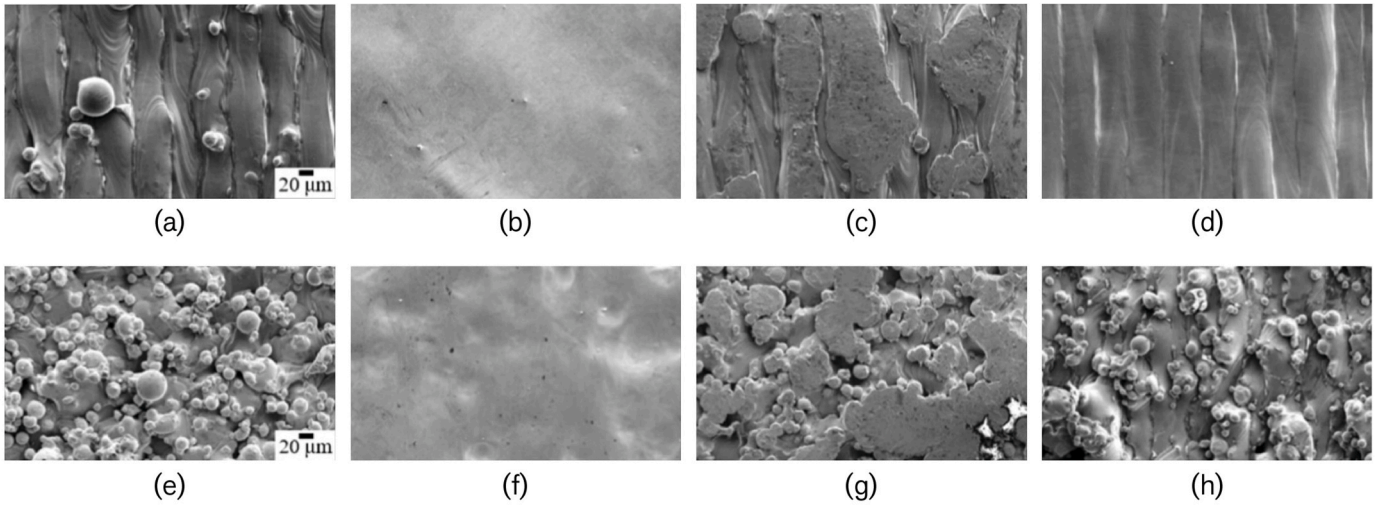

Fig. 28. The changes in surface topography of PBF-LB/316L samples induced by different post-processing methods. SEM images of finished surfaces for the top (a–d) and side orientations (e–h) with distinct surface topographies; as-built (a, e), electropolished (b, f), vibratory finished (c, g), contour scan/re-melting (d, h). Adapted from Ref. [249].

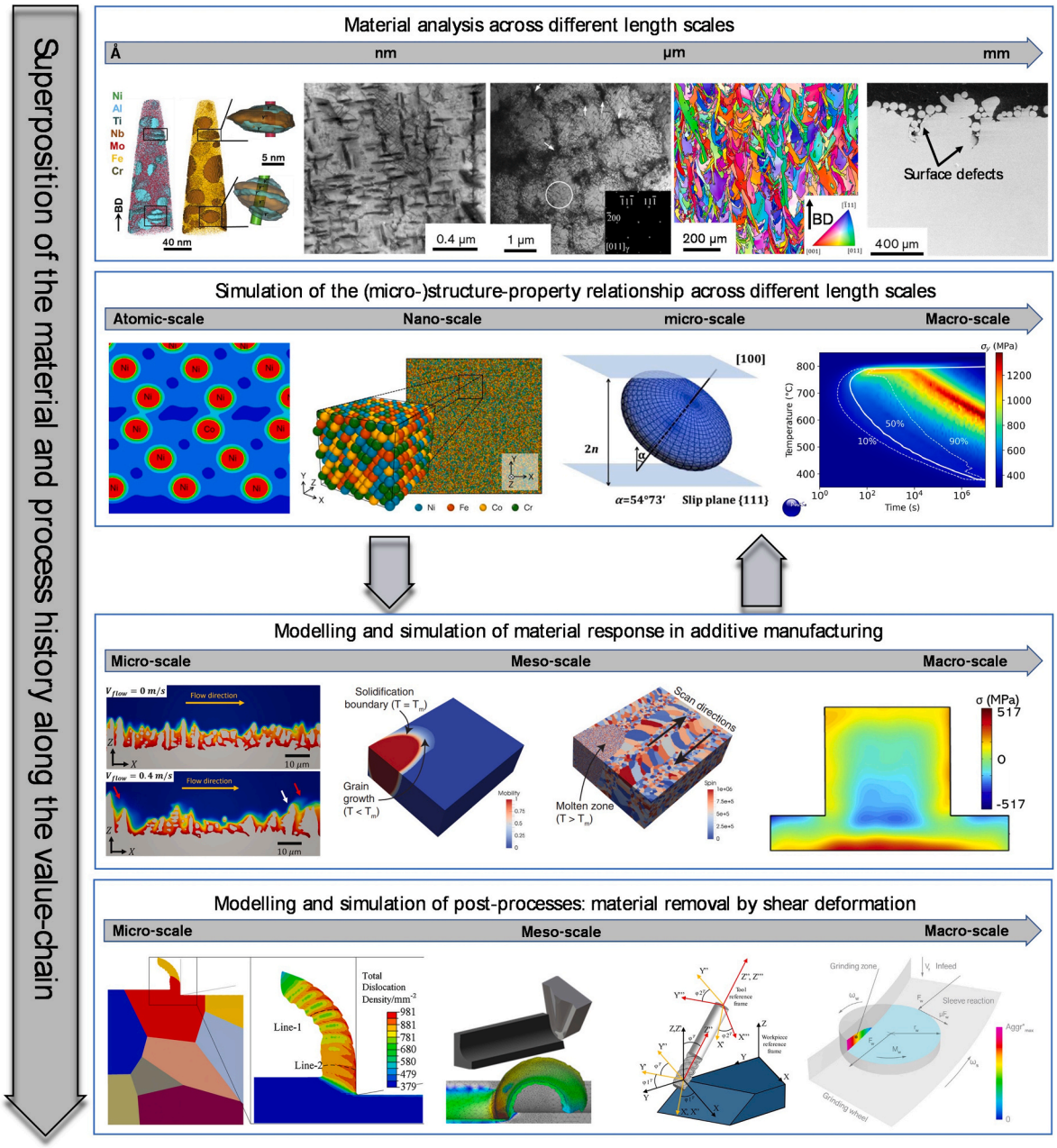

Fig. 29. Integrated Computational Materials Engineering (ICME) framework for superposition of the material and process history along the value-chain to develop generic physics-based platforms for prediction of material response during post-processes involving shear deformation, e.g., cutting and abrasive finishing [4,46,49,68,257–266].

nano- and micro-scale inclusions, micro-segregation of elements, texture and grain, and the density and size of surface defects [7,249]. This means the enhanced corrosion properties can be achieved only when the AM process itself and subsequent thermal and finishing post-treatments are optimised.

6. Summary and outlook

- The accelerated adoption of metal AM parts in a number of industrial sectors will to a large extent depend on the success of post-processing operations (process steps) taken after the completion of an AM build cycle in order to achieve the required properties in the final product. The surface roughness of as-built AM parts does not meet the precision requirements in the industry, so post-processing is unavoidable in most cases. Next to surface roughness, the lack of robustness in as-built and post-processed surface integrity – characterised by variations in material microstructure, residual stresses, defects, etc. – further impedes wider industrialisation of AM. A fundamental understanding of the surface integrity resulting from both additive manufacturing and post-processing is needed to properly design the interlinked manufacturing routes and to improve the resultant performance and functionality of AM parts.
- The surface properties and microstructural characteristics of the additively manufactured parts depend largely on the AM technology and the applied process parameters. In addition, the surface topography and roughness properties are not consistent in as-built parts and vary, for example, with the build angle and the position of the parts on the build plate. The numerous material, design and process variables involved in fabrication of AM components pose a major challenge in predicting the precursor microstructural characteristics.

Even so with the optimised process parameters, it is still challenging to generate the same characteristic features for a given alloy if the production equipment is replaced. For example, PBF-LB machines generally possess different characteristics (e.g., beam control systems and chamber designs). Furthermore, the machine manufacturers often provide certified process recipes and powder characteristics for a given metallic alloy to be used for fabrication of the parts. Hence, different surface integrity characteristics would be observed in parts manufactured using the same technology, but on a different machine. These factors showcase the complexity involved within the process itself.

- Today, a generic understanding regarding achievable surface properties and microstructural characteristics is limited to only a few alloys. The microstructural characteristics of additively manufactured materials are generally different from those of their conventionally manufactured counterparts, and thus very different responses would be observed during material removal processes by shear deformation (e.g., when machining and abrasive fine-finishing). This is partly because the distinct microstructural characteristics of AM materials, e.g., crystallographic texture and cellular structure, as well as the shape and distribution of grains and phases, would lead to very different flow stress behaviours during material deformation as compared with those of cast or wrought alloys. The process-induced microstructure variations lead to a large spread in flow stress properties (e.g., ductility and work-hardening) and thus a very different response would be observed during post-processing (finishing), even within the domain of a specific AM technology. The readily available mechanical properties like hardness, yield strength and ultimate tensile strength do not necessarily provide reliable metrics for prediction of the material response during finishing operations like machining (i.e., for machinability assessment). A physics-based understanding [46,49,67,250–254] of how process-induced microstructure variations influence the flow stress properties can provide a more generic view on machinability assessment of additively manufactured materials. This fundamental approach can be used to explain the reasons behind the contradictory observations reported in literature regarding the material response during different post-processing operations. Further research on developing physics-based and microstructure-sensitive modelling platforms – in line with the Integrated Computational Materials Engineering (ICME) paradigm [255,256] – is deemed essential for machinability assessment in view of a large spread in achievable microstructural characteristics and physical properties of AM materials. Fig. 29 shows an example of the ICME approach integrating the material and process history data along the value-chain to simulate the response of AM materials during post-processes that involve shear deformation, e.g., cutting and abrasive finishing. In principle, such ICME frameworks can also be developed for non-contact post-processing/finishing operations such as electrochemical machining and laser polishing, provided that the underlying mechanisms are understood.
- In order to meet the quality requirements in terms of form, accuracy and surface integrity, AM parts must have their as-built surface texture reduced via machining and/or finishing. Surface improvement is a challenging post-processing task, especially when the required surface roughness is below Ra = 0.1 μm. This is because the process-induced variations in surface and microstructural characteristics do not allow standardisation of surface finish post-treatments for a given material. Surface refinement typically requires multi-stage post-processing. For example, removal of semi-sintered particles on the as-built surface can be first achieved by abrasive blasting, followed by a two-step isotropic (mass) finishing. The majority of available research on the finishing of AM parts is incomplete. A number of studies claim the superior capability of a concerned process and a significant result, but their findings cannot be reproduced because 1) the process itself is not clearly identified or uses erroneous terminology; 2) important process data, such as use of abrasives, are not revealed; 3) of poor experimental design. With respect to the latter, it was observed that a number of experimental studies were poorly designed, due to lack of fundamental knowledge in finishing technology. For example, vibratory-finishing technologies are efficient if the "incoming" surface roughness is in the range of Ra = 0.2–0.3 μm. Many researchers attempt to quickly tap the benefits of abrasive fine finishing by directly finishing as-built AM surfaces with high initial roughness values, e.g., Ra = 10–50 μm. This type of manufacturing shortcutting results in notoriously time-consuming finishing, lasting for days instead of the 2–3 h typical for abrasive fine-finishing of ground parts. Moreover, such excessive finishing distorts the size and geometrical accuracy. In this consideration it is important to carry out finishing in multiple steps, with each process carefully designed according to its optimal incoming surface roughness. Such a finishing plan documenting process sequences relevant to the finishing of an AM part, including specified "roughness acceptance" criteria at each step is challenging in view of the lack of standards and a large number of available post processes. To overcome these overarching challenges, it is recommended to use an established (manufacturing technology) terminology to clearly identify the reference finishing processes, thoroughly describe the experimental methods/work, put more effort into properly designing experiments, and share research data underlining published results and conclusions.
- AM finishing with abrasives to a large extent depends on a number of abrasive fine-finishing technologies, as these utilise unbonded abrasives and a pressure-copying material-removal principle capable of smoothing freeform surfaces. Grinding, in contrast, uses bonded abrasives in a motion-copying process, replicating the datum surface of the tool to the workpiece. As such, conventional grinding is not capable of finishing complex surface geometries, characteristic for AM-build parts. This might be the reason for a very limited number of research papers on grinding and grindability of AM materials. Shape-adaptive grinding (SAG) is a notable exception, in view of its capability to finish freeform surfaces. The process, however, is unfortunately still not widely used in the industry, even though it can be implemented on a 5-axis machining centre if corrective polishing software is integrated. The implementation is rather complex and still requires experimentally determining the Preston's law coefficient for a specific workpiece material-tool pair.
- The very limited body of literature on grinding of AM clearly shows that specific attention is needed to address the grindability, especially in view of the material-microstructural effects on the process (e.g., specific grinding energy). Whereas fundamental material-removal mechanisms in grinding are relatively well understood, this is not the case for abrasive fine-finishing processes. Here, the material removal rate is typically governed by Preston's law, which requires tedious experimental effort and identification of the process kinematics. Fundamental process parameters, such as dimensionless aggressiveness number [174], are not used in modelling of abrasive fine finishing. There is only one paper available systematically investigating and mapping specific energy and equivalent chip-thickness values [150]. Similarly, there is a need to carefully address fundamental laws governing laser-based processes, for example used in laser polishing. These time-dependent and non-linear processes also involve a number of interrelated control parameters (e.g., power/energy, exposure/dwell time, geometry of the laser spot) affecting the outcome of material/surface modification (e.g., re-melting). The optimisation of such processes is typically time-consuming, especially if based on complex multi-physics models. To circumvent this problem, Axinte and Billingham [267] postulated an inverse problem-solving approach, where the input is a targeted surface to be created (e.g., laser polished), and the outputs are control parameters needed to achieve this surface. The extent to which the inverse-problem approach is adopted by researchers in the

field is still limited, as the majority of beam modelling/optimisation approaches continue to be trial-and-error. This optimisation issue, of course, also applies to material-consolidation processes in additive manufacturing. The thermal aspects determining the melting process, can be fundamentally characterised by two dimensionless parameters, as demonstrated by Rubenchik et al. [268]. The proposed scaling law captures the underlying physical law behind a phenomenon and offers a useful tool to optimise laser-beam process parameters used during a build cycle for an arbitrary material and AM machine.

- The available literature on the influence of post-processing on fatigue, tribological and corrosion properties is limited to certain alloys and processes. Fatigue, corrosion and tribological properties like wear resistance largely depend on microstructural properties like cell and melt pool boundaries, nano- and micro-scale inclusions, micro-segregation of elements, texture and grain morphology [7,83,249]. This makes it difficult to present a general assessment on the influence of post-processing on the functional performance of AM materials. Yet available investigations suggest that surface finish treatments can improve the fatigue performance of AM materials, provided that the density of process-induced defects is minimal. This shows the importance of AM process optimisation and subsequent thermal post-treatments (HIP) to achieve desired properties after subtractive (or surface modification) post-processing. In principle, a similar argument holds for corrosion and tribological properties. Further research is deemed necessary to reveal the relative role of the microstructural characteristics for a given alloy before and after surface finish processing.

Credit author statement

Amir Malakizadi: Writing - Original Draft, Conceptualization, Methodology. **Dinesh Mallipeddi**: Writing - Original Draft, Methodology. **Sasan Dadbakhsh**: Writing - Original Draft. **Rachid M'Saoubi**: Writing - Original Draft. **Peter Krajnik**: Writing - Original Draft.

Declaration of competing interest

The authors declare that they have no known competing financial interests or personal relationships that could have appeared to influence the work reported in this paper.

Acknowledgments

This review was prepared under the umbrella of Chalmers Centre for Metal Cutting Research (MCR). The authors thank Fengzhou Fang, Samuel Milton, Wang Hao, and Yeo Swee Hock for their input in the preparation of this paper.

Appendix A. Supplementary data

Supplementary data to this article can be found online at https://doi.org/10.1016/j.ijmachtools.2022.103908.

References

[1] ISO/ASTM 52900, Additive Manufacturing — General Principles — Fundamentals and Vocabulary, 2021.
[2] J.P. Kruth, Material incress manufacturing by rapid prototyping techniques, CIRP Ann. 40 (2) (1991) 603–614.
[3] J.P. Kruth, M.C. Leu, T. Nakagawa, Progress in additive manufacturing and rapid prototyping, CIRP Ann. 47 (2) (1998) 525–540.
[4] P. Krajnik, F. Hashimoto, B. Karpuschewski, E.J. da Silva, D. Axinte, Grinding and fine finishing of future automotive powertrain components, CIRP Ann. 70 (2) (2021) 589–610.
[5] T.H. Becker, P. Kumar, U. Ramamurty, Fracture and fatigue in additively manufactured metals, Acta Mater. 219 (2021), 117240.
[6] C. Tan, F. Weng, S. Sui, Y. Chew, G. Bi, Progress and perspectives in laser additive manufacturing of key aeroengine materials, Int. J. Mach. Tool Manufact. 170 (2021), 103804.
[7] H.M. Khan, Y. Karabulut, O. Kitay, Y. Kaynak, I.S. Jawahir, Influence of the post-processing operations on surface integrity of metal components produced by laser powder bed fusion additive manufacturing: a review, Mach. Sci. Technol. 25 (1) (2021) 118–176.
[8] J.-Y. Lee, A.P. Nagalingam, S.H. Yeo, A review on the state-of-the-art of surface finishing processes and related ISO/ASTM standards for metal additive manufactured components, Virtual Phys. Prototyp. 16 (1) (2021) 68–96.
[9] Z. Liao, et al., Surface integrity in metal machining - Part I: fundamentals of surface characteristics and formation mechanisms, Int. J. Mach. Tool Manufact. 162 (2021), 103687.
[10] A. la Monaca, et al., Surface integrity in metal machining - Part II: functional performance, Int. J. Mach. Tool Manufact. 164 (2021), 103718.
[11] V. Benoist, L. Arnaud, M. Baili, A new method of design for additive manufacturing including machining constraints, Int. J. Adv. Manuf. Technol. 111 (1) (2020) 25–36.
[12] J.D. Pérez-Ruiz, F. Marin, S. Martínez, A. Lamikiz, G. Urbikain, L.N. López de Lacalle, Stiffening near-net-shape functional parts of Inconel 718 LPBF considering material anisotropy and subsequent machining issues, Mech. Syst. Signal Process. 168 (2022), 108675.
[13] T.P. Moran, P.E. Carrion, S. Lee, N. Shamsaei, N. Phan, D.H. Warner, Hot isostatic pressing for fatigue critical additively manufactured Ti-6Al-4V, Materials 15 (6) (2022) 2051.
[14] P. Krajnik, F. Hashimoto, Finishing, in: CIRP Encyclopedia of Production Engineering, P. The International Academy for, Springer Berlin Heidelberg, Berlin, Heidelberg, 2018, pp. 1–9.
[15] D. Sarker, E. Toyserkani, O.O. Ibhadode, F. Liravi, P. Russo, K. Taherkhani, Metal Additive Manufacturing, 2021.
[16] D. Herzog, V. Seyda, E. Wycisk, C. Emmelmann, Additive manufacturing of metals, Acta Mater. 117 (2016) 371–392.
[17] A. Agapovichev, A. Sotov, V. Kokareva, V. Smelov, Possibilities and limitations of titanium alloy additive manufacturing, MATEC Web Conf 224 (2018), 01064.
[18] E. Hosseini, V.A. Popovich, A review of mechanical properties of additively manufactured Inconel 718, Addit. Manuf. 30 (2019), 100877.
[19] E.M. Trent, P.K. Wright, Metal Cutting, Butterworth-Heinemann, Boston, 2000.
[20] J.-E. Ståhl, Metal Cutting-Theories and Models Lund, Lund University Press, Sweden, 2012.
[21] P. Hoier, et al., Influence of batch-to-batch material variations on grindability of a medium-carbon steel, J. Manuf. Process. 73 (2022) 463–470.
[22] V.P. Astakhov, Machinability: existing and advanced concepts, in: Machinability of Advanced Materials, 2014, pp. 1–56.
[23] W. König, J. Messer, Influence of the composition and structure of steels on grinding process, CIRP Ann. 30 (2) (1981) 547–552.
[24] J.-E. Ståhl, M. Andersson, Polar machinability diagrams-a model to predict the machinability of a work material, in: Swedish Production Symposium, 2007.
[25] S. Olovsjö, P. Hammersberg, P. Avdovic, J.-E. Ståhl, L. Nyborg, Methodology for evaluating effects of material characteristics on machinability—theory and statistics-based modelling applied on Alloy 718, Int. J. Adv. Manuf. Technol. 59 (1–4) (2012) 55–66.
[26] P. Avdovic, L. Xu, M. Andersson, J.-E. Ståhl, Evaluating the machinability of inconel 718 using polar diagrams, J. Eng. Gas Turbines Power 133 (7) (2011), 072101-072101-7.
[27] J. Johansson, H. Persson, J.E. Ståhl, J.M. Zhou, V. Bushlya, F. Schultheiss, Machinability evaluation of low-lead brass alloys, Procedia Manuf. 38 (2019) 1723–1730.
[28] L. Xu, F. Schultheiss, M. Andersson, J.-E. Ståhl, General conception of polar diagrams for the evaluation of the potential machinability of workpiece materials, Int. J. Mach. Mach. Mater. 14 (1) (2013) 24–44.
[29] M.C. Shaw, A quantized theory of strain hardening as applied to the cutting of metals, J. Appl. Phys. 21 (6) (1950) 599–606.
[30] V. Singh, P. Venkateswara Rao, S. Ghosh, Development of specific grinding energy model, Int. J. Mach. Tool Manufact. 60 (2012) 1–13.
[31] S. Kobayashi, S. Kobayashi, S.-I. Oh, T. Altan, Metal Forming and the Finite-Element Method, Oxford University Press on Demand, 1989.
[32] J. Badger, Grindability of conventionally produced and powder-metallurgy high-speed steel, CIRP Ann. 56 (1) (2007) 353–356.
[33] P. Hoier, A. Malakizadi, U. Klement, P. Krajnik, Characterization of abrasion- and dissolution-induced tool wear in machining, Wear 426–427 (2019) 1548–1562.
[34] P. Hoier, A. Malakizadi, P. Stuppa, S. Cedergren, U. Klement, Microstructural characteristics of Alloy 718 and Waspaloy and their influence on flank wear during turning, Wear 400–401 (2018) 184–193.
[35] R. Komanduri, M. Shaw, Grindability of AISI T-15 tool steel produced by the consolidation of atomized metal powder, in: 1975 Proceedings- Third North American Metalworking Research Conference, Carnegie Press, Pittsburgh, Pa, 1975, pp. 481–497, 1974.
[36] P. Hoier, A. Malakizadi, S. Friebe, U. Klement, P. Krajnik, Microstructural variations in 316L austenitic stainless steel and their influence on tool wear in machining, Wear 428 (2019) 315–327.
[37] A. Bjerke, et al., Onset of the degradation of CVD α-Al2O3 coating during turning of Ca-treated steels, Wear 477 (2021), 203785.
[38] H. Persson, F. Lenrick, L. Franca, J.-E. Ståhl, V. Bushlya, Wear mechanisms of PcBN tools when machining AISI 316L, Ceram. Int. 47 (22) (2021) 31894–31906.

[39] P. Hoier, A. Malakizadi, S. Friebe, U. Klement, P. Krajnik, Microstructural variations in 316L austenitic stainless steel and their influence on tool wear in machining, Wear 428–429 (2019) 315–327.
[40] B. Wang, X. Xiao, V.P. Astakhov, Z. Liu, The effects of stress triaxiality and strain rate on the fracture strain of Ti6Al4V, Eng. Fract. Mech. 219 (2019), 106627.
[41] S. Buchkremer, F. Klocke, D. Lung, Finite-element-analysis of the relationship between chip geometry and stress triaxiality distribution in the chip breakage location of metal cutting operations, Simulat. Model. Pract. Theor. 55 (2015) 10–26.
[42] E. Rabinowicz, A. Mutis, Effect of abrasive particle size on wear, Wear 8 (5) (1965) 381–390.
[43] M.F.C. Andrade, R.P. Martinho, F.J.G. Silva, R.J.D. Alexandre, A.P.M. Baptista, Influence of the abrasive particles size in the micro-abrasion wear tests of TiAlSiN thin coatings, Wear 267 (1) (2009) 12–18.
[44] M. Binder, F. Klocke, B. Doebbeler, Abrasive wear behavior under metal cutting conditions, Wear 376–377 (2017) 165–171.
[45] S. Sanchez, et al., Powder Bed Fusion of nickel-based superalloys: a review, Int. J. Mach. Tool Manufact. 165 (2021), 103729.
[46] A. Malakizadi, et al., The role of microstructural characteristics of additively manufactured Alloy 718 on tool wear in machining, Int. J. Mach. Tool Manufact. 171 (2021), 103814.
[47] Y.M. Wang, et al., Additively manufactured hierarchical stainless steels with high strength and ductility, Nat. Mater. 17 (1) (2018) 63–71.
[48] P. Fernandez-Zelaia, V. Nguyen, H. Zhang, A. Kumar, S.N. Melkote, The effects of material anisotropy on secondary processing of additively manufactured CoCrMo, Addit. Manuf. 29 (2019), 100764.
[49] J.D. Pérez-Ruiz, L.N.L. de Lacalle, G. Urbikain, O. Pereira, S. Martínez, J. Bris, On the relationship between cutting forces and anisotropy features in the milling of LPBF Inconel 718 for near net shape parts, Int. J. Mach. Tool Manufact. 170 (2021), 103801.
[50] L. Lizzul, M. Sorgato, R. Bertolini, A. Ghiotti, S. Bruschi, Influence of additive manufacturing-induced anisotropy on tool wear in end milling of Ti6Al4V, Tribol. Int. 146 (2020), 106200.
[51] R. Bejjani, E. Bamford, S. Cedergren, A. Archenti, A. Rashid, Variations in the surface integrity of Ti-6Al-4V by combinations of additive and subtractive manufacturing processes, Materials 13 (8) (2020).
[52] R.J. Bourcier, D.A. Koss, R.E. Smelser, O. Richmond, The influence of porosity on the deformation and fracture of alloys, Acta Metall. 34 (12) (1986) 2443–2453.
[53] X. Zhao, S. Dadbakhsh, A. Rashid, Contouring strategies to improve the tensile properties and quality of EBM printed Inconel 625 parts, J. Manuf. Process. 62 (2021) 418–429.
[54] X. Zhao, A. Rashid, A. Strondl, C. Hulme-Smith, N. Stenberg, S. Dadbakhsh, Role of superficial defects and machining depth in tensile properties of electron beam melting (EBM) made inconel 718, J. Mater. Eng. Perform. 30 (3) (2021) 2091–2101.
[55] H. Atkinson, S. Davies, Fundamental aspects of hot isostatic pressing: an overview, Metall. Mater. Trans. 31 (12) (2000) 2981–3000.
[56] N.P. Lavery, et al., Effects of hot isostatic pressing on the elastic modulus and tensile properties of 316L parts made by powder bed laser fusion, Mater. Sci. Eng., A 693 (2017) 186–213.
[57] E. Liverani, A.H.A. Lutey, A. Ascari, A. Fortunato, The effects of hot isostatic pressing (HIP) and solubilization heat treatment on the density, mechanical properties, and microstructure of austenitic stainless steel parts produced by selective laser melting (SLM), Int. J. Adv. Manuf. Technol. 107 (1) (2020) 109–122.
[58] J.C.Y. Koh, A. Fortini, Prediction of thermal conductivity and electrical resistivity of porous metallic materials, Int. J. Heat Mass Tran. 16 (11) (1973) 2013–2022.
[59] M.J. Peet, H.S. Hasan, H.K.D.H. Bhadeshia, Prediction of thermal conductivity of steel, Int. J. Heat Mass Tran. 54 (11) (2011) 2602–2608.
[60] S. Sartori, L. Moro, A. Ghiotti, S. Bruschi, On the tool wear mechanisms in dry and cryogenic turning Additive Manufactured titanium alloys, Tribol. Int. 105 (2017) 264–273.
[61] J. Yang, Theory of thermal conductivity, in: T.M. Tritt (Ed.), Thermal Conductivity: Theory, Properties, and Applications, Springer US, Boston, MA, 2004, pp. 1–20.
[62] S. Goel, H. Mehtani, S.-W. Yao, I. Samajdar, U. Klement, S. Joshi, As-built and post-treated microstructures of an electron beam melting (EBM) produced nickel-based superalloy, Metall. Mater. Trans. 51 (12) (2020) 6546–6559.
[63] E.M. Fayed, M. Saadati, D. Shahriari, V. Brailovski, M. Jahazi, M. Medraj, Optimization of the post-process heat treatment of inconel 718 superalloy fabricated by laser powder bed fusion process, Metals 11 (1) (2021) 144.
[64] K.M. Bertsch, G. Meric de Bellefon, B. Kuehl, D.J. Thoma, Origin of dislocation structures in an additively manufactured austenitic stainless steel 316L, Acta Mater. 199 (2020) 19–33.
[65] D. Hull, D.J. Bacon, Introduction to Dislocations, Elsevier, 2011.
[66] L. Cui, S. Jiang, J. Xu, R.L. Peng, R.T. Mousavian, J. Moverare, Revealing relationships between microstructure and hardening nature of additively manufactured 316L stainless steel, Mater. Des. 198 (2021), 109385.
[67] M.A. Galindo-Fernández, K. Mumtaz, P.E.J. Rivera-Díaz-del-Castillo, E.I. Galindo-Nava, H. Ghadbeigi, A microstructure sensitive model for deformation of Ti-6Al-4V describing Cast-and-Wrought and Additive Manufacturing morphologies, Mater. Des. 160 (2018) 350–362.
[68] J. Xu, T. Ma, R.L. Peng, S. Hosseini, Effect of post-processes on the microstructure and mechanical properties of laser powder bed fused IN718 superalloy, Addit. Manuf. 48 (2021), 102416.
[69] F. Yan, W. Xiong, E. Faierson, G.B. Olson, Characterization of nano-scale oxides in austenitic stainless steel processed by powder bed fusion, Scripta Mater. 155 (2018) 104–108.
[70] B.J. Hayes, et al., Predicting tensile properties of Ti-6Al-4V produced via directed energy deposition, Acta Mater. 133 (2017) 120–133.
[71] I. Ghamarian, P. Samimi, V. Dixit, P.C. Collins, A constitutive equation relating composition and microstructure to properties in Ti-6Al-4V: as derived using a novel integrated computational approach, Metall. Mater. Trans. 46 (11) (2015) 5021–5037.
[72] M. Benedetti, et al., The effect of post-sintering treatments on the fatigue and biological behavior of Ti-6Al-4V ELI parts made by selective laser melting, J. Mech. Behav. Biomed. Mater. 71 (2017) 295–306.
[73] R. M, S. Koppoju, G. Telasang, R. Korla, P. G, Effect of solutionizing temperature on the microstructural evolution during double aging of powder bed fusion-additive manufactured IN718 alloy, Mater. Char. 172 (2021), 110868.
[74] O. Bletton, R. Duet, P. Pedarre, Influence of oxide nature on the machinability of 316L stainless steels, Wear 139 (2) (1990) 179–193.
[75] H. Du, A.V. Karasev, P.G. Jönsson, Influence of non-metallic inclusions in 316L stainless steels on machining using different cutting speeds, ISIJ Int. 61 (9) (2021) 2426–2434, https://doi.org/10.2355/isijinternational.ISIJINT-2021-079.
[76] J.C. Outeiro, D. Umbrello, R. M'Saoubi, Experimental and numerical modelling of the residual stresses induced in orthogonal cutting of AISI 316L steel, Int. J. Mach. Tool Manufact. 46 (14) (2006) 1786–1794.
[77] J.C. Outeiro, A.M. Dias, J.L. Lebrun, V.P. Astakhov, Machining residual stresses in AISI 316L steel and their correlation with the cutting parameters, Mach. Sci. Technol. 6 (2) (2002) 251–270.
[78] D. Riabov, M. Rashidi, E. Hryha, S. Bengtsson, Effect of the powder feedstock on the oxide dispersion strengthening of 316L stainless steel produced by laser powder bed fusion, Mater. Char. 169 (2020), 110582.
[79] L.-E. Rännar, A. Koptyug, J. Olsén, K. Saeidi, Z. Shen, Hierarchical structures of stainless steel 316L manufactured by Electron Beam Melting, Addit. Manuf. 17 (2017) 106–112.
[80] D.-R. Eo, S.-H. Park, J.-W. Cho, Inclusion evolution in additive manufactured 316L stainless steel by laser metal deposition process, Mater. Des. 155 (2018) 212–219.
[81] C. Pauzon, E. Hryha, P. Forêt, L. Nyborg, Effect of argon and nitrogen atmospheres on the properties of stainless steel 316L parts produced by laser-powder bed fusion, Mater. Des. 179 (2019), 107873.
[82] A. Saboori, et al., An investigation on the effect of powder recycling on the microstructure and mechanical properties of AISI 316L produced by Directed Energy Deposition, Mater. Sci. Eng., A 766 (2019), 138360.
[83] M. Bahshwan, C.W. Myant, T. Reddyhoff, M.-S. Pham, The role of microstructure on wear mechanisms and anisotropy of additively manufactured 316L stainless steel in dry sliding, Mater. Des. 196 (2020), 109076.
[84] Y. Kaynak, O. Kitay, The effect of post-processing operations on surface characteristics of 316L stainless steel produced by selective laser melting, Addit. Manuf. 26 (2019) 84–93.
[85] V.P. Alexeev, A.V. Balyakin, A.I. Khaimovich, Influence of the direction of selective laser sintering on machinability of parts from 316L steel, IOP Conf. Ser. Mater. Sci. Eng. 177 (2017), 012120.
[86] Y. Gong, P. Li, Analysis of tool wear performance and surface quality in post milling of additive manufactured 316L stainless steel, J. Mech. Sci. Technol. 33 (5) (2019).
[87] S. Cedergren, C. Frangoudis, A. Archenti, R. Pederson, G. Sjöberg, Influence of work material microstructure on vibrations when machining cast Ti-6Al-4V, Int. J. Adv. Manuf. Technol. 84 (9) (2016) 2277–2291.
[88] M.S. Dargusch, S. Sun, J.W. Kim, T. Li, P. Trimby, J. Cairney, Effect of tool wear evolution on chip formation during dry machining of Ti-6Al-4V alloy, Int. J. Mach. Tool Manufact. 126 (2018) 13–17.
[89] J. Barry, G. Byrne, D. Lennon, Observations on chip formation and acoustic emission in machining Ti–6Al–4V alloy, Int. J. Mach. Tool Manufact. 41 (7) (2001) 1055–1070.
[90] M. Bermingham, J. Kirsch, S. Sun, S. Palanisamy, M. Dargusch, New observations on tool life, cutting forces and chip morphology in cryogenic machining Ti-6Al-4V, Int. J. Mach. Tool Manufact. 51 (6) (2011) 500–511.
[91] R. Lindvall, F. Lenrick, R. M'Saoubi, J.-E. Ståhl, V. Bushlya, Performance and wear mechanisms of uncoated cemented carbide cutting tools in Ti6Al4V machining, Wear 477 (2021), 203824.
[92] E.O. Ezugwu, J. Bonney, R.B. Da Silva, O. Çakir, Surface integrity of finished turned Ti–6Al–4V alloy with PCD tools using conventional and high pressure coolant supplies, Int. J. Mach. Tool Manufact. 47 (6) (2007) 884–891.
[93] A. Pramanik, G. Littlefair, Machining of titanium alloy (Ti-6Al-4V)—theory to application, Mach. Sci. Technol. 19 (1) (2015) 1–49.
[94] K. Palaniappan, M. Sundararaman, H. Murthy, R. Jeyaraam, B.C. Rao, Influence of workpiece texture and strain hardening on chip formation during machining of Ti–6Al–4V alloy, Int. J. Mach. Tool Manufact. (2021), 103849.
[95] R. Lindvall, F. Lenrick, H. Persson, R. M'Saoubi, J.-E. Ståhl, V. Bushlya, Performance and wear mechanisms of PCD and pcBN cutting tools during machining titanium alloy Ti6Al4V, Wear 454–455 (2020), 203329.
[96] M.J. Donachie, Titanium: a Technical Guide, ASM international, 2000.
[97] J. Mezzetta, et al., Microstructure-properties relationships of Ti-6Al-4V parts fabricated by selective laser melting, Int. J. Precis. Eng. Manuf.-Green Technol. 5 (5) (2018) 605–612.
[98] M. Neikter, P. Åkerfeldt, R. Pederson, M.L. Antti, V. Sandell, Microstructural characterization and comparison of Ti-6Al-4V manufactured with different additive manufacturing processes, Mater. Char. 143 (2018) 68–75.

[99] H. Shipley, et al., Optimisation of process parameters to address fundamental challenges during selective laser melting of Ti-6Al-4V: a review, Int. J. Mach. Tool Manufact. 128 (2018) 1–20.
[100] C.M. Cepeda-Jiménez, F. Potenza, E. Magalini, V. Luchin, A. Molinari, M.T. Pérez-Prado, Effect of energy density on the microstructure and texture evolution of Ti-6Al-4V manufactured by laser powder bed fusion, Mater. Char. 163 (2020), 110238.
[101] C. Liu, et al., Effect of hot isostatic pressing on microstructures and mechanical properties of Ti6Al4V fabricated by electron beam melting, Metals 10 (5) (2020).
[102] A.M. Beese, B.E. Carroll, Review of mechanical properties of Ti-6Al-4V made by laser-based additive manufacturing using powder feedstock, JOM (J. Occup. Med.) 68 (3) (2016) 724–734.
[103] R. Zhao, et al., On the role of volumetric energy density in the microstructure and mechanical properties of laser powder bed fusion Ti-6Al-4V alloy, Addit. Manuf. 51 (2022), 102605.
[104] M. Shunmugavel, A. Polishetty, M. Goldberg, R. Singh, G. Littlefair, A comparative study of mechanical properties and machinability of wrought and additive manufactured (selective laser melting) titanium alloy – Ti-6Al-4V, Rapid Prototyp. J. 23 (6) (2017) 1051–1056.
[105] A. Bordin, S. Sartori, S. Bruschi, A. Ghiotti, Experimental investigation on the feasibility of dry and cryogenic machining as sustainable strategies when turning Ti6Al4V produced by Additive Manufacturing, J. Clean. Prod. 142 (2017) 4142–4151.
[106] S. Sartori, A. Bordin, A. Ghiotti, S. Bruschi, Analysis of the surface integrity in cryogenic turning of Ti6Al4V produced by direct melting laser sintering, Proc. CIRP 45 (2016) 123–126.
[107] A. Bordin, S. Bruschi, A. Ghiotti, F. Bucciotti, L. Facchini, Comparison between wrought and EBM Ti6Al4V machinability characteristics, Key Eng. Mater. 611–612 (2014) 1186–1193.
[108] D. Mallipeddi, et al., Surface integrity of machined electron beam melted Ti6Al4V alloy manufactured with different contour settings and heat treatment, Proc. CIRP 87 (2020) 327–332.
[109] O. Oyelola, P. Crawforth, R. M'Saoubi, A.T. Clare, On the machinability of directed energy deposited Ti6Al4V, Addit. Manuf. 19 (2018) 39–50.
[110] F. Veiga, A. Gil Del Val, A. Suárez, U. Alonso, Analysis of the machining process of titanium Ti6Al-4V parts manufactured by wire arc additive manufacturing (WAAM), Materials 13 (3) (2020) 766.
[111] X. Tan, et al., Graded microstructure and mechanical properties of additive manufactured Ti–6Al–4V via electron beam melting, Acta Mater. 97 (2015) 1–16.
[112] W.-S. Woo, E.-J. Kim, H.-I. Jeong, C.-M. Lee, Laser-assisted machining of Ti-6Al-4V fabricated by DED additive manufacturing, Int. J. Precis. Eng. Manuf.-Green Technol. 7 (3) (2020) 559–572.
[113] S. Milton, et al., Microstructure effects on the machinability behaviour of Ti6Al4V produced by selective laser melting and electron beam melting process, Mater. Sci. Eng., A 823 (2021), 141773.
[114] S. Milton, A. Morandeau, F. Chalon, R. Leroy, Influence of finish machining on the surface integrity of Ti6Al4V produced by selective laser melting, Proc. CIRP 45 (2016) 127–130.
[115] S. Milton, A. Duchosal, F. Chalon, R. Leroy, A. Morandeau, Thermal study during milling of Ti6Al4V produced by Electron Beam Melting (EBM) process, J. Manuf. Process. 38 (2019) 256–265.
[116] K.S. Al-Rubaie, S. Melotti, A. Rabelo, J.M. Paiva, M.A. Elbestawi, S.C. Veldhuis, Machinability of SLM-produced Ti6Al4V titanium alloy parts, J. Manuf. Process. 57 (2020) 768–786.
[117] F. de Oliveira Campos, A.C. Araujo, A.L. Jardini Munhoz, S.G. Kapoor, The influence of additive manufacturing on the micromilling machinability of Ti6Al4V: a comparison of SLM and commercial workpieces, J. Manuf. Process. 60 (2020) 299–307.
[118] F. Hojati, A. Daneshi, B. Soltani, B. Azarhoushang, D. Biermann, Study on machinability of additively manufactured and conventional titanium alloys in micro-milling process, Precis. Eng. 62 (2020) 1–9.
[119] G. Bonaiti, P. Parenti, M. Annoni, S. Kapoor, Micro-milling machinability of DED additive titanium Ti-6Al-4V, Procedia Manuf. 10 (2017) 497–509.
[120] W. Khaliq, C. Zhang, M. Jamil, A.M. Khan, Tool wear, surface quality, and residual stresses analysis of micro-machined additive manufactured Ti–6Al–4V under dry and MQL conditions, Tribol. Int. 151 (2020), 106408.
[121] D. Xu, Z. Liao, D. Axinte, M. Hardy, A novel method to continuously map the surface integrity and cutting mechanism transition in various cutting conditions, Int. J. Mach. Tool Manufact. 151 (2020), 103529.
[122] S. Razanica, A. Malakizadi, R. Larsson, S. Cedergren, B.L. Josefson, FE modeling and simulation of machining Alloy 718 based on ductile continuum damage, Int. J. Mech. Sci. (2019), 105375.
[123] R. M'Saoubi, et al., Surface integrity analysis of machined Inconel 718 over multiple length scales, CIRP Ann. 61 (1) (2012) 99–102.
[124] R. S, M. A, L. R, C. S, and J. B. L, "FE modeling and simulation of machining Alloy 718 based on ductile continuum damage," International Journal of Mechanical Sciences, vol. 171, p. 105375, 2020.
[125] J. Johansson, C. Persson, H. Lai, M. Hörnqvist Colliander, Microstructural examination of shear localisation during high strain rate deformation of Alloy 718, Mater. Sci. Eng., A 662 (2016) 363–372.
[126] A. Hagberg, P. Malm, Material Deformation Mechanisms during Machining of Superalloys, Chalmers University of Technology, 2010.
[127] S. Olovsjö, A. Wretland, G. Sjöberg, The effect of grain size and hardness of wrought Alloy 718 on the wear of cemented carbide tools, Wear 268 (9–10) (2010) 1045–1052.
[128] V. Bushlya, et al., Tool wear mechanisms of PcBN in machining Inconel 718: analysis across multiple length scale, CIRP Ann. 70 (1) (2021) 73–78, https://doi.org/10.1016/j.cirp.2021.04.008.
[129] N. Tamil Alagan, P. Hoier, P. Zeman, U. Klement, T. Beno, A. Wretland, Effects of high-pressure cooling in the flank and rake faces of WC tool on the tool wear mechanism and process conditions in turning of alloy 718, Wear 434–435 (2019), 102922.
[130] C. Furusho, Y. Kousai, M. Osaki, K. Uno, Development of new alloy 718 with super machinability, in: Proceedings of the 9th International Symposium on Superalloy 718 & Derivatives: Energy, Aerospace, and Industrial Applications, Springer, 2018, pp. 1073–1085.
[131] E.M. Fayed, M. Saadati, D. Shahriari, V. Brailovski, M. Jahazi, M. Medraj, Effect of homogenization and solution treatments time on the elevated-temperature mechanical behavior of Inconel 718 fabricated by laser powder bed fusion, Sci. Rep. 11 (1) (2021) 2020.
[132] Y. Kaynak, E. Tascioglu, Finish machining-induced surface roughness, microhardness and XRD analysis of selective laser melted Inconel 718 alloy, Proc. CIRP 71 (2018) 500–504.
[133] Y. Kaynak, E. Tascioglu, Post-processing effects on the surface characteristics of Inconel 718 alloy fabricated by selective laser melting additive manufacturing, Prog. Addit. Manuf. 5 (2) (2020) 221–234.
[134] L. Chen, Q. Xu, Y. Liu, G. Cai, J. Liu, Machinability of the laser additively manufactured Inconel 718 superalloy in turning, Int. J. Adv. Manuf. Technol. 114 (3) (2021) 871–882.
[135] F. Careri, D. Umbrello, K. Essa, M.M. Attallah, S. Imbrogno, The effect of the heat treatments on the tool wear of hybrid Additive Manufacturing of IN718, Wear 470–471 (2021), 203617.
[136] O. Gokcekaya, T. Ishimoto, S. Hibino, J. Yasutomi, T. Narushima, T. Nakano, Unique crystallographic texture formation in Inconel 718 by laser powder bed fusion and its effect on mechanical anisotropy, Acta Mater. 212 (2021), 116876.
[137] T. Ostra, U. Alonso, F. Veiga, M. Ortiz, P. Ramiro, A. Alberdi, Analysis of the machining process of inconel 718 parts manufactured by laser metal deposition, Materials 12 (13) (2019) 2159.
[138] A. Calleja, G. Urbikain, H. González, I. Cerrillo, R. Polvorosa, A. Lamikiz, Inconel® 718 superalloy machinability evaluation after laser cladding additive manufacturing process, Int. J. Adv. Manuf. Technol. 97 (5) (2018) 2873–2885.
[139] S. Periane, et al., Selection of machining condition on surface integrity of additive and conventional Inconel 718, Proc. CIRP 87 (2020) 333–338.
[140] E. Ducroux, G. Fromentin, F. Viprey, D. Prat, A. D'Acunto, New mechanistic cutting force model for milling additive manufactured Inconel 718 considering effects of tool wear evolution and actual tool geometry, J. Manuf. Process. 64 (2021) 67–80.
[141] D.M. Kim, E. Park, N. Kim, H.W. Park, Experimental investigation on tool wear during the milling processes for the post-processing of selective laser melted Inconel 718 alloys, in: International Manufacturing Science and Engineering Conference, vol. 51357, American Society of Mechanical Engineers, 2018. V001T01A011.
[142] E. Park, D.M. Kim, H.W. Park, Y.-B. Park, N. Kim, Evaluation of tool life in the dry machining of inconel 718 parts from additive manufacturing (AM), Int. J. Precis. Eng. Manuf. 21 (1) (2020) 57–65.
[143] B. Kirsch, H. Hotz, J. Hartig, S. Greco, M. Zimmermann, J.C. Aurich, Pendulum and creep feed grinding of additively manufactured AISI 316L, Proc. CIRP 101 (2021) 166–169.
[144] C. Keller, E. Hug, X. Feaugas, Microstructural size effects on mechanical properties of high purity nickel, Int. J. Plast. 27 (4) (2011) 635–654.
[145] M. Kadivar, B. Azarhoushang, U. Klement, P. Krajnik, The role of specific energy in micro-grinding of titanium alloy, Precis. Eng. 72 (2021) 172–183.
[146] A. Beaucamp, Y. Namba, P. Charlton, Process mechanism in shape adaptive grinding (SAG), CIRP Ann. 64 (1) (2015) 305–308.
[147] A.T. Beaucamp, Y. Namba, P. Charlton, S. Jain, A.A. Graziano, Finishing of additively manufactured titanium alloy by shape adaptive grinding (SAG), Surf. Topogr. Metrol. Prop. 3 (2) (2015), 024001.
[148] W.-L. Zhu, Y. Yang, H.N. Li, D. Axinte, A. Beaucamp, Theoretical and experimental investigation of material removal mechanism in compliant shape adaptive grinding process, Int. J. Mach. Tool Manufact. 142 (2019) 76–97.
[149] J. Chaves-Jacob, A. Beaucamp, W. Zhu, D. Kono, J.-M. Linares, Towards an understanding of surface finishing with compliant tools using a fast and accurate simulation method, Int. J. Mach. Tool Manufact. 163 (2021), 103704.
[150] F. Hashimoto, et al., Abrasive fine-finishing technology, CIRP Ann. 65 (2) (2016) 597–620.
[151] S. Bagehorn, J. Wehr, H.J. Maier, Application of mechanical surface finishing processes for roughness reduction and fatigue improvement of additively manufactured Ti-6Al-4V parts, Int. J. Fatig. 102 (2017) 135–142.
[152] J. Guo, et al., Novel rotating-vibrating magnetic abrasive polishing method for double-layered internal surface finishing, J. Mater. Process. Technol. 264 (2019) 422–437.
[153] M. Kahlin, et al., Improved fatigue strength of additively manufactured Ti6Al4V by surface post processing, Int. J. Fatig. 134 (2020), 105497.
[154] R.W. Overholser, R.J. Stango, R.A. Fournelle, Morphology of metal surface generated by nylon/abrasive filament brush, Int. J. Mach. Tool Manufact. 43 (2) (2003) 193–202.
[155] C. Peng, Y. Fu, H. Wei, S. Li, X. Wang, H. Gao, Study on improvement of surface roughness and induced residual stress for additively manufactured metal parts by abrasive flow machining, Proc. CIRP 71 (2018) 386–389.

[156] T. Furumoto, T. Ueda, T. Amino, A. Hosokawa, A study of internal face finishing of the cooling channel in injection mold with free abrasive grains, J. Mater. Process. Technol. 211 (11) (2011) 1742–1748.
[157] Y. Makiuchi, F. Hashimoto, A. Beaucamp, Model of material removal in vibratory finishing, based on Preston's law and discrete element method, CIRP Ann. 68 (1) (2019) 365–368.
[158] M. Ihara, A. Matsubara, A. Beaucamp, Study on removal mechanism at the tool rotational center in bonnet polishing of glass, Wear 454–455 (2020), 203321, 2020/08/15/.
[159] W.-L. Zhu, A. Beaucamp, Non-Newtonian fluid based contactless sub-aperture polishing, CIRP Ann. 69 (1) (2020) 293–296.
[160] W.-L. Zhu, A. Beaucamp, Compliant grinding and polishing: a review, Int. J. Mach. Tool Manufact. 158 (2020), 103634.
[161] Y. Yang, H. Li, Z. Liao, D. Axinte, W. Zhu, A. Beaucamp, Controlling of compliant grinding for low-rigidity components, Int. J. Mach. Tool Manufact. 152 (2020), 103543.
[162] F. Preston, The theory and design of plate glass polishing machines, J. Glass Technol. 11 (44) (1927) 214–256.
[163] J. Zhang, H. Wang, Generic model of time-variant tool influence function and dwell-time algorithm for deterministic polishing, Int. J. Mech. Sci. 211 (2021), 106795.
[164] J. Zhang, H. Wang, A. Senthil Kumar, M. Jin, Experimental and theoretical study of internal finishing by a novel magnetically driven polishing tool, Int. J. Mach. Tool Manufact. 153 (2020), 103552.
[165] Y. Cui, S.C. Kottilingam, B.L. Tollison, D. Lin, D.E. Schick, Component Surface Finishing Systems and Methods, Google Patents, 2015.
[166] J. Zhang, J. Hu, H. Wang, A.S. Kumar, A. Chaudhari, A novel magnetically driven polishing technique for internal surface finishing, Precis. Eng. 54 (2018) 222–232.
[167] P.-Y. Wu, H. Yamaguchi, Material removal mechanism of additively manufactured components finished using magnetic abrasive finishing, Proc. Manuf. 26 (2018) 394–402.
[168] H. Yamaguchi, O. Fergani, P.-Y. Wu, Modification using magnetic field-assisted finishing of the surface roughness and residual stress of additively manufactured components, CIRP Ann. 66 (1) (2017) 305–308.
[169] A. Teramachi, J. Yan, Improving the surface integrity of additive-manufactured metal parts by ultrasonic vibration-assisted burnishing, J. Micro Nano-Manuf. 7 (2) (2019).
[170] J. Ratay, P.-Y. Wu, A. Feirvezers, H. Yamaguchi, Characteristics of diamond abrasive used in magnetic abrasive finishing of nickel-based superalloys, J. Micro Nano-Manuf. 8 (3) (2020).
[171] J. Zhang, A. Chaudhari, H. Wang, Surface quality and material removal in magnetic abrasive finishing of selective laser melted 316L stainless steel, J. Manuf. Process. 45 (2019) 710–719.
[172] F. Hashimoto, S.P. Johnson, Modeling of vibratory finishing machines, CIRP Ann. 64 (1) (2015) 345–348.
[173] F. Hashimoto, S.P. Johnson, R.G. Chaudhari, Modeling of material removal mechanism in vibratory finishing process, CIRP Ann. 65 (1) (2016) 325–328.
[174] R. Dražumerič, J. Badger, R. Roininen, P. Krajnik, On geometry and kinematics of abrasive processes: the theory of aggressiveness, Int. J. Mach. Tool Manufact. 154 (2020), 103567.
[175] I. Malkorra, et al., Identification of interaction mechanisms during drag finishing by means of an original macroscopic numerical model, Int. J. Mach. Tool Manufact. 168 (2021), 103779.
[176] P.S. Millet, Method for smoothing and polishing metals via ion transport via free solid bodies and solid bodies for performing the method, Patent US 2020/0270761 A1 (2020).
[177] Y. Bai, et al., Dry mechanical-electrochemical polishing of selective laser melted 316L stainless steel, Mater. Des. 193 (2020), 108840.
[178] F. Hashimoto, R.-S. Zhou, K. Howlett, Bearing surfaces with isotropic finish, US Patent 5503481 (1996).
[179] E. Atzeni, et al., Performance assessment of a vibro-finishing technology for additively manufactured components, Proc. CIRP 88 (2020) 427–432.
[180] A. Bernhardt, et al., Surface conditioning of additively manufactured titanium implants and its influence on materials properties and in vitro biocompatibility, Mater. Sci. Eng. C 119 (2021), 111631.
[181] L. Yang, N. Laugel, J. Housden, L. Espitalier, A. Matthews, A. Yerokhin, Plasma additive layer manufacture smoothing (PALMS) technology – an industrial prototype machine development and a comparative study on both additive manufactured and conventional machined AISI 316 stainless steel, Addit. Manuf. 34 (2020), 101204.
[182] S. Zhang, Y. Zhou, H. Zhang, Z. Xiong, S. To, Advances in ultra-precision machining of micro-structured functional surfaces and their typical applications, Int. J. Mach. Tool Manufact. 142 (2019) 16–41.
[183] A. Lu, Y. Gao, T. Jin, X. Luo, Q. Zeng, Z. Shang, Effects of surface roughness and texture on the bacterial adhesion on the bearing surface of bio-ceramic joint implants: an in vitro study, Ceram. Int. 46 (5) (2020) 6550–6559.
[184] A. Lu, et al., Modeling and prediction of surface topography and surface roughness in dual-axis wheel polishing of optical glass, Int. J. Mach. Tool Manufact. 137 (2019) 13–29.
[185] K.L. Tan, M.S. Vohra, W.L. Tan, A.P. Nagalingam, S.H. Yeo, A. Wee, Finishing a Surface of a Component Made by Additive Manufacturing, United States Patent, 2021.
[186] B. Pečnik, M. Hočevar, B. Širok, B. Bizjan, Scale deposit removal by means of ultrasonic cavitation, Wear 356–357 (2016) 45–52.
[187] K.L. Tan, S.H. Yeo, Surface modification of additive manufactured components by ultrasonic cavitation abrasive finishing, Wear 378–379 (2017) 90–95.
[188] K.L. Tan, S.H. Yeo, Surface finishing on IN625 additively manufactured surfaces by combined ultrasonic cavitation and abrasion, Addit. Manuf. 31 (2020), 100938.
[189] S.H. Yeo, A.P. Nagalingam, A Method and Apparatus for Finishing a Surface of a Component, 2020. Great Britain.
[190] A.P. Nagalingam, H.K. Yuvaraj, S.H. Yeo, Synergistic effects in hydrodynamic cavitation abrasive finishing for internal surface-finish enhancement of additive-manufactured components, Addit. Manuf. 33 (2020), 101110.
[191] A.P. Nagalingam, H.K. Yuvaraj, V. Santhanam, S.H. Yeo, Multiphase hydrodynamic flow finishing for surface integrity enhancement of additive manufactured internal channels, J. Mater. Process. Technol. 283 (2020), 116692.
[192] A.P. Nagalingam, S.H. Yeo, Surface finishing of additively manufactured Inconel 625 complex internal channels: a case study using a multi-jet hydrodynamic approach, Addit. Manuf. 36 (2020), 101428.
[193] A.P. Nagalingam, J.-Y. Lee, S.H. Yeo, Multi-jet hydrodynamic surface finishing and X-ray computed tomography (X-CT) inspection of laser powder bed fused Inconel 625 fuel injection/spray nozzles, J. Mater. Process. Technol. 291 (2021), 117018.
[194] K.P. Rajurkar, D. Zhu, J.A. McGeough, J. Kozak, A. De Silva, New developments in electro-chemical machining, CIRP Ann. 48 (2) (1999) 567–579.
[195] P.A. Jacquet, Electrolytic method for obtaining bright copper surfaces, Nature 135 (3426) (1935), 1076-1076.
[196] W. Han, F. Fang, Fundamental aspects and recent developments in electropolishing, Int. J. Mach. Tool Manufact. 139 (2019) 1–23.
[197] D. Landolt, Fundamental aspects of electropolishing, Electrochim. Acta 32 (1) (1987) 1–11.
[198] ISO 15730:2000: Metallic and Other Inorganic Coatings — Electropolishing as a Means of Smoothing and Passivating Stainless Steel, 2000.
[199] H. Wolfgang, H. Selma, S. Gabriela, Electropolishing Method and Electrolyte for Same, 2020.
[200] L. Wegrelius, F. Falkenberg, I. Olefjord, Passivation of stainless steels in hydrochloric acid, J. Electrochem. Soc. 146 (4) (1999) 1397–1406.
[201] Y. Zhang, J. Li, S. Che, Electropolishing mechanism of Ti-6Al-4V alloy fabricated by selective laser melting, Int. J. Electrochem. Sci. 13 (5) (2018) 4792–4807.
[202] R. Yi, Y. Zhang, X. Zhang, F. Fang, H. Deng, A generic approach of polishing metals via isotropic electrochemical etching, Int. J. Mach. Tool Manufact. 150 (2020), 103517.
[203] C. Rotty, A. Mandroyan, M.L. Doche, J.Y. Hihn, Electropolishing of CuZn brasses and 316L stainless steels: influence of alloy composition or preparation process (ALM vs. standard method), Surf. Coating. Technol. 307 (2016) 125–135.
[204] C. Zhao, N. Qu, X. Tang, Removal of adhesive powders from additive-manufactured internal surface via electrochemical machining with flexible cathode, Precis. Eng. 67 (2021) 438–452.
[205] V. Urlea, V. Brailovski, Electropolishing and electropolishing-related allowances for powder bed selectively laser-melted Ti-6Al-4V alloy components, J. Mater. Process. Technol. 242 (2017) 1–11.
[206] W. Hansal, S. Hansal, R. Mann, G. Sandulache, Electropolishing method and system therefor, Patent US 2019/0345628 A1 (2019).
[207] J. Mitchell-Smith, A. Speidel, J. Gaskell, A.T. Clare, Energy distribution modulation by mechanical design for electrochemical jet processing techniques, Int. J. Mach. Tool Manufact. 122 (2017) 32–46.
[208] A. Speidel, R. Sélo, I. Bisterov, J. Mitchell-Smith, A.T. Clare, Post processing of additively manufactured parts using electrochemical jet machining, Mater. Lett. 292 (2021), 129671.
[209] S. Hansal, W. Hansal, G. Sandulache, Method for removing metal supporting structures on an additively manufactured metal component, Patent US2021/0395915 A1 (2021).
[210] A. Rashid, F.M.A. Asif, P. Krajnik, C.M. Nicolescu, Resource Conservative Manufacturing: an essential change in business and technology paradigm for sustainable manufacturing, J. Clean. Prod. 57 (2013) 166–177.
[211] P.A. Temple, W.H. Lowdermilk, D. Milam, Carbon dioxide laser polishing of fused silica surfaces for increased laser-damage resistance at 1064 nm, Appl. Opt. 21 (18) (1982) 3249–3255.
[212] A.M. Ozkan, A.P. Malshe, W.D. Brown, Sequential multiple-laser-assisted polishing of free-standing CVD diamond substrates, Diam. Relat. Mater. 6 (12) (1997) 1789–1798, 1997/12/01/.
[213] S.M. Pimenov, et al., Laser polishing of diamond plates, Appl. Phys. A 69 (1) (1999) 81–88.
[214] A.M.K. Hafiz, E.V. Bordatchev, R.O. Tutunea-Fatan, Influence of overlap between the laser beam tracks on surface quality in laser polishing of AISI H13 tool steel, J. Manuf. Process. 14 (4) (2012) 425–434.
[215] T. Deng, J. Li, Z. Zheng, Fundamental aspects and recent developments in metal surface polishing with energy beam irradiation, Int. J. Mach. Tool Manufact. 148 (2020), 103472.
[216] Y. Liu, et al., Improving surface quality and superficial microstructure of LDED Inconel 718 superalloy processed by hybrid laser polishing, J. Mater. Process. Technol. 300 (2022), 117428.
[217] J. Xu, P. Zou, D. Kang, W. Wang, Theoretical and experimental study of bulge formation in laser polishing of 304 stainless steel, J. Manuf. Process. 66 (2021) 39–52, 2021/06/01/.
[218] S.A. Khairallah, A.T. Anderson, A. Rubenchik, W.E. King, Laser powder-bed fusion additive manufacturing: physics of complex melt flow and formation mechanisms of pores, spatter, and denudation zones, Acta Mater. 108 (2016) 36–45.

[219] J. Kumstel, B. Kirsch, Polishing titanium- and nickel-based alloys using cw-laser radiation, Phys. Procedia 41 (2013) 362–371.
[220] Y.-D. Chen, W.-J. Tsai, S.-H. Liu, J.-B. Horng, Picosecond laser pulse polishing of ASP23 steel, Opt Laser. Technol. 107 (2018) 180–185.
[221] Y.-H. Li, et al., Material characterization, thermal analysis, and mechanical performance of a laser-polished Ti alloy prepared by selective laser melting, Metals 9 (2) (2019) 112.
[222] A. Lamikiz, J.A. Sánchez, L.N. López de Lacalle, J.L. Arana, Laser polishing of parts built up by selective laser sintering, Int. J. Mach. Tool Manufact. 47 (12) (2007) 2040–2050.
[223] L. Chen, B. Richter, X. Zhang, X. Ren, F.E. Pfefferkorn, Modification of surface characteristics and electrochemical corrosion behavior of laser powder bed fused stainless-steel 316L after laser polishing, Addit. Manuf. 32 (2020), 101013.
[224] L. Chen, B. Richter, X. Zhang, K.B. Bertsch, D.J. Thoma, F.E. Pfefferkorn, Effect of laser polishing on the microstructure and mechanical properties of stainless steel 316L fabricated by laser powder bed fusion, Mater. Sci. Eng., A 802 (2021), 140579.
[225] M.A. Obeidi, E. McCarthy, B. O'Connell, I. Ul Ahad, D. Brabazon, Laser polishing of additive manufactured 316L stainless steel synthesized by selective laser melting, Materials 12 (6) (2019) 991.
[226] S. Marimuthu, A. Triantaphyllou, M. Antar, D. Wimpenny, H. Morton, M. Beard, Laser polishing of selective laser melted components, Int. J. Mach. Tool Manufact. 95 (2015) 97–104.
[227] Y. Tian, et al., Material interactions in laser polishing powder bed additive manufactured Ti6Al4V components, Addit. Manuf. 20 (2018) 11–22.
[228] K.C. Yung, T.Y. Xiao, H.S. Choy, W.J. Wang, Z.X. Cai, Laser polishing of additive manufactured CoCr alloy components with complex surface geometry, J. Mater. Process. Technol. 262 (2018) 53–64.
[229] A. Batal, A. Michalek, P. Penchev, A. Kupisiewicz, S. Dimov, Laser processing of freeform surfaces: a new approach based on an efficient workpiece partitioning strategy, Int. J. Mach. Tool Manufact. 156 (2020), 103593.
[230] D. Bhaduri, et al., Laser polishing of 3D printed mesoscale components, Appl. Surf. Sci. 405 (2017) 29–46.
[231] L. Hackel, J.R. Rankin, A. Rubenchik, W.E. King, M. Matthews, Laser peening: a tool for additive manufacturing post-processing, Addit. Manuf. 24 (2018) 67–75.
[232] J. Lu, H. Lu, X. Xu, J. Yao, J. Cai, K. Luo, High-performance integrated additive manufacturing with laser shock peening –induced microstructural evolution and improvement in mechanical properties of Ti6Al4V alloy components, Int. J. Mach. Tool Manufact. 148 (2020), 103475.
[233] N.E. Uzan, S. Ramati, R. Shneck, N. Frage, O. Yeheskel, On the effect of shot-peening on fatigue resistance of AlSi10Mg specimens fabricated by additive manufacturing using selective laser melting (AM-SLM), Addit. Manuf. 21 (2018) 458–464.
[234] Z. Wang, Z. Liao, D. Axinte, X. Dong, D. Xu, G. Augustinavicius, Analytical model for predicting residual stresses in abrasive waterjet peening, Mater. Des. 212 (2021), 110209.
[235] B. Blinn, et al., Influence of microstructural defects and the surface topography on the fatigue behavior of "additively-subtractively" manufactured specimens made of AISI 316L, Mater. Werkst. 52 (5) (2021) 561–577.
[236] R. Shrestha, J. Simsiriwong, N. Shamsaei, Fatigue behavior of additive manufactured 316L stainless steel parts: effects of layer orientation and surface roughness, Addit. Manuf. 28 (2019) 23–38.
[237] C. Elangeswaran, et al., Effect of post-treatments on the fatigue behaviour of 316L stainless steel manufactured by laser powder bed fusion, Int. J. Fatig. 123 (2019) 31–39.
[238] D.B. Witkin, D.N. Patel, H. Helvajian, L. Steffeney, A. Diaz, Surface treatment of powder-bed fusion additive manufactured metals for improved fatigue life, J. Mater. Eng. Perform. 28 (2) (2019) 681–692.
[239] T. Childerhouse, E. Hernandez-Nava, R. M'Saoubi, N. Tapoglou, M. Jackson, Surface and sub-surface integrity of Ti-6Al-4V components produced by selective electron beam melting with post-build finish machining, Proc. CIRP 87 (2020) 309–314.
[240] T. Childerhouse, et al., The influence of finish machining depth and hot isostatic pressing on defect distribution and fatigue behaviour of selective electron beam melted Ti-6Al-4V, Int. J. Fatig. 147 (2021), 106169.
[241] Y. Kok, et al., Anisotropy and heterogeneity of microstructure and mechanical properties in metal additive manufacturing: a critical review, Mater. Des. 139 (2018) 565–586.
[242] Z. Wang, K. Guan, M. Gao, X. Li, X. Chen, X. Zeng, The microstructure and mechanical properties of deposited-IN718 by selective laser melting, J. Alloys Compd. 513 (2012) 518–523.
[243] J. Gockel, L. Sheridan, B. Koerper, B. Whip, The influence of additive manufacturing processing parameters on surface roughness and fatigue life, Int. J. Fatig. 124 (2019) 380–388.
[244] A.R. Balachandramurthi, J. Moverare, N. Dixit, R. Pederson, Influence of defects and as-built surface roughness on fatigue properties of additively manufactured Alloy 718, Mater. Sci. Eng., A 735 (2018) 463–474.
[245] D.B. Witkin, D. Patel, T.V. Albright, G.E. Bean, T. McLouth, Influence of surface conditions and specimen orientation on high cycle fatigue properties of Inconel 718 prepared by laser powder bed fusion, Int. J. Fatig. 132 (2020), 105392.
[246] S. Lee, S. Shao, D.N. Wells, M. Zetek, M. Kepka, N. Shamsaei, Fatigue behavior and modeling of additively manufactured IN718: the effect of surface treatments and surface measurement techniques, J. Mater. Process. Technol. 302 (2022), 117475.
[247] H.Y. Wan, et al., Effects of surface roughness and build thickness on fatigue properties of selective laser melted Inconel 718 at 650 °C, Int. J. Fatig. 137 (2020), 105654.
[248] E. Guenther, M. Kahlert, M. Vollmer, T. Niendorf, C. Greiner, Tribological performance of additively manufactured AISI H13 steel in different surface conditions, Materials 14 (4) (2021) 928.
[249] M.A. Melia, J.G. Duran, J.R. Koepke, D.J. Saiz, B.H. Jared, E.J. Schindelholz, How build angle and post-processing impact roughness and corrosion of additively manufactured 316L stainless steel, NPJ Mater. Degrad. 4 (1) (2020) 21.
[250] L.-E. Lindgren, A. Lundbäck, M. Fisk, R. Pederson, J. Andersson, Simulation of additive manufacturing using coupled constitutive and microstructure models, Addit. Manuf. 12 (2016) 144–158.
[251] D. Wedberg, L.-E. Lindgren, Modelling flow stress of AISI 316L at high strain rates, Mech. Mater. 91 (2015) 194–207.
[252] M. Fisk, J.C. Ion, L.-E. Lindgren, Flow stress model for IN718 accounting for evolution of strengthening precipitates during thermal treatment, Comput. Mater. Sci. 82 (2014) 531–539.
[253] P. Fernandez-Zelaia, S. Melkote, T. Marusich, S. Usui, A microstructure sensitive grain boundary sliding and slip based constitutive model for machining of Ti-6Al-4V, Mech. Mater. 109 (2017) 67–81.
[254] H. Liu, et al., The state of the art for numerical simulations of the effect of the microstructure and its evolution in the metal-cutting processes, Int. J. Mach. Tool Manufact. 177 (2022), 103890.
[255] S.A.H. Motaman, et al., Optimal design for metal additive manufacturing: an integrated computational materials engineering (ICME) approach, JOM 72 (3) (2020) 1092–1104.
[256] W. Yi Wang, J. Li, W. Liu, Z.-K. Liu, Integrated computational materials engineering for advanced materials: a brief review, Comput. Mater. Sci. 158 (2019) 42–48.
[257] T.M. Rodgers, J.D. Madison, V. Tikare, Simulation of metal additive manufacturing microstructures using kinetic Monte Carlo, Comput. Mater. Sci. 135 (2017) 78–89.
[258] N. Kouraytem, et al., A recrystallization heat-treatment to reduce deformation anisotropy of additively manufactured Inconel 718, Mater. Des. 198 (2021), 109228.
[259] Z. Wang, et al., Crystal plasticity finite element modeling and simulation of diamond cutting of polycrystalline copper, J. Manuf. Process. 38 (2019) 187–195.
[260] Y. Yu, et al., Impact of fluid flow on the dendrite growth and the formation of new grains in additive manufacturing, Addit. Manuf. 55 (2022), 102832.
[261] H.-J. Lee, H.-K. Kim, H.-U. Hong, B.-S. Lee, Influence of the focus offset on the defects, microstructure, and mechanical properties of an Inconel 718 superalloy fabricated by electron beam additive manufacturing, J. Alloys Compd. 781 (2019) 842–856.
[262] A. Balan, et al., Precipitation of γ″ in Inconel 718 alloy from microstructure to mechanical properties, Materialia 20 (2021), 101187.
[263] X. Zhang, H. Deng, S. Xiao, X. Li, W. Hu, Atomistic simulations of solid solution strengthening in Ni-based superalloy, Comput. Mater. Sci. 68 (2013) 132–137.
[264] S. Hayakawa, H. Xu, Temperature-dependent mechanisms of dislocation–twin boundary interactions in Ni-based equiatomic alloys, Acta Mater. 211 (2021), 116886.
[265] N.C. Levkulich, S.L. Semiatin, J.E. Gockel, J.R. Middendorf, A.T. DeWald, N. W. Klingbeil, The effect of process parameters on residual stress evolution and distortion in the laser powder bed fusion of Ti-6Al-4V, Addit. Manuf. 28 (2019) 475–484.
[266] M.R. Ahmadi, et al., Coherency strengthening of oblate precipitates extended in the {100} plane of fcc crystals: modeling and experimental validation, Materialia 21 (2022), 101328.
[267] D. Axinte, J. Billingham, Time-dependent manufacturing processes lead to a new class of inverse problems, Proc. Natl. Acad. Sci. USA 116 (12) (2019) 5341.
[268] A.M. Rubenchik, W.E. King, S.S. Wu, Scaling laws for the additive manufacturing, J. Mater. Process. Technol. 257 (2018) 234–243.